ULTRA-HIGH PERFORMANCE CONCRETE (UHPC) FOR CLOSURE POURS BETWEEN PRECAST CONCRETE DECK PANELS

A Thesis
Presented to
The Academic Faculty

by

Sung Yeob Lim

In Partial Fulfillment
of the Requirements for the Degree
Master of Science in the
School of Civil and Environmental Engineering

Georgia Institute of Technology
May 2021

ULTRA-HIGH PERFORMANCE CONCRETE (UHPC) FOR CLOSURE POURS BETWEEN PRECAST CONCRETE DECK PANELS

Approved by:

Dr. Lauren Stewart, Advisor
School of Civil and Environmental Engineering
Georgia Institute of Technology

Dr. Kimberly Kurtis
School of Civil and Environmental Engineering
Georgia Institute of Technology

Dr. Giovanni Loreto
College of Architecture and Construction
Kennesaw State University

Date Approved: April 30, 2021

ACKNOWLEDGEMENTS

I would like to express my sincere gratitude to Dr. Lauren Stewart who decided to have me on board as part of her research team. I never would have had the opportunity to learn so much during the past few semesters if it weren't for this project. I would also like to thank Drs. Lawrence Kahn, Kimberly Kurtis, and Giovanni Loreto for their guidance and help throughout this research. It isn't an everyday experience to be able to work for professors who are extremely renown in their respective fields.

Jeremy Mitchell, Andy Udell, and Dr. Nan Gao have been tremendously helpful and very generous with their times to help me get through my tests. I cannot imagine having to work in the lab without their help. I would like to thank all undergraduate and graduate students (Gino Pagliaro, Griffin Fish, Isaac Wasson, Miranda Tan, DC Burney, and Noel Flores) who helped me make UHPC on Monday mornings or during an exam week. I would also like to thank Maria Warren for proofreading my thesis and giving me valuable tips and comments. Kevin Kirkley and John Michael Romano from Tindall Corporation have been extremely helpful with construction of deck panels that are used in this project.

Lastly, I want to thank my parents and my sister for their endless love and support especially throughout the years I have been halfway around the world from home.

TABLE OF CONTENTS

LIST OF TABLES

LIST OF FIGURES

LIST OF SYMBOLS AND ABBREVIATIONS

ABC	Accelerated Bridge Construction
ASTM	American Society for Testing and Materials
BS	British Standards
COV	Coefficient of Variability
DOT	Department of Transportation
EA	Exposed Aggregate
ERDC	Engineer Research and Development Center
FHWA	Federal Highway Administration
f_r	Modulus of rupture
GDOT	Georgia DOT
HPC	High Performance Concrete
HRWR	High-Range Water Reducer
in.	Inches
ksi	Kips per square inch
LVDT	Linear Variable Differential Transformer
mm	Millimeters
psi	Pounds per square inch
MDOT	Michigan DOT
MDT	Montana DOT
M_{cr}	Cracking moment
M_y	Yield moment
M_n	Nominal moment capacity
NYSDOT	New York State DOT
SEML	Structural Engineering and Mechanics Laboratory
SCM	Supplementary Cementitious Materials
UHPC	Ultra-High Performance Concrete
VPG	Vishay Precision Group, Inc.
w/cm	Water-to-cementitious materials ratio
σ_{equi}	Maximum equivalent bending stress

SUMMARY

Ultra-high performance concrete (UHPC) is a relatively new type of concrete that has been implemented in bridge construction in many states. UHPC has improved mechanical properties such as higher compressive and tensile strengths than conventional concrete. In bridge construction, UHPC can be used as joint pour between precast structural elements such as deck panels and bulb-T girders. The usage of UHPC can significantly reduce construction time and long-term maintenance cost of bridges. However, commercially available UHPC is prohibitively expensive and, therefore, is not currently widely in bridge construction. For this reason, many studies have worked to develop a non-proprietary UHPC mix design. Often, silica fume is used as a key component in UHPC, however, it is not easily accessible in Georgia. This research focuses on developing and evaluating a non-proprietary UHPC mix design using locally-available materials in the state of Georgia. Metakaolin and Type F fly ash are used as supplementary cementitious materials (SCMs) instead of silica fume.

In this investigation, a UHPC mix is designed, implemented, and tested to meet baseline mechanical properties. The mix design demonstrates the required 28-day compressive strength of at least 18,000 psi and tensile strength of at least 750 psi. The UHPC mix then underwent testing to further investigate its feasibility in a structural application. Precast concrete deck panels were joined together by a closure pour filled with UHPC and these panels were tested to determine UHPC joint performance. The deck panel specimen tested in this research has demonstrated that the non-proprietary UHPC performs

satisfactorily in a structural load test. Further research is needed to better evaluate and validify the integrity of the non-proprietary UHPC mix developed in this investigation.

CHAPTER 1. INTRODUCTION

1.1 Problem Statement

With ever-growing populations comes an increasing need for sustainable transportation infrastructure. To meet modern transportation demands, it is necessary to build new infrastructure and rehabilitate existing roads and bridges. Work must be completed efficiently to mitigate construction-induced traffic congestion, delays, and disruptions. Many states' Departments of Transportation (DOTs) have adopted accelerated bridge construction (ABC) to minimize the negative impacts of infrastructure improvement. ABC is a construction technique that can significantly reduce construction time and potentially improve service lives of bridges. ABC allows state DOTs to efficiently build and rehabilitate bridges without additional strain on already-congested highways.

The temporal advantage of ABC stems partially from use of precast structural elements. Bridge components, such as deck panels and decked bulb tee girders, can be made offsite and brought to the construction site. These structural elements are then joined together at connection regions using grout or concrete that are able to transfer the required shear and moment induced from traffic loads. In order to successfully join multiple structural elements, the connection regions require significant width and extensive reinforcement detailing. The involved processes in constructing joint connections and assembling the structural elements are often labor-intensive and expensive.

The development of ultra-high performance concrete (UHPC) has paved the way to simplify the construction processes of the aforementioned connection details. Due to its

improved mechanical properties compared to conventional concrete and high performance concrete (HPC), UHPC can reduce connection width and reinforcement detailing. However, commercially available UHPC is proprietary and costs approximately $2,000 per cubic yard [1]. The steep price of commercially available UHPC inhibits its potential for widespread use in infrastructure development and rehabilitation projects.

Across the United States, significant research has been conducted and is ongoing to develop non-proprietary UHPC mix designs at the state and federal levels. Georgia DOT (GDOT) is among the many entities investigating the application of non-proprietary UHPC mix comprised of locally-available materials. However, there is a lack of comprehensive experimental data on UHPC made with materials from Georgia. This research addresses this gap through testing to characterize mechanical properties, including compressive strength and flexural tensile strength, of UHPC made with Georgia-sourced materials and demonstrates its use for precast deck closure pours.

1.2 Research Objectives

The objectives of this research are as follows:

1. To develop and evaluate a satisfactory non-proprietary UHPC mix that uses materials locally available from the state of Georgia and is able to achieve a 28-day compressive strength of at least 18,000 psi and a tensile strength of 750 psi.
2. To create a material testing protocol that demonstrates the required mechanical properties.

3. To develop a structural experiment that shows the ability of the UHPC material to be used for precast deck panel closure pours.
4. To conduct a proof-of-concept experiment to demonstrate the structural experimental technique.
5. To provide recommendations for future phases of testing that will focus on optimization of the closure pour and UHPC design.

1.3 Outline of Thesis

Chapter 2 discusses numerous studies of UHPC that have been conducted across different entities. General material composition of UHPC is examined. This chapter also presents and compares mechanical properties of UHPC such as compressive strength, flexural performance, and chloride ion penetration.

Chapter 3 presents the procedures and steps taken in mixing and testing the non-proprietary UHPC. This chapter discusses, in detail, the necessary mixing procedure and rationale for the mixing protocol.

Chapter 4 delves into the specifics of the mix design as well as the mechanical properties of UHPC. Compressive strength and flexural performance of the non-proprietary UHPC are presented in this chapter.

Chapter 5 includes the structural experiments. It outlines the construction of structural test specimens and the experimental setup as well as results from a proof-of-concept experiment.

Chapter 6 includes the concluding remarks of the thesis as they relate to the research objectives. It also provides recommendations for future work and includes specific modifications for future phases of experiments.

CHAPTER 2. LITERATURE REVIEW

UHPC is a relatively new type of concrete that has sparked the interest of the civil engineering industry. In the United States, UHPC has been used in prestressed concrete girder bridges, precast concrete deck panels, and field-cast connections between prefabricated bridge components [2]. Compared to conventional concrete, UHPC has improved mechanical properties including higher compressive strength, higher ductility, and efficient particle packing density. The lack of coarse aggregates in the mix design and the usage of fine aggregates and cementitious materials such as fly ash and silica fume contribute to the efficient particle packing density and low porosity of UHPC. UHPC has very low water-to-cementitious materials (w/cm) ratio compared to conventional concrete. Because the w/cm is so low, workability is achieved by using high-range water reducers (HRWR) that allow the concrete mix to be easily placed without compromising strength. Due to its favorable mechanical properties and versatility, many studies have investigated optimizing the mix design of UHPC to accommodate local material availability and investigated UHPC as a vital construction material in bridge rehabilitation [3].

2.1 Material Composition of UHPC

Unlike conventional concrete, the material composition of UHPC does not include coarse aggregates and has a significantly lower w/cm ratio. Fine sand, generally between 150 and 600 μm, is used in making UHPC and is the largest constituent in the mix apart from steel fibers [4]. The next largest particle is cement, which has a typical particle size of 1 to 50 μm. Ground quartz, with a size of 10 μm, is also widely used. Silica fume, the smallest particle among the constituents, has a size of 0.1 – 0.3 μm. Silica fume is a widely

used material for UHPC due to its high reactivity and ultra-fine particle size [5]. The particle sizes of the constituents allow UHPC to have a finely graded and homogeneous matrix [6].

Steel fibers are also a key component of the UHPC mix design. The addition of steel fibers allows UHPC to have more ductility and tensile load carrying capacity than conventional concrete. The tensile strength and dimensions of steel fibers vary depending on the manufacturer. Table 1 shows the typical material composition of UHPC.

Table 1: Typical UHPC composition [4]

Material	**Weight (lb) per cubic yard**	**Percent by Weight**
Portland Cement	1,200	28.5
Fine Sand	1,720	40.8
Silica Fume	390	9.3
Ground Quartz	355	8.4
Superplasticizer	51.8	1.2
Accelerator	50.5	1.2
Steel Fibers	263	6.2
Water	184	4.4

Due to the low w/cm ratio in UHPC, workability is acquired through the use of HRWR. In this study, MasterGlenium 7920®, a poly-carboxylate based admixture from Master Builders Solutions, is used.

2.2 Mechanical Properties of UHPC

2.2.1 Compressive Strength

Across numerous studies, a wide range of mechanical properties is observed depending on the materials used and the manner in which UHPC was cured. In Federal Highway Administration's (FHWA) 2006 report [6], mechanical properties of a commercially available UHPC, Ductal®, were investigated. Steam-treated and untreated UHPC specimens demonstrated an average strength of 28.0 ksi and 18.3 ksi, respectively [6]. Another study showed compressive strength of UHPC to be 25.8 ksi when cured at room temperature [7]. Table 2 summarizes compressive strength of various UHPC mix designs across numerous studies.

Table 2: 28-day compressive strength of UHPC from previous research.

Research led by	**Compressive Strength (ksi)**
Graybeal	18.3 – 28.0 [8]
US Army Corps of Engineers	25.9 – 31.3 [9]
Kim Huy Hoang, Philipp Hadl, Nguyen Viet Tue	27.7 – 28.6 [10]
MDOT, Ahlborn, Peuse, Misson	23.9 – 31.1 [11]
MDT, Berry	19.2 [12]
Ahmad, Hakeem, Maslehuddin	23.4 [13]

The variation of compressive strength in the above table is due to a number of factors such as varying material composition, w/cm, percentage of steel fibers by volume, and curing regime. For example, variation of curing conditions caused specimens from

Graybeal to vary from 18.3 – 28.0 ksi. One curing regime subjected specimens to 48 hours of curing in a steam environment (90˚C, 95% humidity) followed by a standard laboratory environment (22˚C, varying humidity) until testing [8]. The other specimens in this research were only subjected to standard laboratory environment until testing. The average 28-day compressive strength of steam-treated specimens was 28 ksi, versus 18.3 ksi for untreated specimens.

The above studies also used silica fume as a key component in the mix design. Silica fume helps improve mechanical properties of the matrix by eliminating voids between particles due to its fineness. It also enhances rheology and secondary hydrates [14]. However, careful attention must be given in determining the amount of silica fume used in the mix design. A high amount of silica fume in the UHPC mix will require a larger dose of HRWR because of the relatively high surface area to volume ratio of the particles. Using excessive amount of HRWR can cause bleeding or segregation of constituents in UHPC [14].

2.2.2 Tensile Strength

Different experimental methods such as direct tension, splitting cylinder, and four-point bending of beams were used to determine tensile capacity of UHPC specimens across numerous studies [15]. Graybeal followed procedures from ASTM E8, which is typically used for tension testing of metallic materials, to measure the direct tensile strength of UHPC specimens. Pilot tests were conducted using 1.0 in. by 2.0 in. by 11.9 in. rectangular prisms to determine viability of applying the concepts of the mechanical tests for metals to strain-hardening concretes [16]. After adjusting various parameters such as configuration,

thickness, shape, and bond length of grip plates, Graybeal confirmed viability of applying ASTM E8 procedures to test the tensile strength of UHPC. Specimens with 2 in. cross section and lengths of 12 in. and 17 in. were gripped at each end and subjected to a maximum tensile load of approximately 180 kN (40.4 kip) [16]. Figure 1 shows the configuration used in this study for the two types of specimens. Strain measurements were taken along the gauge length centered on the mid-length cross section. A parallel ring extensometer with four linear variable differential transformers (LVDTs) were used to measure strain. The results from this study showed a range of 1.24 ksi to 1.68 ksi of average ultimate strength of specimens.

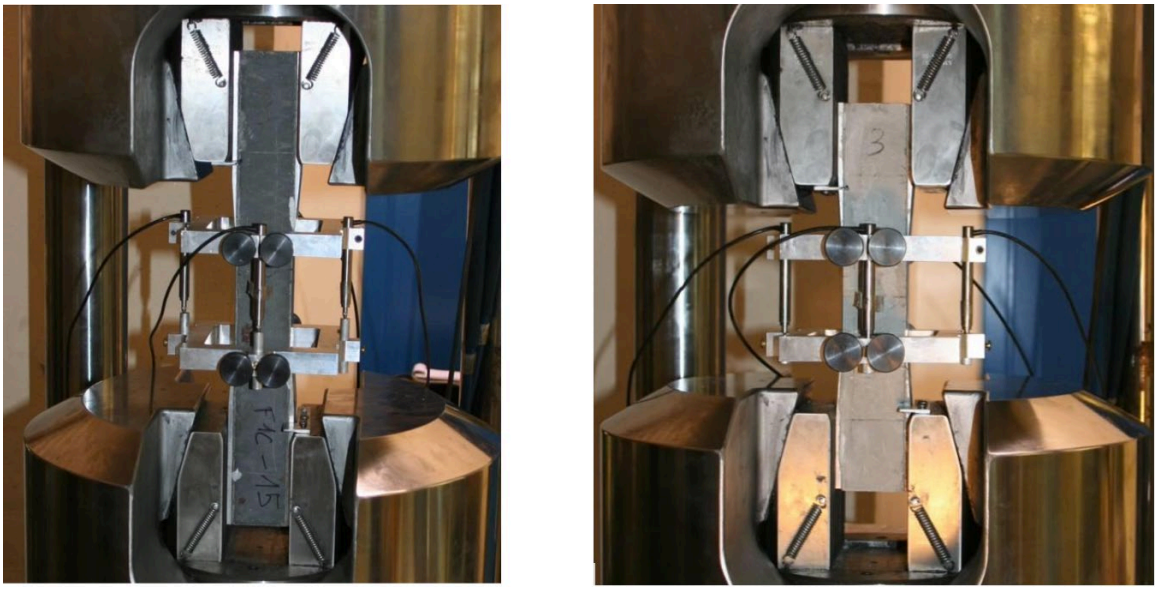

Figure 1: UHPC direct tension test configuration for 17 in. (left) and 12 in. (right) [16].

Graybeal also measured flexural tensile capacity of UHPC specimens according to procedures outlined in ASTM C1609. Peak strength at first crack and peak strength beyond first crack are determined. Figure 2 shows a typical configuration of the four-point bending test. This research employed three different four-point bend test geometries to investigate

flexural behavior of UHPC, labeled as “L”, “B”, and “S”, as shown in Figure 3. Load and midspan deflection were measured during the test period. The associated maximum equivalent bending stress, σ_{equi}, is calculated using Equation 1. The results are summarized in Table 3 for different UHPC batches and test configurations.

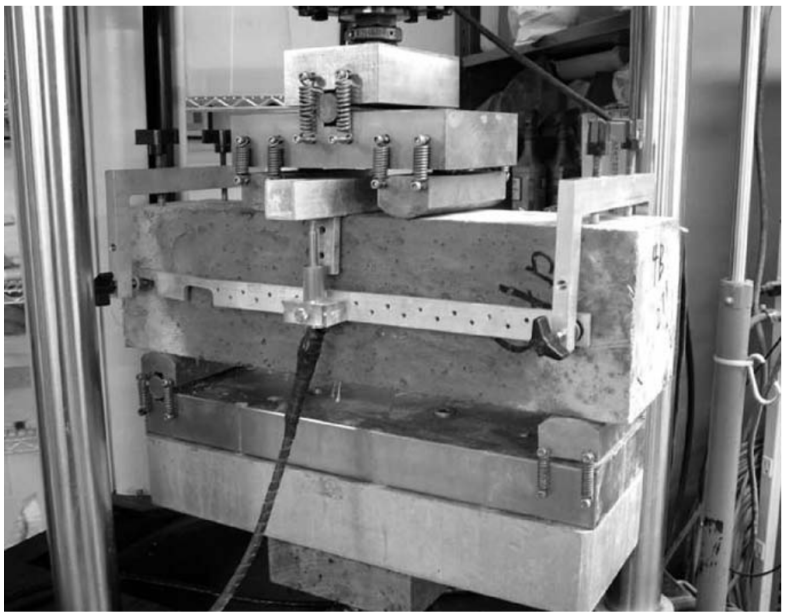

Figure 2: ASTM C1609 four-point bending configuration [17].

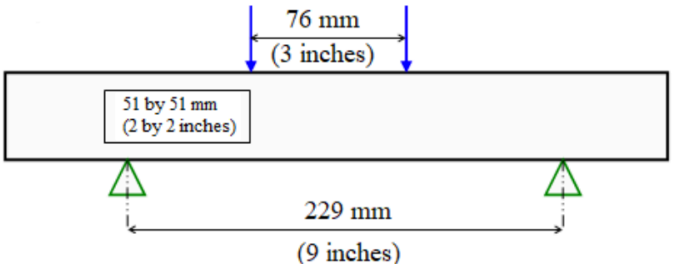

A. Bending configuration S.

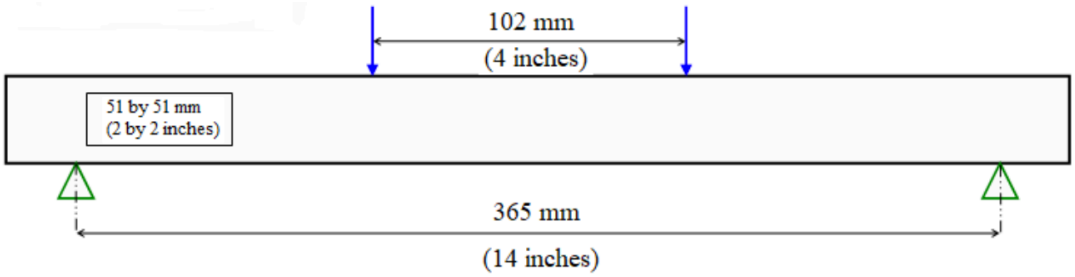

B. Bending configuration L.

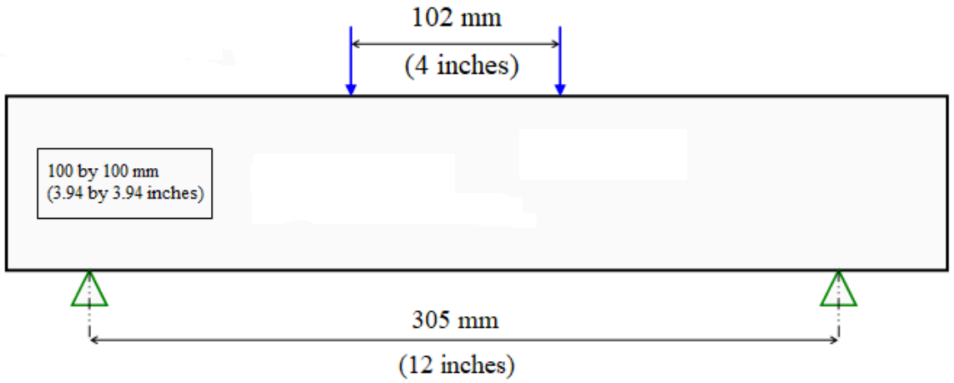

C. Bending configuration B.

Figure 3: Different four-point bending test configurations used to evaluate flexural performance of UHPC [16].

$$\sigma_{equi} = \frac{6M}{bh^2} \quad (1)$$

where
M: maximum moment
b: base of cross section
h: height of cross section.

Table 3: Maximum average equivalent bending stress for varying UHPC batches and test configurations [16].

Batch Name	Test Configuration	Number of Specimens Tested	σ_{equi} (ksi)
B2	S	5	4.07
	L	6	4.20
	B	6	3.82
F1A	S	6	3.50
	L	5	3.92
F2A	S	6	2.62
	L	5	3.42
F1B	S	6	3.10
	L	5	3.21
F1C	S	6	4.04
	L	5	4.13

Another research effort performed by Engineer Research and Development Center (ERDC) at U.S. Army Corps of Engineers investigated the flexural performance of UHPC. ERDC investigated and evaluated the performance of Cor-Tuf, a UHPC mix developed at ERDC. Three different dimensions of UHPC beams were tested with and without fibers using steps outlined in ASTM C1609. Table 4 summarizes the average flexural strength of different beam specimens with steel fiber reinforcement. Flexural strength was also calculated using Equation 1. Test results of total applied load versus midspan displacement

of 25 mm (0.984 in.) beams with fibers are shown in Figure 4. Steel fibers with tensile strength of 1100 MPa (159.5 ksi) used in this research are shown in Figure 5. The legend shows labels F1 to F9, which represent batch numbers of UHPC with fiber reinforcement. The fibers are 30 mm (1.18 in.) long with a diameter of 0.55 mm (0.217 in.) and are hooked at both ends. Cor-Tuf batches used in this research employed 3.6% of steel fibers by volume.

Table 4: Flexural performance of Cor-Tuf beam specimens [18].

Beam dimension [l by w by h] in mm (in.)	**Average Flexural Strength (psi)**	**Standard deviation (psi)**	**Coefficient of variation (%)**
356 by 102 by 25 (14 by 4 by 1)	3480	276	8
356 by 102 by 102 (14 by 4 by 4)	4293	116	2.8
1016 by 102 by 102 (40 by 4 by 4)	3466	391	11

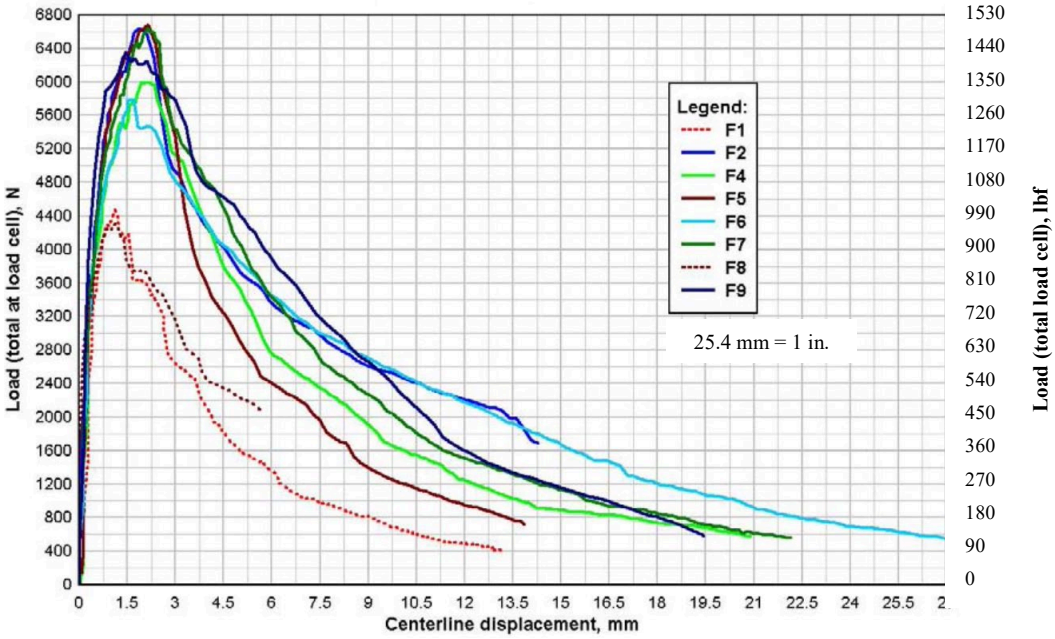

Figure 4: Applied load versus centerline displacement graph from Cor-Tuf flexural performance test [18].

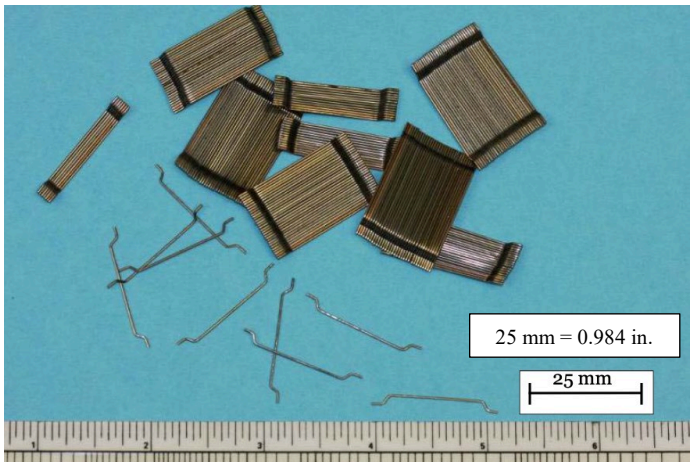

Figure 5: Hooked end fibers used in Cor-Tuf mix design [18].

As shown in Figure 4, the initial response of all the specimens is relatively linear. After the linear response, the specimens shifted to a nonlinear response until reaching the peak load, followed by a softening response [18]. Disregarding the two outliers, the greatest variability between specimen responses is observed after the peak load. Two possible

causes for this variability are the material characteristic and effects due to experimental setup. The random distribution and orientation of steel fibers could be the main contributing factor in variability of the post peak load response of specimens.

2.2.3 Chloride Ion Penetration

The durability of concrete is defined as its capability to continue performing its designed functions while maintaining dimensional stability in a given environment [11]. High permeability can be a significant cause of durability failure in concrete [19]. Highly permeable concrete is vulnerable to chloride ingress, which corrodes embedded steel reinforcement. Corroded steel reinforcement may expand up to 600%. [11], leading to cracking and spalling of the adjacent concrete and structural damage.

Previous studies show that UHPC has very low to negligible permeability and thus is very durable against chloride ingress. The densely packed matrix and low w/cm ratio of UHPC allows it to have very low permeability compared to ordinary concrete, increasing its durability. ASTM C1202 is a common testing method to determine whether concrete is susceptible to chloride ingress. Graybeal measured the amount of electrical current that passed through a 4 in. diameter cylinder by applying a 60V DC potential [4]. A sodium chloride solution was applied to one face of the cylinder and sodium hydroxide solution was applied to the other side. Table 5 compares the amount of Coulombs passed in UHPC specimens that were exposed to different curing regimes.

Table 5: Graybeal's rapid chloride ion penetrability results [4].

Curing Regime	Age (days)	No.	Coulombs Passed		Chloride Ion Penetrability
			Average	Standard Deviation	
Steam	28	3	18	1	Negligible
Air	28	2	360	2	Very Low
Air	56	3	76	18	Negligible
Tempered Steam	28	3	39	1	Negligible
Tempered Steam	56	3	26	4	Negligible
Delayed Steam	28	3	18	5	Negligible

As shown in Table 5, all specimens exhibited chloride ion penetrability ranging from "very low" to "negligible". Air treated UHPC specimens at 28 days showed relatively higher amounts of Coulombs passed than those exposed to tempered and delayed steam treatment, but still exhibited very low penetrability. A similar conclusion was drawn by Ahlborn, Peuse, and Misson [11]. Thermally-treated specimens were tested at 7 and 28 days and air-treated specimens were tested at 28 days. Table 6 summarizes the test results. The values of coefficient of variation (COV) for each curing regime are higher than those reported by Graybeal, but still well within the ASTM C1202 standard [20].

Table 6: Michigan Tech rapid chloride ion penetrability results [11].

Curing regime	Age at testing (days)	No. Specimens	Charge passed (Coulombs)			Chloride ion penetrability
			Average	Standard deviation	COV (%)	
Air	28	4	75	15	20	Negligible
TT	7	3*	10	1.5	15	Negligible
TT	28	4	15	3.5	24	Negligible

*one specimen tested at 8 days

2.3 UHPC as Joint Pour Between Structural Elements

Shear keys are used to transfer forces through joints and to prevent relative vertical displacements between structural elements, such as deck panels and decked bulb-T girders. The structural integrity and durability of concrete used in the shear key is vital to the successful performance of a bridge constructed using precast concrete components [21]. Two advantages of using UHPC as connection material are simplicity and performance. UHPC allows for small, simple connections without requiring post-tensioning or large volumes of field-cast concrete [22]. When used as a connection material between structural elements, UHPC allows for a significantly simpler reinforcement layout compared to when field cast grout is used, as shown in Figure 6. The dense and discontinuous pore structure that is further reinforced with steel fibers allows UHPC to have a more homogeneous stress distribution, better confinement of embedded rebar, and reduced development and splice lengths compared to ordinary concrete [23].

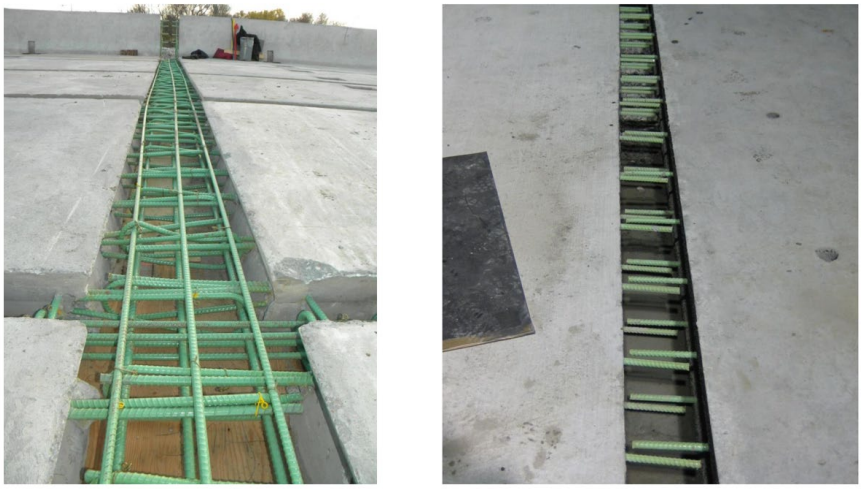

Figure 6: Joint detail using field cast grout (left). Joint detail using UHPC (right) [24].

Figure 7 shows a UHPC connection detail between precast structural decks used by New York State DOT (NYSDOT) on I-81 in Syracuse, New York. The rebars extrude into the UHPC connection area by 5-1/4 in. with lap length of only 4 in.

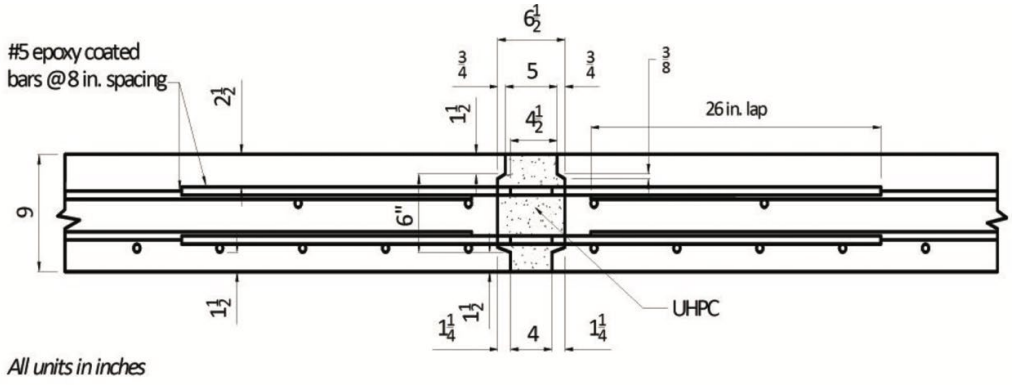

Figure 7: Joint detail of precast concrete decks used by NYSDOT [22].

As seen from the above figures, using UHPC as a connection material can help reduce the connection width. Along with simpler reinforcement layout, the reduced amount of material needed in the connection region can compensate for the relatively higher price

of UHPC. The simplicity of connection details can also reduce the cost in labor, formwork, and materials.

2.3.1 Experimentation of UHPC Joint Between Precast Concrete Deck Panels

NYSDOT in conjunction with FHWA has conducted experiments to assess the performance of UHPC closure pour connections [25]. The tests focused on the structural performance of UHPC connection undergoing cyclic and monotonic truck wheel loading. Figure 8 and Figure 9 show the test setup used to assess longitudinal and transverse UHPC connection performance.

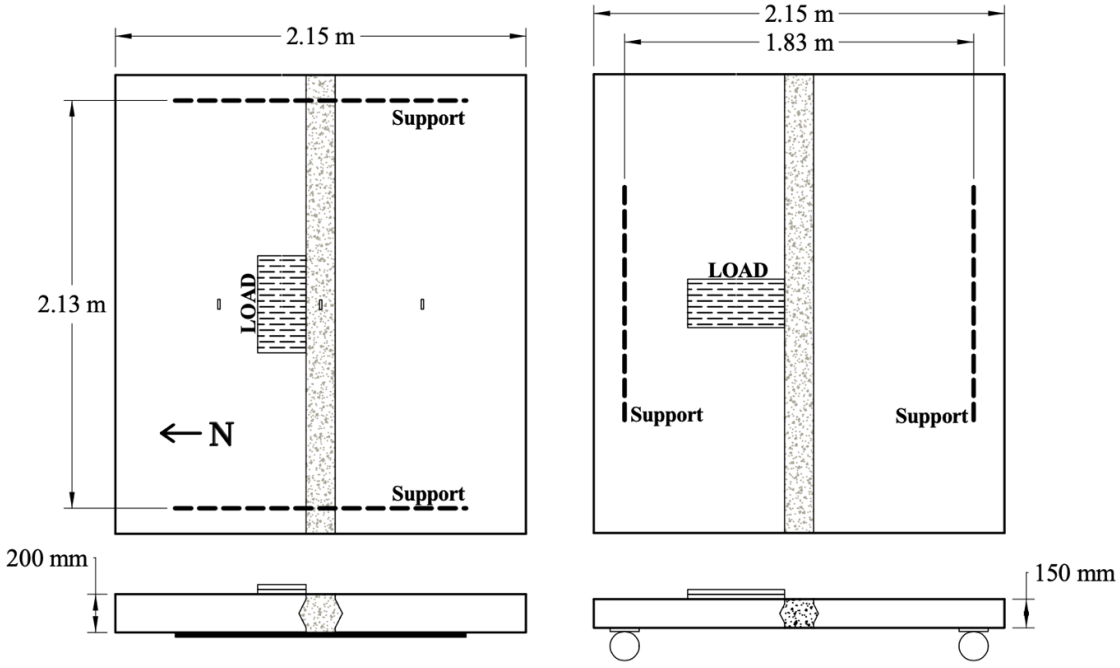

Figure 8: Cyclic loading test configuration for deck panels connected using UHPC joint [25].

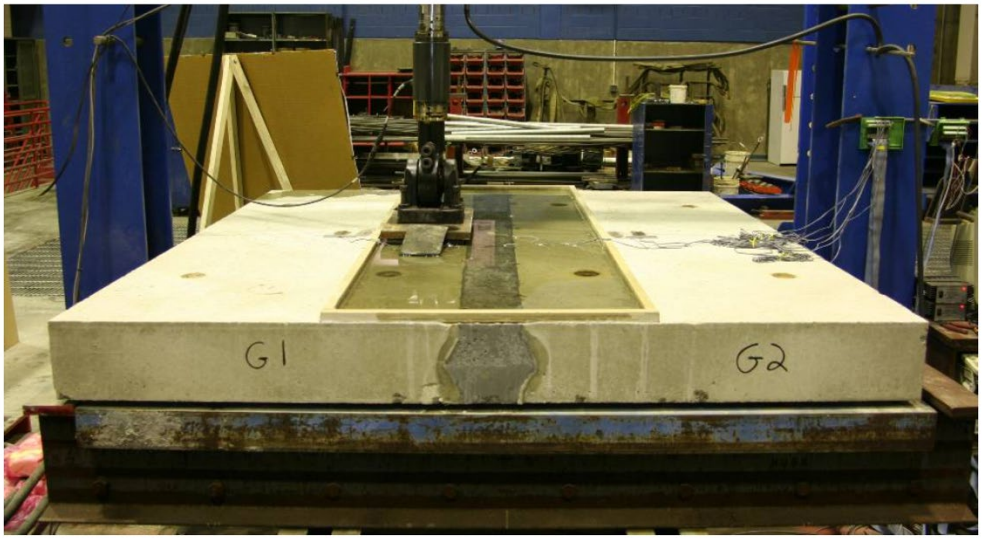

Figure 9: Cyclic loading configuration using triangular shear key [25].

In the above setup, the specimens were subjected to cyclic loads over a load range which generates a maximum tensile strain of 100 microns. This tensile strain value was used as a conservative upper limit estimate of what a concrete bridge deck would undergo during service. Initially, 2 million cycles with a peak load of 16 kips were applied. Then, absent signs of degradation, the load range was increased by a factor of 1.33 and 5 million additional cycles were applied. After the cyclic loads, each specimen was subjected to monotonically increasing load until failure. The specimens were monitored visually and electronically throughout the duration of the test for signs of concrete cracking, interface debonding, and flexural stiffness and strain distribution of specimens.

Figure 10 shows the strain and displacement results for one of the specimens. The strain per applied load remains relatively constant during the two phases of cyclic loading. This indicates that the load distribution across the joint through the bonds between the UHPC and precast concrete remained intact throughout the test.

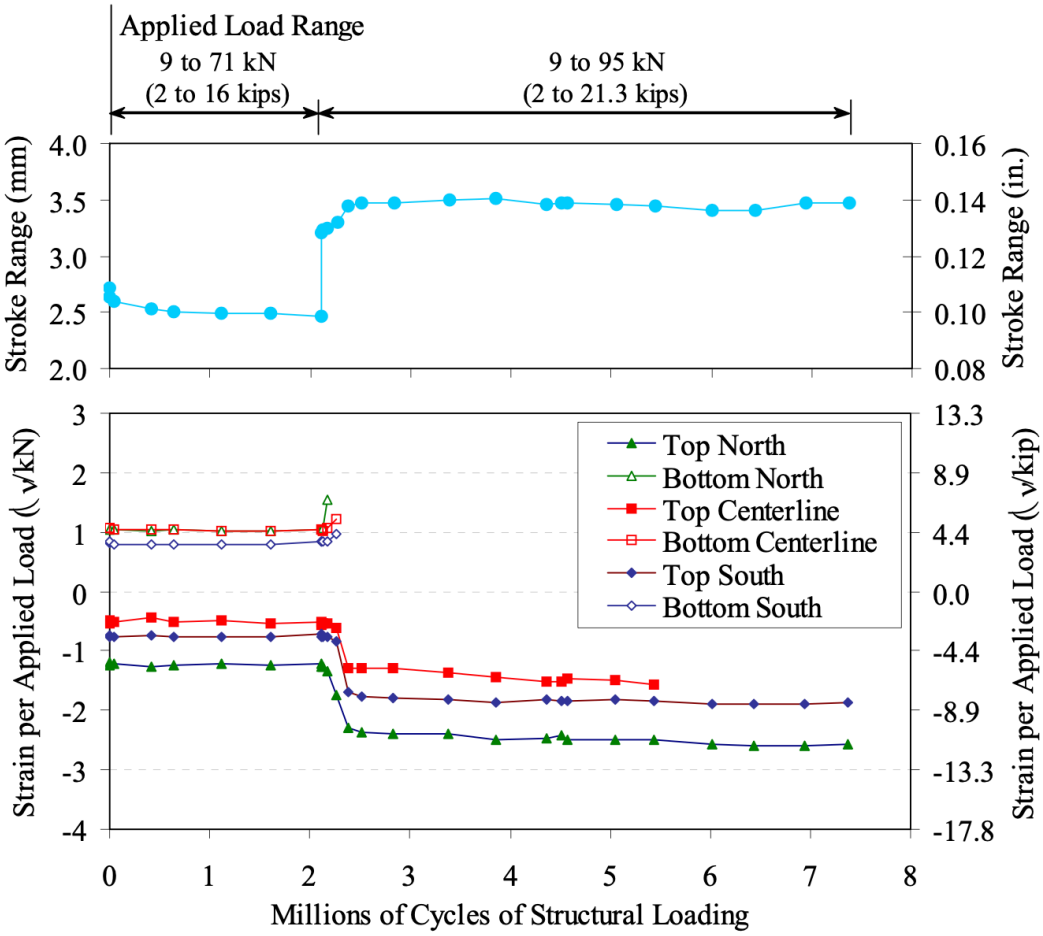

Figure 10: Strain and displacement results from cyclic loading test [25].

In addition to the UHPC connection, FHWA has also conducted tests that compare the performance of different field-cast grout materials and connection details of precast concrete deck panels [26]. The general details of specimens used in this research are shown in Figure 11. The variation in lap splice lengths within the connection region between two deck panels is due to the varying development lengths of rebars embedded in different grout materials. The grout materials are G1, G1IC, M1, E1, and U2, which stand for non-shrink cementitious grout, non-shrink cementitious grout with internal curing, magnesium phosphate grout, epoxy grout, and UHPC, respectively.

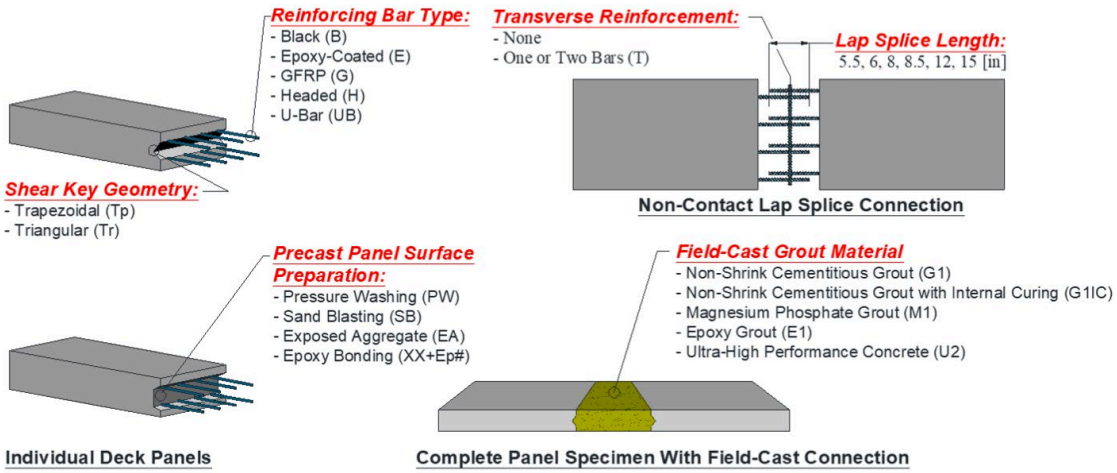

Figure 11: Deck level connection specimens and test variables [26].

The UHPC used in this experiment is a proprietary mix that was pre-blended and pre-bagged by the manufacturer. The pre-bagged powder was mixed with a phosphonate plasticizer, a polycarboxylate HRWR, a non-chloride accelerator, and steel fibers. The fibers were provided by a separate manufacturer from the UHPC. The nominal length and diameter of the fibers are 13 mm (0.512 in.) and 0.2 mm (0.008 in.), respectively. The tensile strength of fibers was specified by the manufacturer as 290 ksi [26]. The surface of the deck panels along the length of the joint had exposed aggregate (EA) finish with amplitude of 1/4 in. to provide bond between the grout materials and the concrete deck panels, as shown in Figure 12.

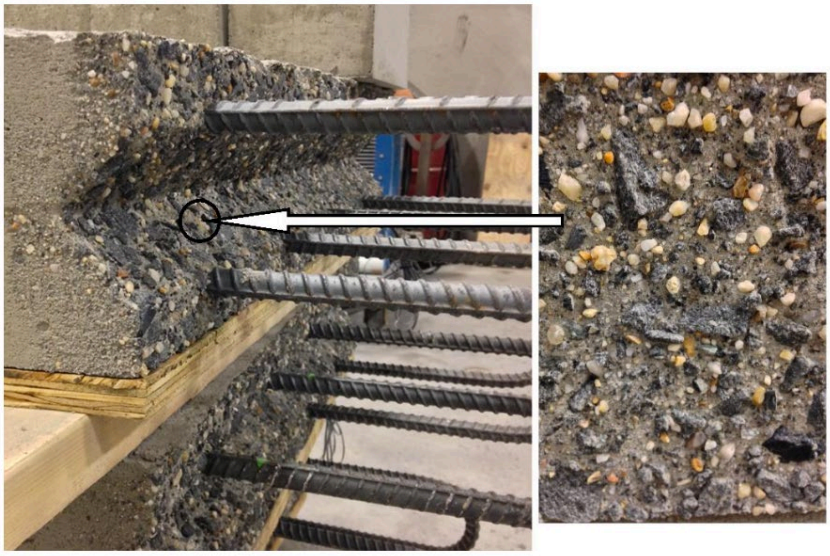

Figure 12: EA surface of a precast concrete deck [26].

The specimens in this experiment were subjected to three different loading procedures applied in succession: pre-crack cyclic loading, post-cracking fatigue loading, and monotonic ultimate loading. If a specimen lost the capability to withstand further loading during one of the loading procedures, then subsequent loading was not applied [26]. Figure 13 shows the setup for a four-point bending test of the specimens.

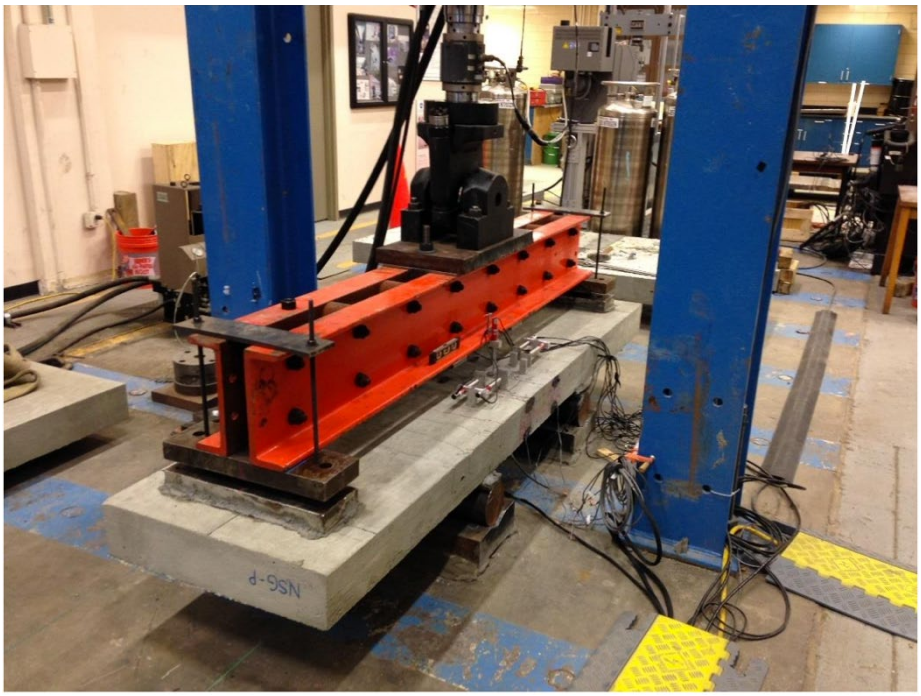

Figure 13: Deck panel specimen during loading [26].

The applied load during pre-crack cyclic loading procedure ranged between 10 and 120 percent of the cracking moment, M_{cr}. During this procedure, observations were made to identify first cracking at the interface between precast concrete and grout materials. Premature interface cracking can lead to durability issues because external agents such as water and chloride can penetrate through the cracks. The majority of specimens that employed a non-shrink cementitious grout (G1) showed interface cracking even before the loads were applied due to shrinkage. All specimens that employed a magnesium phosphate rapid-setting cementitious grout (M1) showed interface cracking after $0.8M_{cr}$ cycles. G1 and M1 grouts showed poor bonding with the precast concrete surfaces regardless of joint surface preparation. Specimens that used epoxy (E1) and UHPC (U2) grout fared well. Interface cracking were observed for all the specimens with sand-blasted joint surfaces using E1 grout at the $0.8\ M_{cr}$ cycles. The remaining specimens showed interface cracking

between 1.0 M_{cr} and the end of the loading procedure. The specimens that employed U2 grout without EA joint surface showed interface cracking at 0.8 M_{cr} cycles. All the specimens that had EA joint surface exhibited interface cracking beyond at least 1.2 M_{cr} cycle. The observations during and after the pre-crack cyclic loading indicate that UHPC performed better than all the other connection materials when EA surface preparation was employed. Figure 14 shows representative photographs of the connection regions after the loading procedure. Figure 15 shows a computerized drawing of cracks that occurred in the specimens using UHPC connection. The drawing shows that there were no cracks that occurred due to shrinkage.

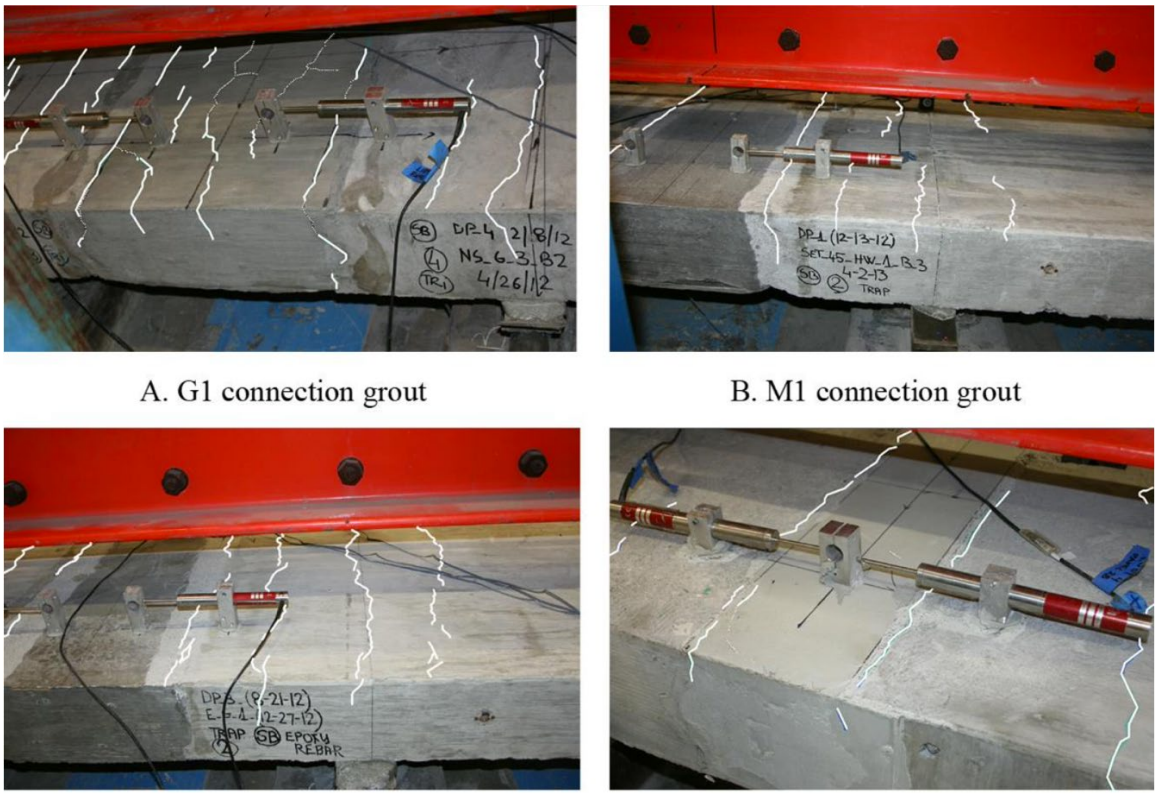

A. G1 connection grout

B. M1 connection grout

C. E1 connection grout

D. U2 connection grout

Figure 14: Representative photos of deck-level connection regions pre-cracking cyclic loading [26].

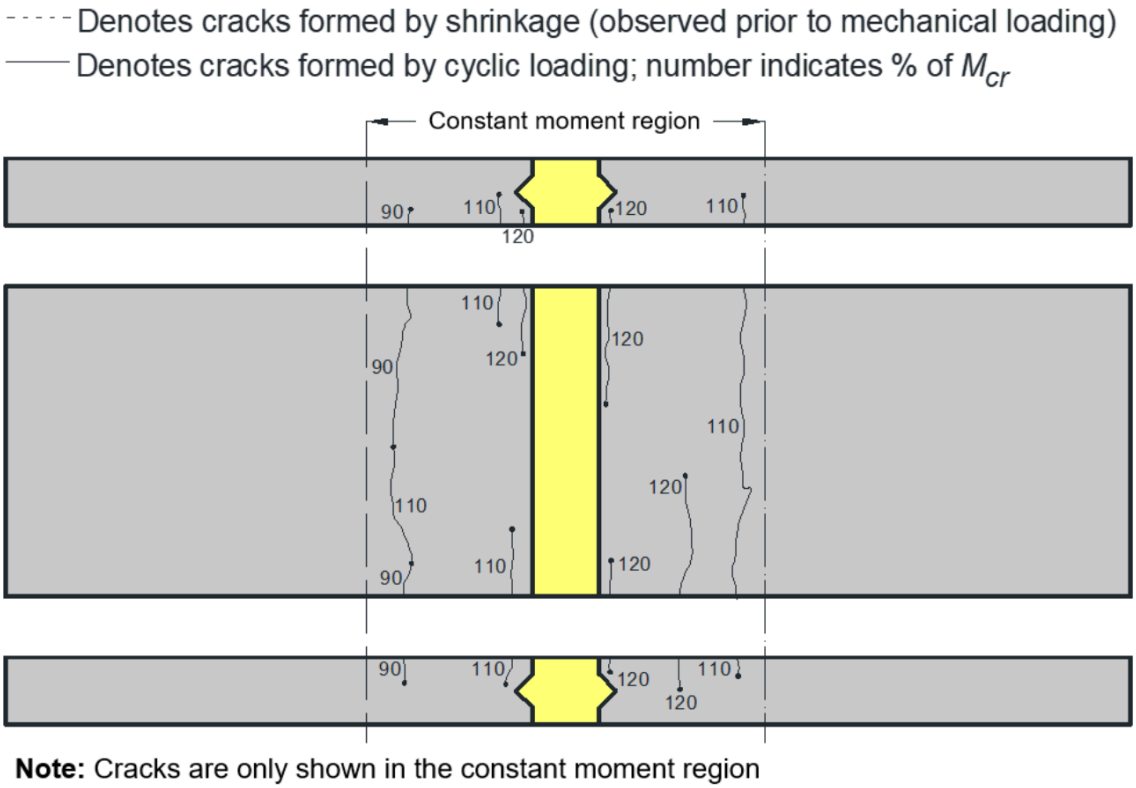

Figure 15: Computerized illustration of damage progression during pre-cracking cyclic loading for a specimen employing UHPC connection [26].

The lack of cracks within the connection region during pre-cracking cyclic loading indicates that when the UHPC connection fails, it will do so after the panels have failed. This particular investigation showed that the full flexural capacity of the deck panels was realized before failure occurred, due to concrete crushing, for specimens that employed UHPC connections [26]. The UHPC connections allowed the deck panel specimen to behave as though it were monolithically cast. The simpler connection detail, long-term maintenance cost, and durability of UHPC are some of the advantages of employing it as a connection material [26].

CHAPTER 3. METHODOLOGY FOR MATERIAL AND MECHANICAL TESTING

In the interest of using materials that are easily procurable in the state of Georgia, a non-proprietary mix design using metakaolin and Class F fly ash was designed. This design had to be feasible to mix and pour in the field. This chapter outlines the procedures developed for this mix design that resulted in consistent strength and workability of the mix. Also, the mechanical properties of the mix design are evaluated based on two proposed strength parameters: a compressive strength of 18,000 psi and sufficient flexural tensile strength at 28 days. These criteria were assessed though compressive and flexural testing of the UHPC mix designs. This chapter also includes description of specimen preparation and methodologies for mechanical testing carried out in Chapter 4.

3.1 Mixing Procedure

An intensive mixer manufactured by Eirich USA was used to make all UHPC in this study. The model of the mixer is R08W, which has a capacity of 75 L (2.65 ft^3) and 120 kg (265 lbs) [28]. Figure 16 and Figure 17 illustrate the mixing method and turning geometry of R08W. The rotor and mixing pan rotate in opposite directions allowing materials to mix thoroughly. The fixed scraper also agitates the concrete mix. The combination of high rotating speeds and geometry produces optimum homogenization of different materials [29]. Figure 18 is a picture of the R08W used to make UHPC in this study.

Figure 16: Mixing method and turning geometry of the Eirich Intensive Mixer (R08W) [29].

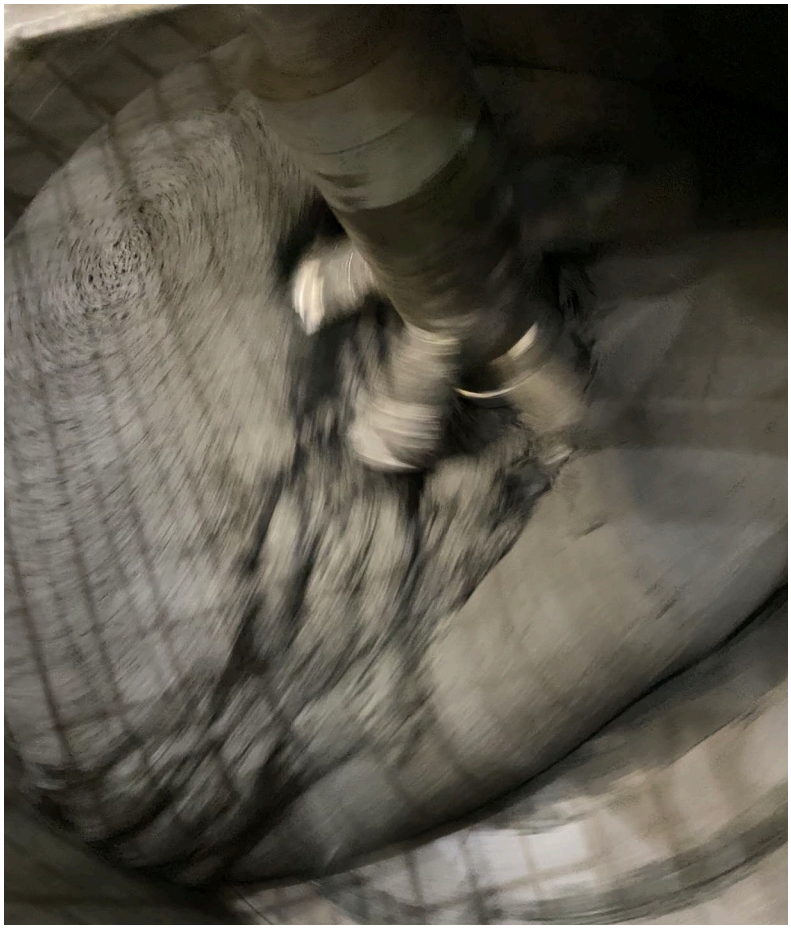

Figure 17: UHPC being mixed with R08W.

Figure 18: Eirich R08W used to make all UHPC in this investigation.

To achieve optimum workability and consistency in the UHPC mix, several procedures were implemented. Masonry sand, metakaolin, cement, and fly ash are initially dry mixed for a total of 10 minutes in order to break up any agglomerations and ensure that materials are evenly dispersed. It has been observed that using metakaolin drives up the temperature of the mix to a noticeable degree. A higher temperature of the mix can decrease the workability of UHPC. To offset the increase in temperature, at least half of the water was replaced with ice cubes. The step-by-step procedure is:

1. Add masonry sand and metakaolin in the mixer. Mix at ~250 rpm for 5 minutes.
2. Add cement and fly ash. Mix at ~250 rpm for 5 minutes.
3. Take 3/4 of HRWR and add to 0.175 of w/cm worth of water. Stir thoroughly.
4. Keep running the mixer at ~250 rpm. Gradually pour the water-HRWR solution into the mix over the course of 1 to 2 minutes.
5. After all of water-HRWR solution has been added, increase the speed to ~400 rpm. Mix for 8 minutes.
6. Pour the remaining 1/4 of HRWR into the remaining 0.005 w/cm worth of water.
7. Gradually pour the remaining water-HRWR into the mixer in 1 minute.
8. Decrease the speed to ~180 rpm. Mix for 5 minutes.
9. Perform flow table test per ASTM C1437 with exceptions outlined in ASTM C1856.
10. Keep the mixer running at ~60 rpm while performing flow test.
11. Once desirable flow diameter is confirmed, gradually add steel fibers to the mix within 1 to 2 minutes. Mix at ~180 rpm for 5 minutes.
12. Cast UHPC.

The mixing procedure was developed through multiple trial pours in the laboratory. Satisfactory workability is achieved when there is a delayed addition of water and HRWR (steps 6 and 7). If all the batch water and HRWR are added at the very beginning of wet mixing, the UHPC has a state of poor workability. The mix also sets up relatively quickly in the mixer and becomes extremely difficult to place into molds. It has been observed that when UHPC is allowed to sit in the mixer for longer than 10 minutes without agitation, a dry skin forms on the surface that makes the mix more difficult to maneuver. Although this

dry skin is easy to break apart manually, it is recommended to agitate the mix using the mixer to avoid difficulties in placing fresh UHPC. In the above procedure, step 10 was implemented to address this issue. This is especially prescient when casting UHPC in multiple layers, since the dry skin can potentially create an interface between layers and reduce the randomness of steel fiber orientation. It is important to determine the flow diameter of freshly mixed UHPC, step 9, prior to adding steel fibers, step 11. When fibers are added without achieving the desired flow diameter of UHPC, the mix stiffens and loses significant workability. This can result in poor quality of casting as shown in Figure 19.

Figure 19: 100 mm cube specimen. The shape is distorted due to poor workability of UHPC.

3.2 Testing Procedure

3.2.1 Compressive Strength Test Procedure

During the development of a non-proprietary mix design, UHPC specimens used to test for compressive strength were cast into 100 mm (3.94 in.) cubic molds. 3 in. by 6 in. cylinders were also cast along with the 100 mm cubes during construction of structural test specimens which will be discussed in detail in Chapter 5. One cubic foot of UHPC was made per batch during the development of non-proprietary UHPC mix design. The dimensions of cube and cylinder specimens and the load rate at which they were tested conform to specifications in British Standards (BS) EN-12390 and ASTM C39, respectively. In order to perform the compressive strength tests, smooth testing surfaces are required. Unlike cylindrical molds, cubic molds allow the specimens to have five smooth surfaces. Grinding down an uneven surface for testing was not necessary, which helped expedite the process. Figure 20 shows the molds used to make compressive test specimens. Cube and cylinder specimens that are ready for testing are shown in Figure 21 and Figure 22, respectively. All compressive strength test specimens were placed in a static servo-hydraulic SATEC compression frame that has a capacity of 800 kips. Testing was displacement-controlled and displacement was increased steadily by the SATEC until automatically stopped, when the specimen lost further load-carrying capacity. The maximum load is recorded for every specimen.

Figure 20: 100 mm cube molds used for casting UHPC.

Figure 21: 100 mm UHPC cube specimen ready for testing.

Figure 22: 3 in. by 6 in. UHPC cylinder ready for testing.

For every batch of UHPC during the mix design development and structural specimen construction, nine cubic specimens were cast and screeded before being covered with plastic wraps in order to prevent moisture loss. Screeding UHPC is not always recommended nor manageable, especially in a larger-scale cast. However, screeding was done in this investigation to ease the preparation process for testing. Cylinder specimens were cast only during the construction of closure pours between precast concrete deck panels. All specimens were removed from their molds 24 hours after being cast. They were subsequently stored in a fog room at 73˚F and allowed to cure until testing. There was no thermal treatment of specimens or any other notable curing regime. Compressive tests were performed 3, 7, and 28 days after casting. Three cube specimens and three cylinder specimens were tested on each test day. The ends of cylinder specimens were ground with

an end-grinder shown in Figure 23 in order to ensure smooth testing surfaces. For cube specimens, the testing procedure adhered to EN-12390-3. The load rate specified in EN-12390-3 is between 0.2 MPa/s (29 psi/s) and 1.0 MPa/s (145 psi/s) [30]. The average value, 0.6 MPa/s (87 psi/s), was chosen for all compressive strength tests of cubic specimens in this study. For cylinder specimens, the load rate of 37 psi/s specified in ASTM C39 was modified to 150 psi/s per Graybeal's previous study [4].

Figure 23: Grinding a 3 in. by 6 in. cylinder to ensure smooth testing surface.

3.2.2 Flexural Test Procedure

Beam specimens were cast in order to evaluate the flexural performance of non-proprietary UHPC. These specimens were cast simultaneously with the cube and cylinder specimens. Specimens were covered with plastic wraps after casting and were demolded

24 hours later. They were then placed in a fog room at 73˚F until testing at 28 days after being cast. Two dimensions of beams were used: 2 in. by 2 in. by 17 in. and 3 in. by 3 in. by 12 in. with span length of 14 in. and 9 in., respectively. Three specimens were cast for each dimension. Different dimensions were used to evaluate the consistency in flexural performance. Figure 24 shows the beam molds that were used to cast specimens. A four-point bending test configuration was followed per ASTM C78 and C1609 as shown in Figure 25. Beam specimens were placed on a test fixture with an adjustable support span. One of the two supports of the bottom fixture was allowed to slide laterally as the specimen was loaded, acting as a roller support. An LVDT is used to measure the midspan displacement throughout the test. A load cell with a capacity of 10 kips was used to measure the load as the specimen was loaded at 0.01 in/min. The load and midspan displacement data were acquired using National Instrument's LabVIEW, a data acquisition program, at a rate of 3 Hz.

Figure 24: 3 in. by 3 in. by 12 in. molds (left) and 2 in. by 2 in. by 17 in. molds (right)

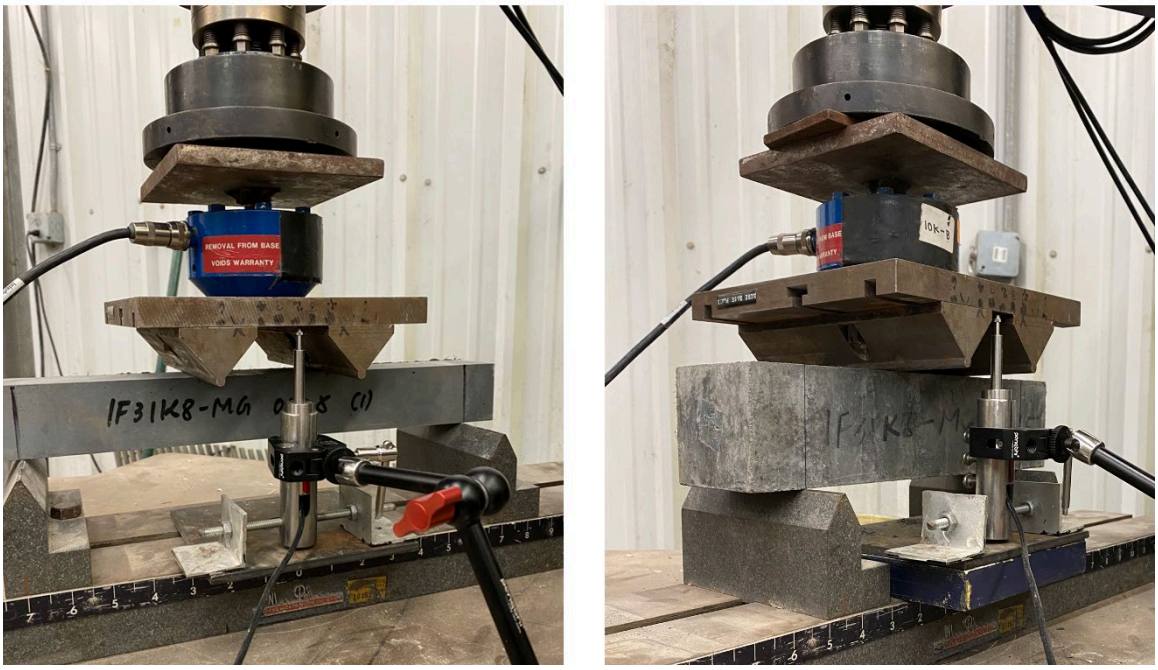

Figure 25: 2 in. by 2 in. by 17 in. beam (left) and 3 in. by 3 in. by 12 in. beam (right) during testing.

CHAPTER 4. EVALUATION OF MATERIAL AND MECHANICAL PROPERTIES OF NON-PROPRIETARY UHPC

A non-proprietary UHPC mix design for GDOT should have a compressive strength of at least 18,000 psi at 28 days and sufficient tensile strength and ductility. The high compressive strength and tensile capacity of UHPC will allow for smaller and simpler joint connections between structural elements in ABC. The materials used to make this UHPC should also be easily acquired within the state of Georgia. This chapter evaluates the material and mechanical properties that satisfy the above requirements.

4.1 Mix Design

Table 7 shows the material composition of the non-proprietary UHPC mix. For comparison, Table 8 shows one of several non-proprietary mixes from a previous study by Graybeal. The mix design in Table 8 is chosen for comparison amongst others because of its high average 28-day compressive strength of 29 ksi and identical amount of cement used in the non-proprietary mix [1]. In order to differentiate the two mix designs, each mix is given a specific nomenclature. The non-proprietary mix in Table 7 is referred to as 1F31K8. The mix with silica fume is referred to as 1F24Sf25. Figure 26 explains the nomenclature in detail. Table 9 summarizes the materials and their respective suppliers.

Table 7: Material composition of 1F31K8.

Materials	Weight (pcy)	Ratio per Cement Weight
Type I Portland Cement	1248	1
Class F Fly ash	387	0.31
Metakaolin	100	0.08
Masonry sand	1997	1.60
HRWR	25.7	0.02
Water	303	0.24
Steel fibers	264.6	0.21

Table 8: Graybeal's non-proprietary mix [1].

Materials	Weight (pcy)	Ratio per Cement Weight
White cement	1248	1
Fly ash	303	0.24
Silica fume	312	0.25
Fine aggregate	1871	1.5
HRWR	45	0.036
Water	287	0.23

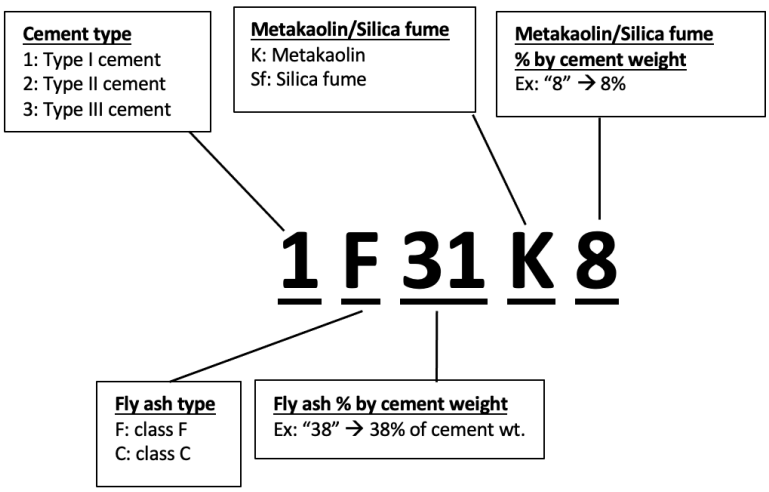

Figure 26: Explanation of nomenclature used to differentiate mixes.

Table 9: Materials and their respective suppliers for 1F31K8.

Materials	Suppliers
Type I Portland Cement	LaFarge-Holcim
Class F Fly Ash	Boral Resources
Metakaolin	BASF Kaolin
Masonry sand	Vulcan Materials
HRWR	MBCC Master Builders Solutions
Steel Fibers	Bekaert

The HRWR used in the non-proprietary mix is MasterGlenium® 7920. It is a polycarboxylate ether HRWR that conforms to ASTM C494 requirements [31]. Steel fibers marketed under the name Dramix® were procured from Bekaert. These fibers have nominal length of 13 mm (0.5 in.), diameter of 0.2 mm (0.008 in.), and tensile capacity of 2,600 MPa (377 ksi) [32]. Masonry sand used in the mix has all particles passing through

the No. 4 sieve and a fineness modulus of 1.59. The absorption capacity and specific gravity of the masonry sand is 0.51% and 2.58, respectively. Figure 27 shows the sieve analysis results for the masonry sand procured from Vulcan Materials' Kennesaw quarry. Details of the sieve analysis of masonry sand used in 1F31K8 are shown in Appendix A.

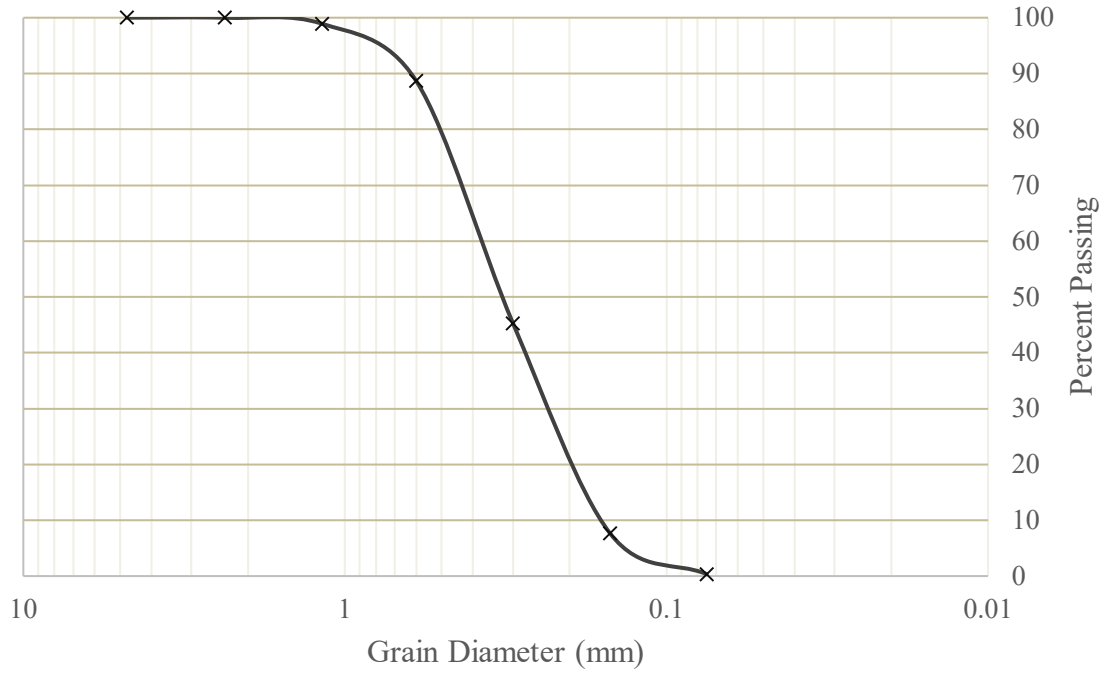

Figure 27: Sieve analysis result of masonry sand used in 1F31K8.

4.2 Initial Observations of UHPC

4.2.1 Observations of 1F31K8

As mentioned previously, it is important to achieve satisfactory workability of UHPC prior to adding fibers. The desired flow diameter of 1F31K8 is at least 9 in., adhering to procedures listed in ASTM C1437 with modifications outlined in ASTM C1856 [26]. This value is chosen based on numerous observations of UHPC mixtures that exhibited either poor workability or too much fluidity. A flow test of UHPC with a diameter

of 7-5/8 in. and relatively poor workability is shown in Figure 28. An acceptable flow diameter of approximately 9-1/4 in. in one direction is shown in Figure 29. Increasing the w/cm ratio of the mix design can help increase the workability of UHPC. However, it should be noted that increasing w/cm ratio can lead to segregation of steel fibers. This can render the UHPC ineffective, as it reduces the randomness of fiber distribution.

Figure 28: Flow diameter of 7-5/8 in. indicative of poor workability.

Figure 29: Flow diameter of 9-1/4 in. indicative of good workability.

4.2.2 Comparison to Mix Design from Literature

In order to directly compare the mix design developed for GDOT's use, the aforementioned 1F24Sf25 was also mixed and tested during this investigation. The main difference is the use of silica fume instead of metakaolin. Silica fume used in this investigation was supplied by Elkem Materials. While mixing 1F24Sf25, there was no significant rise in temperature of the mix unlike in the case of 1F31K8. The reason for this may be due to the absence of metakaolin in 1F24Sf25. Figure 30 shows a flow table test for 1F24Sf25. The average flow diameter was 8-5/8 in. Although the flow diameter is lower than the desired diameter for 1F31K8, 1F24Sf25 displayed satisfactory workability for a prolonged period of time.

Figure 30: Flow test of 1F24Sf25.

It is noteworthy to mention that a 1:1 replacement of silica fume with metakaolin did not result in a successful batch of UHPC. Rougeau and Borys investigated use of ultrafine particles other than silica fume in UHPC mixes. Using metakaolin and pulverized fly ash in UHPC required a higher dosage of superplasticizer and water to achieve the same workability as UHPC using silica fume [33]. Although higher amounts of water can improve the workability of UHPC, it will compromise the strength and quality of the final product. These observations align with those made in this investigation. During the development of 1F31K8, a higher metakaolin to cement ratio resulted in poor workability in several batches. Figure 31 shows a mix with 0.12 of metakaolin-to-cement ratio that became relatively solid and lumpy prior to the flow test. Figure 32 shows a flow diameter

of 4-3/8 in. of the UHPC mix. The mix had very poor workability and did not behave like a self-consolidating concrete.

Figure 31: Indication of poor workability of a UHPC batch with 0.12 metakaolin-to-cement ratio.

Figure 32: Flow diameter of 4-3/8 in. indicates poor workability of the above mix.

4.3 Mechanical Properties

4.3.1 Compressive Strength During Development

For compression tests, one common failure mode was observed across every cube specimen. The steel fibers in the mix design of UHPC allowed specimens to fail in a ductile mode. Figure 33 shows the failure mode of cube specimens. The cubic shape of each specimen is somewhat retained due to the steel fibers. The surface cracks that are shown in Figure 33 reveal how fibers are holding onto the concrete and prevent it from failing abruptly. Delamination of surfaces is a common observation made across all the cube specimens that failed in compression.

Figure 33: Failure mode of 100 mm UHPC cube specimens after compressive strength test.

The average compressive strength test results across nine batches of 1F31K8 during development are shown in Table 10. Average compressive test results for two batches of 1F24Sf25 are shown in Table 11. A bar graph comparing the average strength results

between the two mixes is shown in Figure 34. All test results are summarized in Appendix A.

Table 10: Average compressive strength of 1F31K8 during development.

Days cured	Average Strength (ksi)	Standard deviation (ksi)	COV (%)
3	14.35	0.79	5.48
7	16.14	0.68	4.24
28	18.55	1.11	5.96

Table 11: Compressive test results for 1F24Sf25.

Days cured	Average Strength (ksi)	Standard deviation (ksi)	COV (%)
3	12.86	0.19	1.50
7	14.10	0.81	5.72
28	16.74	0.94	5.59

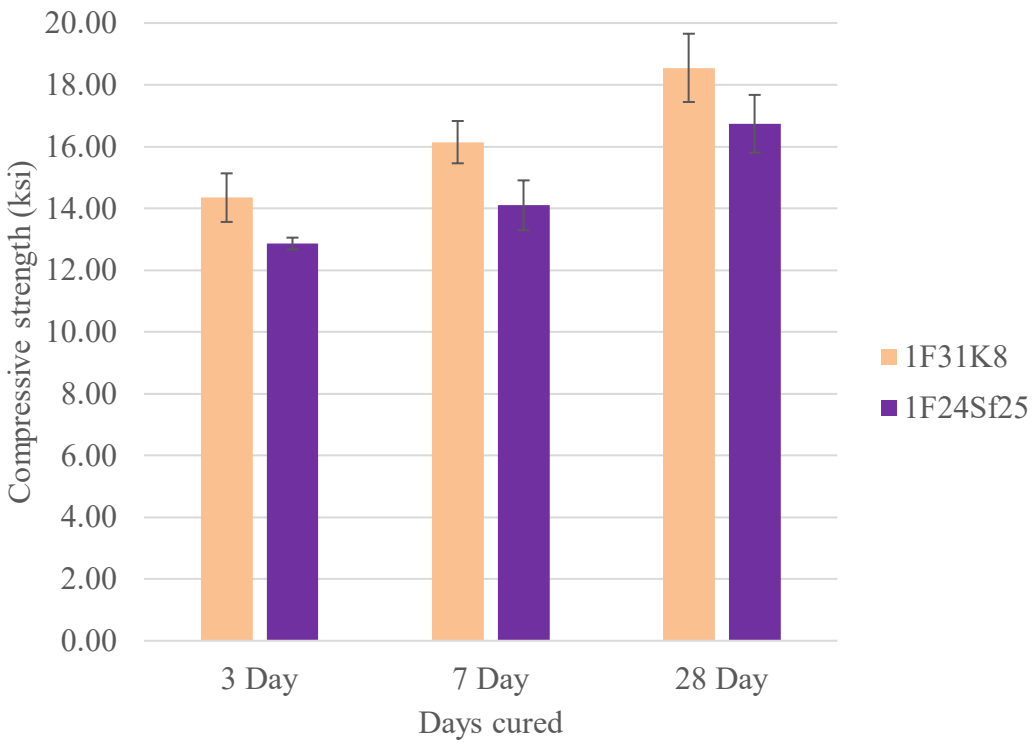

Figure 34: Average compressive strength of two mixes.

It can be seen from the above tables that the values of coefficient of variation in both mix designs across all the batches are less than 6%. This demonstrates consistency in the mixes, likely due to the high shear mixer's ability to homogenize the materials. It is also noted that compressive strength of 1F24Sf25 is lower than that of 1F31K8 for all three curing times. 1F24Sf25 is based on a non-proprietary mix design by Graybeal with a reported compressive strength of 29 ksi [1]. It should be noted that the material suppliers here may not be the same as those used by Graybeal. Also, the mixer used to make the UHPC batches in Graybeal's studies is an open, 1/2 horsepower bench top mixer that is not identical to the one used in this investigation. These reasons could have led to discrepancies in results between literature and this investigation.

4.3.2 Compressive Strength Results of Cubes and Cylinders

Cylinder specimens were cast and tested alongside cube specimens for batches of 1F31K8 that were used as closure pours between precast concrete deck panels. Further detail regarding construction of closure pours between precast concrete deck panels will be discussed in Chapter 5. Figure 35 shows cylinder specimens that failed under compression. Similar to the cube specimens, the cylinder specimens also displayed ductile modes of failure. Delamination of surface is evident in all the cylinder specimens.

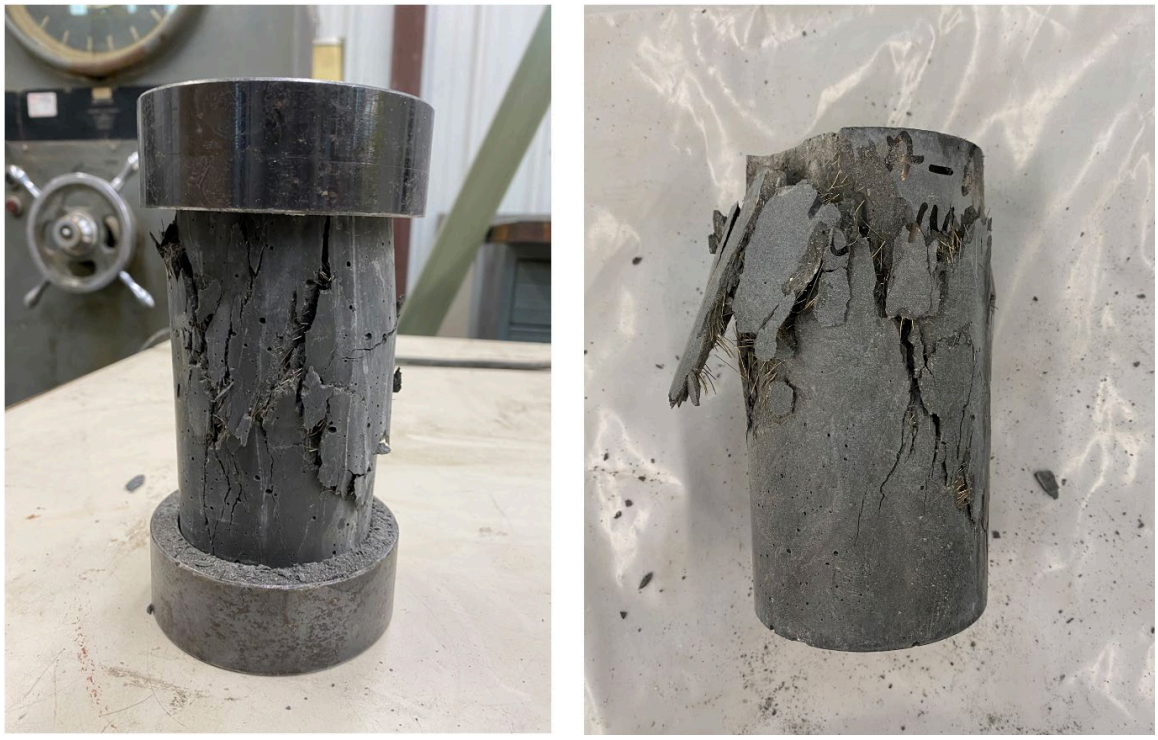

Figure 35: 3 in. by 6 in. cylinders after compression tests.

The compressive strength results of 1F31K8 used in closure pours are summarized in Table 12. Batch numbers that start with the letter “C” indicates that these batches were used to construct closure pours of structural test specimens. The coefficient of variability for these results are summarized in Table 13. The data suggests that there is only a minor

difference in strength values of 3 in. by 6 in. cylinders and 100 mm cubes until the 28-day tests. Coefficient of variability across different batches, test days, and specimen shapes also suggest that there is consistency in the mixes. This suggests that cube specimens may be viable to evaluate the compressive strength of UHPC. Using cube molds for casting UHPC is more convenient because of multiple smooth testing surfaces, whereas cylinders require grinding down both ends to ensure smooth testing surfaces.

Table 12: Average compressive strength of 1F31K8 used in closure pour.

Batch No.	Days Cured					
	3		7		28	
	Cubes	Cylinders	Cubes	Cylinders	Cubes	Cylinders
	Average strength (ksi)					
C1	15.50	15.44	17.45	17.96	21.04	23.92
C2	16.02	16.13	18.34	18.89	20.32	24.31
C3	15.83	15.52	17.66	18.73	--*	--*
C4	16.75	16.57	18.71	20.48	--*	--*

*: specimens are not at 28 days at the time of reporting.

Table 13: Coefficient of variability of compressive strength of cylinders and cubes.

Batch No.	Days Cured					
	3		7		28	
	Cubes	Cylinders	Cubes	Cylinders	Cubes	Cylinders
	Coefficient of variability (%)					
C1	3.06	--*	0.37	--*	2.09	--*
C2	0.49	1.37	1.13	0.25	2.34	0.76
C3	0.82	3.11	2.07	1.62	--**	--**
C4	1.05	0.46	2.27	1.72	--**	--**

*: only one cylinder was tested, no coefficient of variability was calculated.

**: specimens are not at 28 days at the time of reporting.

4.3.3 Flexural Performance

Flexural performance of beam specimens were evaluated using four-point bending configuration, as detailed in Chapter 3. Due to the steel fibers in the UHPC matrix, every specimen failed in a ductile manner. Figure 36 shows how a crack that formed in the middle third of the span gradually increased in size throughout the test. This is in stark contrast to the brittle manner in which an unreinforced UHPC beam fails, as shown in Figure 37. An overview of the failure mode of UHPC beam specimens with fiber reinforcement is shown in Figure 38.

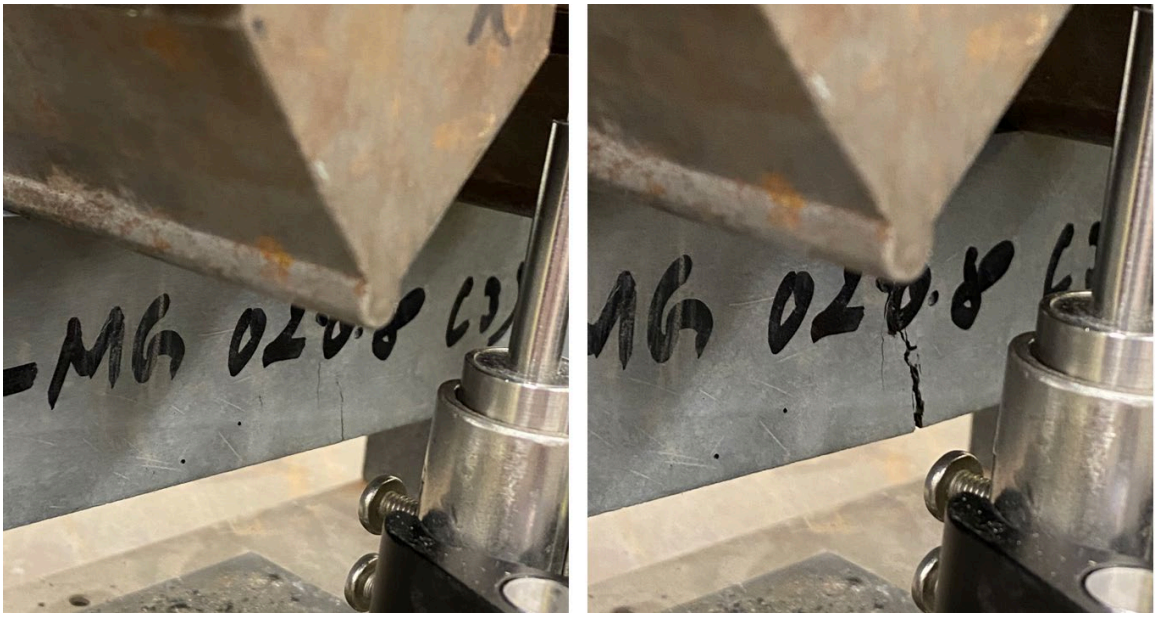

Figure 36: Formation of a major crack in a beam specimen during four-point bending test.

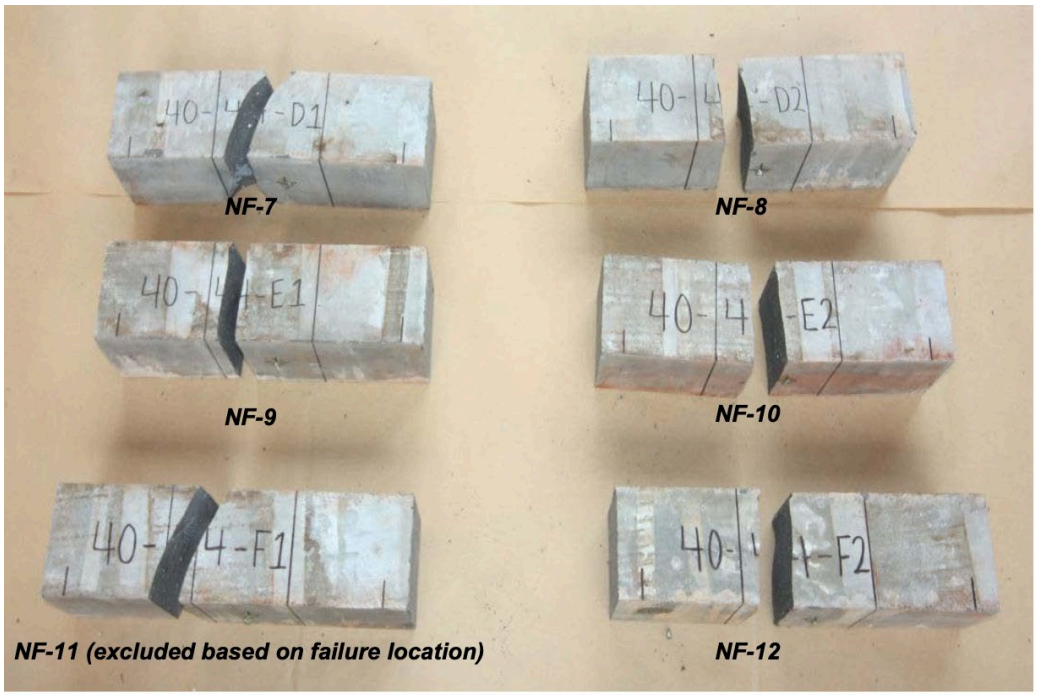

Figure 37: Unreinforced Cor-Tuf beams after failure [9].

Figure 38: UHPC beam specimens after failure.

The ductility of 1F31K8 can be observed quantitatively in the load-displacement graph acquired from testing. Figure 39 and Figure 40 show representative load-displacement graphs of three 2 in. by 2 in. by 17 in. and 3 in. by 3 in. by 12 in. specimens, respectively. All flexural test results are summarized in Appendix A. After the first peak load, the UHPC beams maintain load carrying capacity throughout the duration of the test, until at least a midspan deflection of L/150, where L represents span length. The modulus of rupture, as determined using Equation 2, of 1F31K8 beams cast during development are summarized in Table 14. The same quantities for beams cast during construction of closure pours of structural specimens are summarized in Table 15. The modulus of rupture at both peak load and first peak load are at least 2,000 psi across all specimens that have been tested regardless of their dimensions. To compare with data from literature, Equation 1 was used to calculate the flexural strength of both 2 in. by 2 in. and 3 in. by 3 in. beams. Table 16 and Table 17 summarize the average flexural strength of 1F31K8 beams. The average flexural strength of 2 in. by 2 in. beams across all the batches is 2,895 psi. The average flexural strength of beams of equivalent dimension and span from Graybeal is 3,775 psi (see configuration L in Table 3). The difference in strength may arise from the fact that all the beams in this investigation were tested 28 days after casting and were stored in a curing room until the day of the test. Graybeal's specimens were tested 3 months after casting and a majority of specimens underwent steam curing [16].

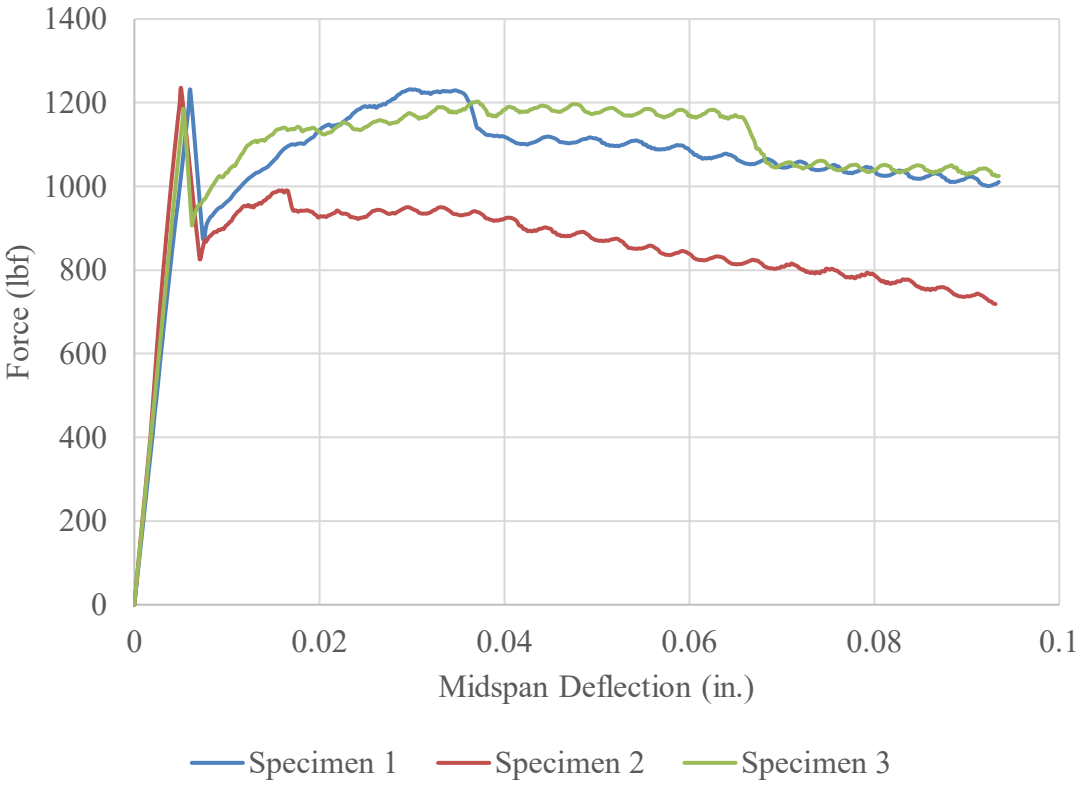

Figure 39: Load versus displacement graph of 2 in. by 2 in. beams.

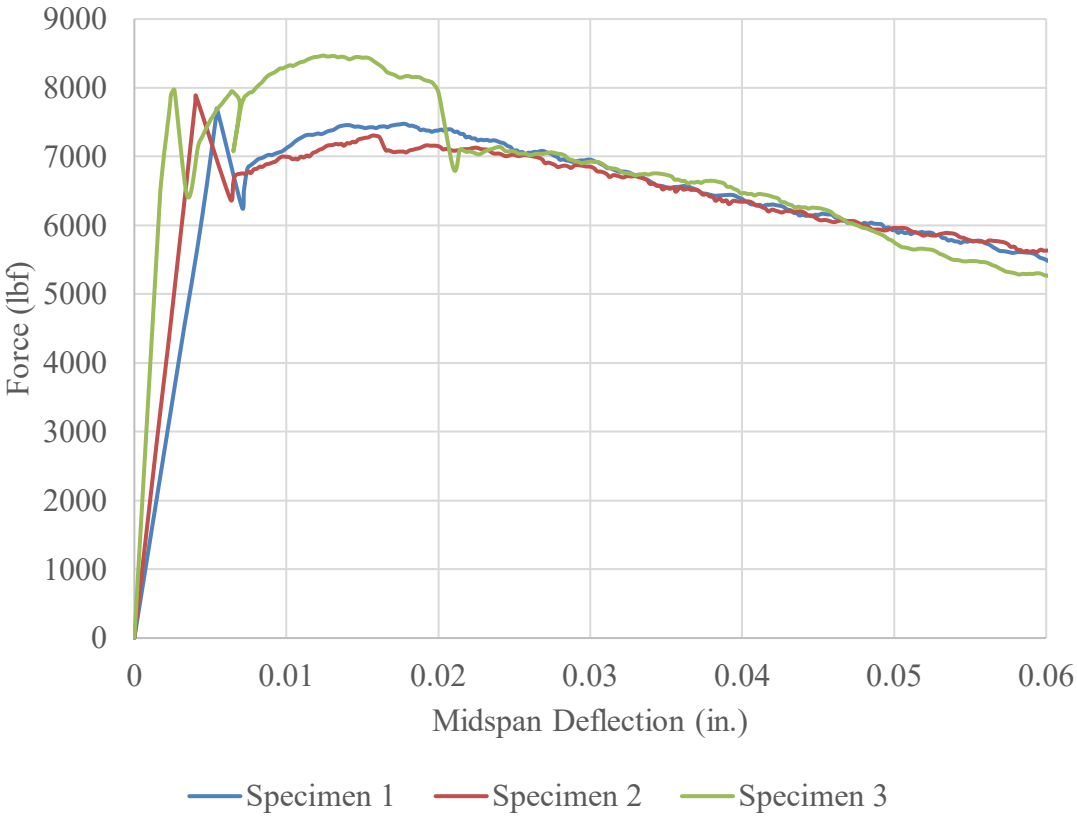

Figure 40: Load versus displacement graph for 3 in. by 3 in. beams.

$$f_r = \frac{PL}{bd^2} \tag{2}$$

where:

f_r: modulus of rupture, psi
P: the load, lbf
L: the span length, in.
b: average width of the specimen at the fracture, as oriented for testing, in., and
d: average depth of the specimen at the fracture, as oriented for testing, in.

Table 14: Average modulus of rupture of 1F31K8 beams cast during development.

Dimension *b* by *h* by *l* (in.)	**Span (in.)**	**f_r @ first peak load (psi)**	**f_r @ peak load (psi)**
2 by 2 by 17	14	2215	2550
3 by 3 by 12	9	2385	2860

Table 15: Average modulus of rupture of 1F31K8 beams cast during closure pour construction.

Dimension *b* by *h* by *l* (in.)	**Span (in.)**	**f_r @ first peak load (psi)**	**f_r @ peak load (psi)**
2 by 2 y 17	14	2845	3045
3 by 3 by 12	9	2735	3250

Table 16: Average flexural strength of beam specimens cast during development using Equation 1.

Dimension *b* by *h* by *l* (in.)	**Span (in.)**	**Average flexural strength (psi)**
2 by 2 by 17	14	2740
3 by 3 by 12	9	2860

Table 17: Average flexural strength of beam specimens cast during closure pour construction using Equation 1.

Dimension *b* by *h* by *l* (in.)	**Span (in.)**	**Average flexural strength (psi)**
2 by 2 by 17	14	3125
3 by 3 by 12	9	3250

Upon completion of each test, specimens were inspected to determine whether the major cracks occurred within the middle third of the respective spans. Data of specimens with cracks that occurred outside of the middle third are not reported. Figure 41 through Figure 44 show major cracks that occurred in 2 in. by 2 in. and 3 in. by 3 in. beams.

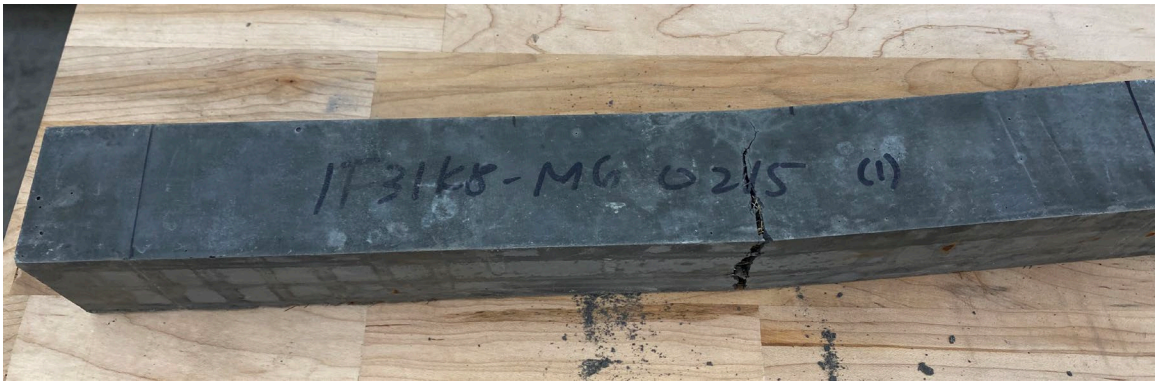

Figure 41: Major crack in the middle third of a 2 in. by 2 in. beam.

Figure 42: Close-up of the major crack that occurred in the 2 in. by 2 in. beam.

Figure 43: Major crack in the middle third of a 3 in. by 3 in. beam.

Figure 44: Close-up of the major crack in the 3 in. by 3 in. beam.

It was observed that the steel fibers bridge the major cracks in the two specimens. The engagement of steel fibers in the cracked zone of the cross section allows for a ductile failure of UHPC beams. Rupture of steel fibers was not observed, which indicates that the failure mode of UHPC beams occurred due to fiber pullout from the matrix. The ductile mode of failure was also observed in the case of compression tests. The ductile behavior of UHPC can potentially allow for reduction of the amount of steel reinforcement as well as the reduction of the development length of individual reinforcement bars.

CHAPTER 5. STRUCTURAL EVALUATION OF NON-PROPRIETARY UHPC

In order to evaluate structural viability of the UHPC with Georgian materials in joint pours, precast concrete deck panels of various dimensions were constructed with reinforcing steel bars protruding from one side. All panels in this investigation were fabricated at Tindall Corporation's precast concrete plant in Conley, Georgia. Two panels of equal dimension and embedment length of reinforcement were connected to each other using UHPC as a closure pour. Much of the design of concrete panels and the test setup were based on Graybeal's previous research on UHPC connections between precast bridge deck elements. This chapter describes the design, construction, and testing processes and results for the structural evaluation of UHPC closure pours.

5.1 Precast Concrete Deck Panels

5.1.1 Design

The precast concrete deck panels that are joined together by UHPC were designed as if they were monolithically cast. Protruding reinforcement from two deck panels were interlaced to create a non-contact lap splice region. This connection region was then filled with UHPC. A plan view of 28 in. by 40 in. and 40 in. by 96 in. panels are shown in Figure 45 and Figure 46, respectively. Four different types of concrete panels were constructed with different dimensions, connection region geometry, and embedment length of reinforcing bars into UHPC. Table 18 summarizes variables in each of the panels. Most of the specimens employ 5 in. of embedment length and 4 in. of non-contact lap splice of

protruding rebars in the UHPC connection. This is a recommendation from Graybeal's previous research. It also followed GDOT's current practice, which specifies a minimum embedment length of 8 times the bar diameter [34]. This requirement applies for No. 8 bar and smaller with yield strength of 75 ksi or less embedded in UHPC with 2% steel fiber content by volume [23].

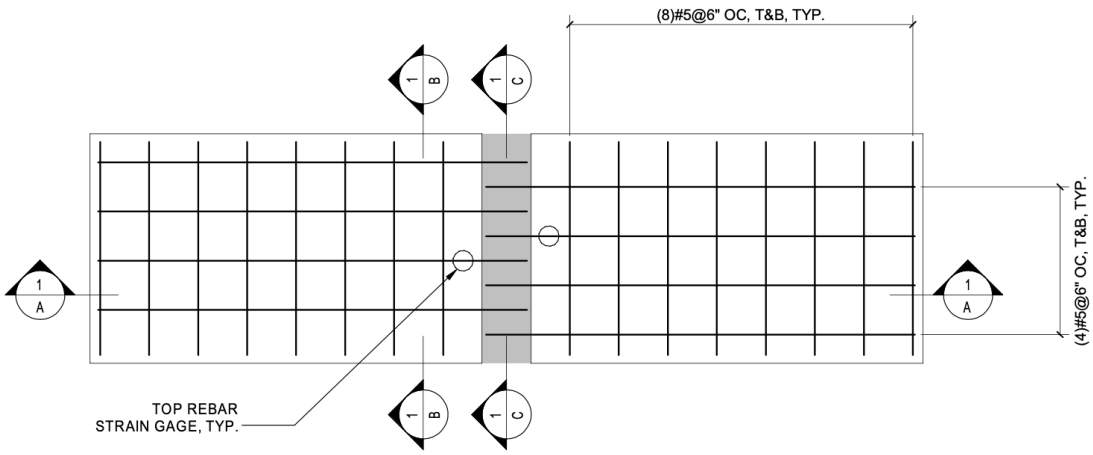

Figure 45: Plan view of a structural test specimen (2) 28 in. by 48 in. panels.

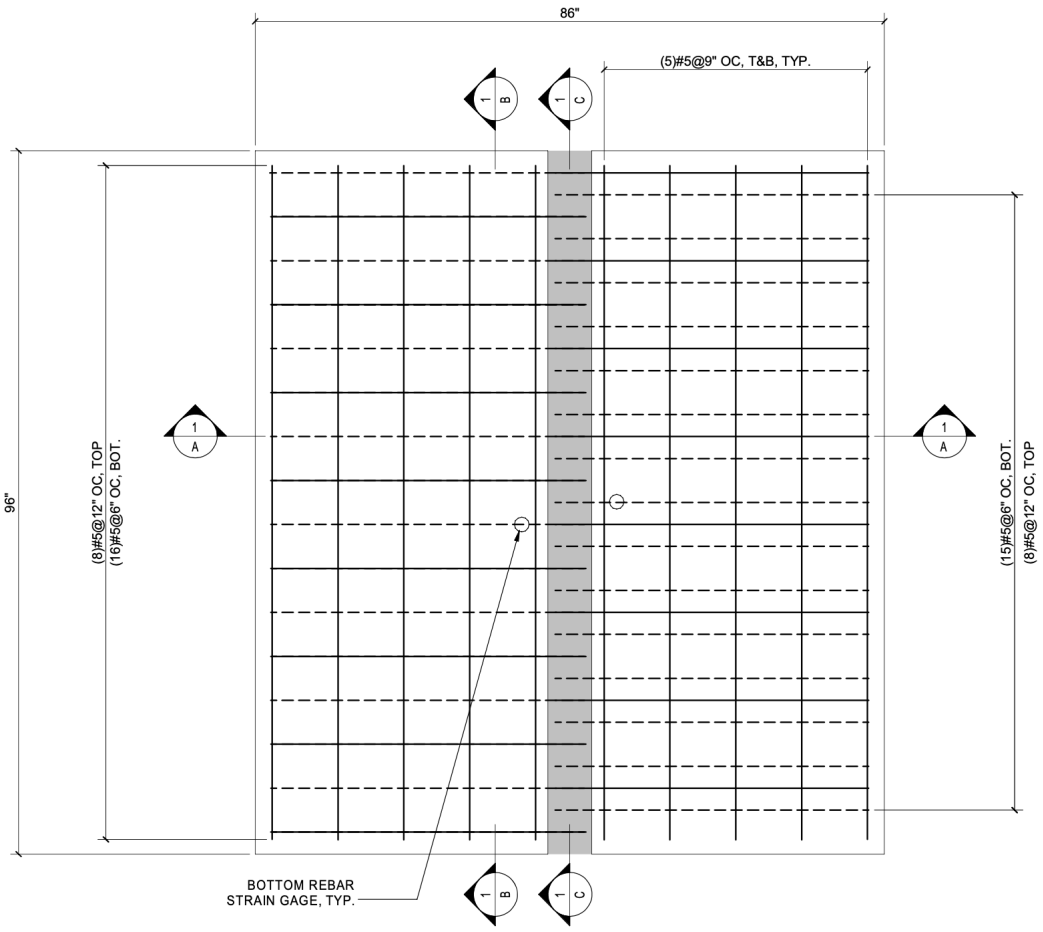

Figure 46: Plan view of a structural test specimen (2) 40 in. by 96 in. panels.

Table 18: Parameters of various precast concrete deck specimens.

Panel dimension *b* by *h* by *l* (in.)	**Embedment length (in.)**	**Non-contact lap splice (in.)**	**Key geometry**	**Quantity**
28 by 40 by 6	5	4	None	4
28 by 40 by 6	5.75	5.5	None	4
28 by 40 by 9	5	4	GDOT specified	4
40 by 96 by 9	5	4	GDOT specified	4

The panels have two types of connection geometry as shown in Figure 47 and Figure 48. In Graybeal's previous research, triangular and trapezoidal shear key geometries were used to increase the bonding area between UHPC and precast concrete as shown in Figure 49. However, such geometries involve more detailed and extensive effort in creating formworks. To address this issue, specimens that do not incorporate key geometries (Figure 47) were constructed along with those that have geometries specified by GDOT (Figure 48). The surfaces of concrete panels that are in contact with UHPC is specified to have EA surface with 1/8 in. amplitude per GDOT's recommendation in order to enhance the bond between UHPC and concrete panels.

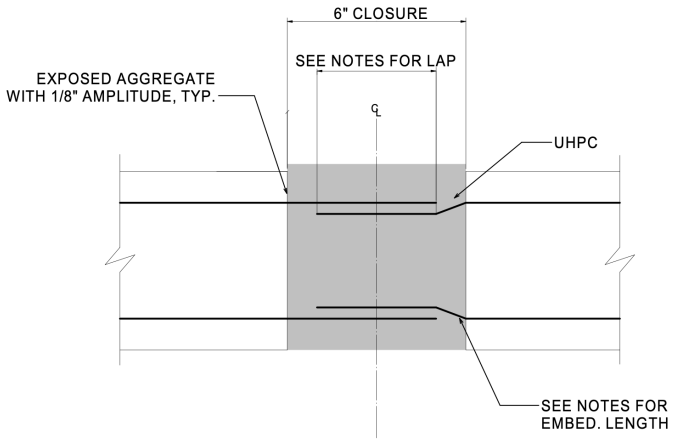

Figure 47: Joint detail without shear key.

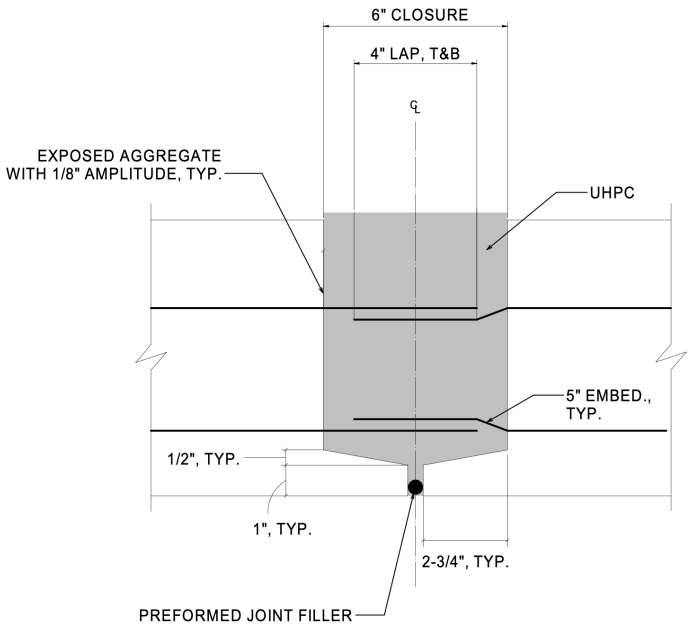

Figure 48: GDOT specified joint detail.

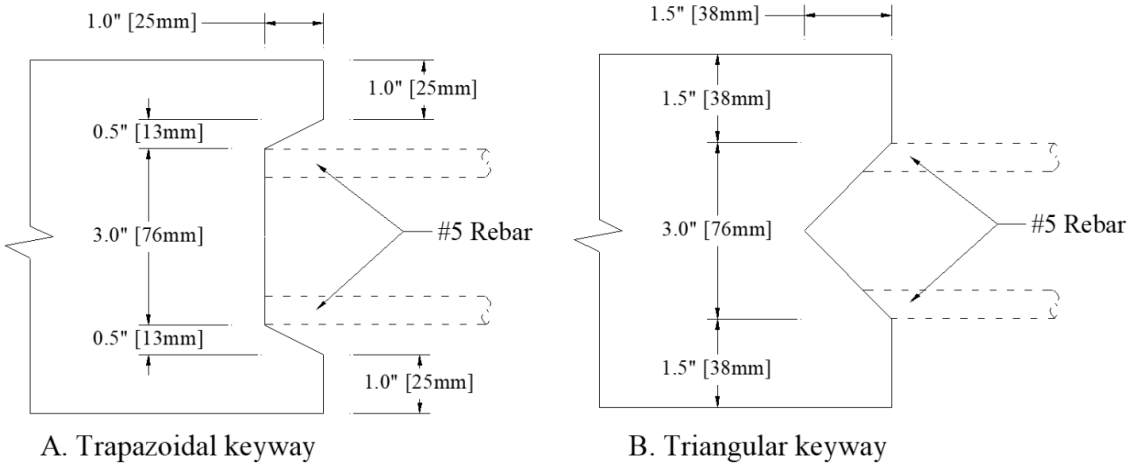

Source: FHWA

Figure 49: Trapezoidal and triangular shear key details [26].

Strength calculations were performed with the assumption that these panels are monolithically cast with continuous reinforcement. Whitney stress block analysis was used to calculate the moment capacity of the panel cross section. The specified compressive

strength of the deck panels is 6,000 psi at 28 days. Detailed calculations can be found in Appendix B. The nominal cracking, yielding, and ultimate moment strengths of 6 in. thick panels are summarized in Table 19. Only No. 5 black bars of Grade 60 are used as reinforcement in this study. Figure 50 shows the cross-sectional used to calculate the moment capacity of deck panels.

Table 19: Cracking, yielding, and nominal moment capacities of panel cross sections.

Final panel dimension *b* by *h* by *l* (in.)	**Cracking moment, M_{cr} (kip-ft)**	**Yield moment, M_y (kip-ft)**	**Nominal moment, M_n (kip-ft)**
28 by 6 by 102	8.85	26.32	27.45

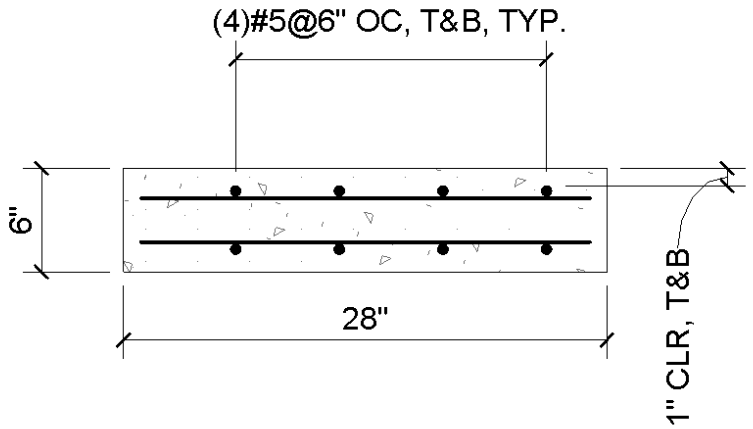

Figure 50: Cross-section of 6 in. thick deck panel specimen.

5.1.2 Construction of Deck Panel Specimens for Structural Test

All precast deck panels were constructed at Tindall Corporation's precast concrete plant in Conley, Georgia. For every deck panel, a strain gauge was installed on one of the

No. 5 bars that will be in tension during structural load testing. Figure 51 shows a No. 5 bar that has been ground to create a smooth surface for strain gauge installation. All strain gauges are from Vishay Precision Group, Inc. (VPG) and have resistance of 350 Ω (±0.3%). The bond agent used to attach these strain gauges to the bars is also from VPG. Strain gauges were wrapped with layers of electric tape and foam tape to provide protection from concrete and water during deck panel construction as shown in Figure 52. Spray on sealant was used to add another layer of protection against water seepage in Figure 53.

Figure 51: Surface preparation for strain gauge attachment.

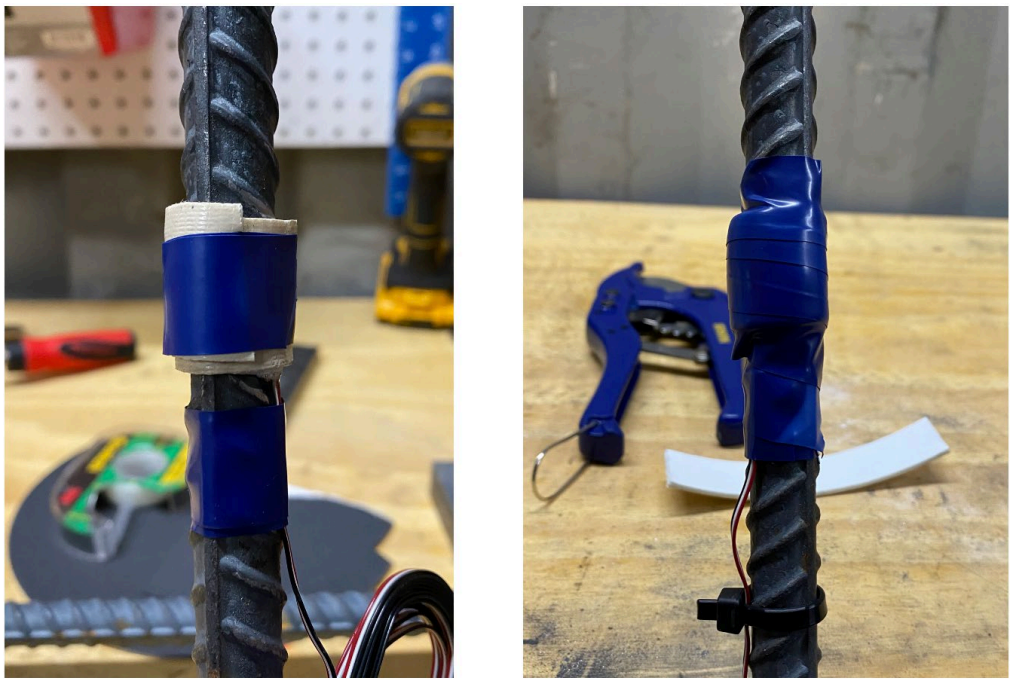

Figure 52: Foam tape and electrical tape used to protect the attached strain gauge.

Figure 53: Spray-on sealant being applied to provide protection against water.

Once strain gauge installation was complete, the bars with strain gauges were placed in their respective locations in the panel formworks. An example of a bar as part of the reinforcement cage is shown in Figure 54. Spacing between reinforcing bars and cover distances were measured to ensure panel construction adheres to the design specifications. Figure 55 shows a measurement being taken to confirm spacing of reinforcing bars. Figure 56 shows another measurement that confirms the cover distance of bottom bars for one of the larger panels. A layout of reinforcing bars for a 28 in. by 48 in. by 9 in. panel is shown in Figure 57. Hooked No. 4 bars were installed prior to casting all the panels for lifting purposes shown in Figure 58.

Figure 54: No. 5 bar with a strain gauge inside reinforcement cage.

Figure 55: Checking reinforcement spacing of 6 in.

Figure 56: Checking bottom cover of steel reinforcement in a specimen.

Figure 57: Reinforcement cage of a 28 in. by 48 in. by 9 in. specimen.

Figure 58: Hooked No. 4 bars placed inside reinforcement cage for lifting purposes.

After placing the reinforcing bars, the deck panels were cast in one batch using a ready-mix truck shown in Figure 59 and Figure 60. Once all the panels were cast, they were covered with tarp to prevent moisture loss, as shown in Figure 61. All the formwork was removed 4 days after casting. Figure 62 shows compression test cylinders that were cast to evaluate concrete strength at 7 and 28 days after casting and also on the day of the structural test. Four cylinders were tested on each of the test days. The compressive strength of concrete used in deck panels is summarized in Table 20. The compressive strength tests adhered to procedures outlined in ASTM C39.

Figure 59: Deck panel specimen being cast with ready-mix truck.

Figure 60: Deck panel specimens being cast.

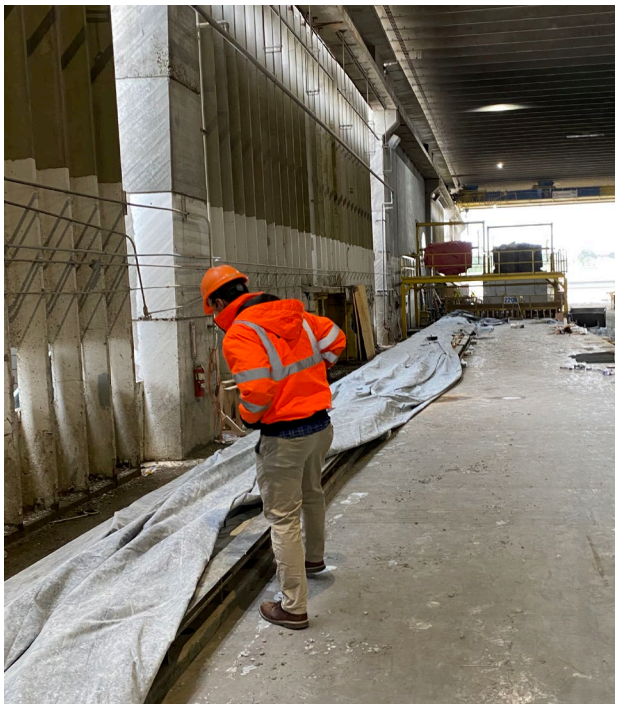

Figure 61: Tarp used to cover all specimens after casting.

Figure 62: 4 in. by 8 in. cylinders cast to evaluate concrete strength.

Table 20: Compressive strength of concrete used in deck panels at 7 and 28 days.

Days after casting	Compressive strength (psi)	COV (%)
7	5,775	11.53
28	6,800	3.12

Once all the formwork was removed, the panels were sand blasted in order to create EA surfaces on the sides where UHPC will come into contact. Sand blasting of the panels is shown in Figure 63. GDOT typically specifies 1/8 in. amplitude of the EA surface for bridge construction in Georgia. The surfaces were constantly checked to ensure correct amplitude of the EA surface shown in Figure 64. An overview of EA finish on one of the panels is shown in Figure 65.

Figure 63: Sand blasting to create EA surface on specimens.

Figure 64: Measurement of 1/8 in. of EA amplitude.

Figure 65: Sand-blasted surface.

Panels were delivered to the Structural Engineering and Mechanics Laboratory (SEML) at Georgia Institute of Technology 28 days after they were cast. During transport,

some of the panels that incorporated GDOT's key geometry suffered damages in the joint area. Figure 66 shows a damaged joint of one of the concrete deck panels during transport. The "lips" of the joint detail are known to be quite fragile, as it is a commonly occurring phenomena in GDOT's construction practices. It is also for this reason that this research is considering deck panels that do not incorporate the "lips" details. Structural test specimens constructed using these deck panels will allow for an evaluation of eliminating joint details to ease construction processes in the field.

Figure 66: Damage to GDOT specified joint detail during transport.

5.2 Structural Test Specimens

5.2.1 Construction of Joint Pours

Structural test specimens were constructed by placing identical deck panels in such a way that each of the panels' EA surfaces face each other. The joint was measured to ensure 6 in. of width in Figure 67. The protruding reinforcement were interlaced and create non-contact lap splice in the connection shown in Figure 68. Setup of a structural test specimen using deck panels that are 6 in. thick is shown in Figure 69.

Figure 67: 6 in. wide joint region between two deck panels.

Figure 68: Non-contact lap splice in the joint region.

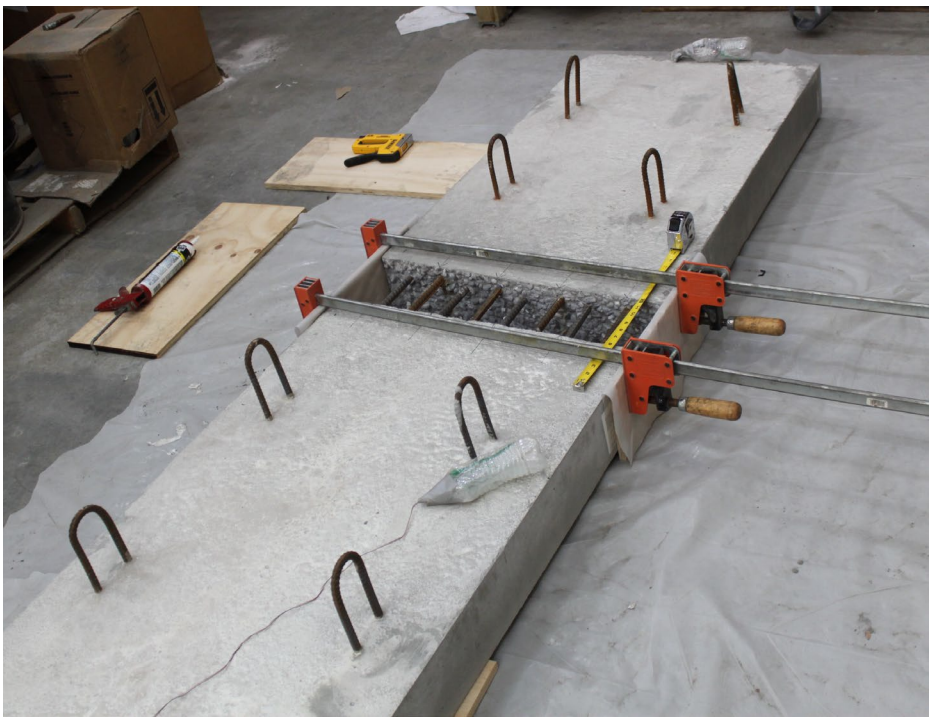

Figure 69: Setup of two deck panels ready for joint pour.

One batch of UHPC was made to construct the closure pours in one structural specimen and to cast compressive and flexural test specimens. Each batch had 1.6 ft^3 of UHPC. Figure 70 shows the construction of the UHPC joint. UHPC was poured at one end of the joint and was allowed to flow to the other end until the joint was filled. Each joint was filled with UHPC in one pour to prevent the formation of interfaces inside the UHPC. A closer look at the joint during and after UHPC pour is shown in Figure 71 and Figure 72, respectively.

Figure 70: UHPC joint pour.

Figure 71: Close-up of UHPC joint pour.

Figure 72: UHPC joint after 3 days of curing time and removal of formwork.

As discussed in Chapters 3 and 4, 100 mm cube and 3 in. by 6 in. cylinder specimens were tested to evaluate compressive strength at 3, 7, and 28 days after casting. Beam specimens were tested 28 days after casting. Cubes, cylinders, and beams were demolded 24 hours after casting. These specimens were placed in a fog room at 73˚F until testing.

5.3 Structural Test Setup and Procedures

Figure 73 shows an overview of the structural test setup. A negative bending configuration was chosen in order to easily observe cracks as well as any debonding between UHPC and precast concrete throughout the test. LVDTs were attached on both the tension and compression faces of the concrete specimen. These LVDTs were used to measure the change in displacement across the UHPC joint region. A string potentiometer was installed on the floor to measure the midspan deflection of the specimen as it is loaded. Strain gauges that were pre-installed on two reinforcing bars inside the deck panel specimen are used to measure strain in steel reinforcement. A load cell with a capacity of 100 kips was attached to a hydraulic ram that was operated by a pump with a shut off valve. The load cell bears on a steel plate via a steel sphere that is allowed to rotate in order to prevent the hydraulic ram from applying the load at an angle. A W8x48 beam was used to spread the load from the hydraulic jack to the two ends of the deck panel specimen. The panel specimen tested in this investigation incorporated steel reinforcing bars with 5 in. of embedment length and 4 in. of non-contact lap splice in the UHPC joint.

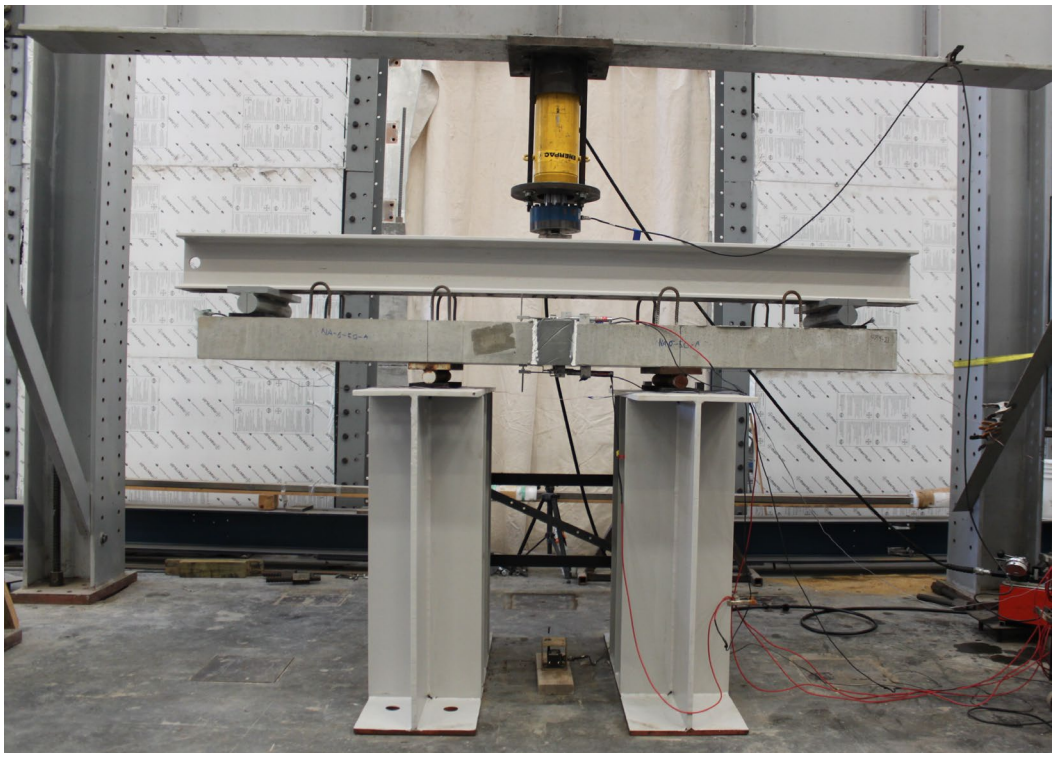

Figure 73: Deck panel specimen ready for load test.

The deck panel specimen underwent quasi-static loading at a rate of approximately 0.02 in./min. During the test, the applied load was held constant at a) M_{cr}, b) between M_{cr} and yield moment, M_y, c) at nominal moment, M_n, and beyond. This was done to identify cracks that occurred in the maximum moment region, particularly near and in the UHPC joint. The concrete deck panels had an average compressive strength of 7,445 psi with COV of 1.66% on the day of the test. Based on this strength, the load to reach M_{cr} was 7.25 kips. The loads to reach M_y and M_n, were 22 and 23 kips, respectively. One deck panel specimen out of four that were cast was tested by the time of reporting.

5.4 Visual Observations

5.4.1 Visual Assessment of Specimen at M_{cr}

Visual inspection of the deck panel specimen was conducted at M_{cr}. Few cracks were observed in the concrete deck in the maximum moment region. There were no cracks that formed inside the UHPC connection region. Figure 74 shows cracks that were traced at M_{cr}. It is important to note that no visible cracks were observed in the UHPC, as expected.

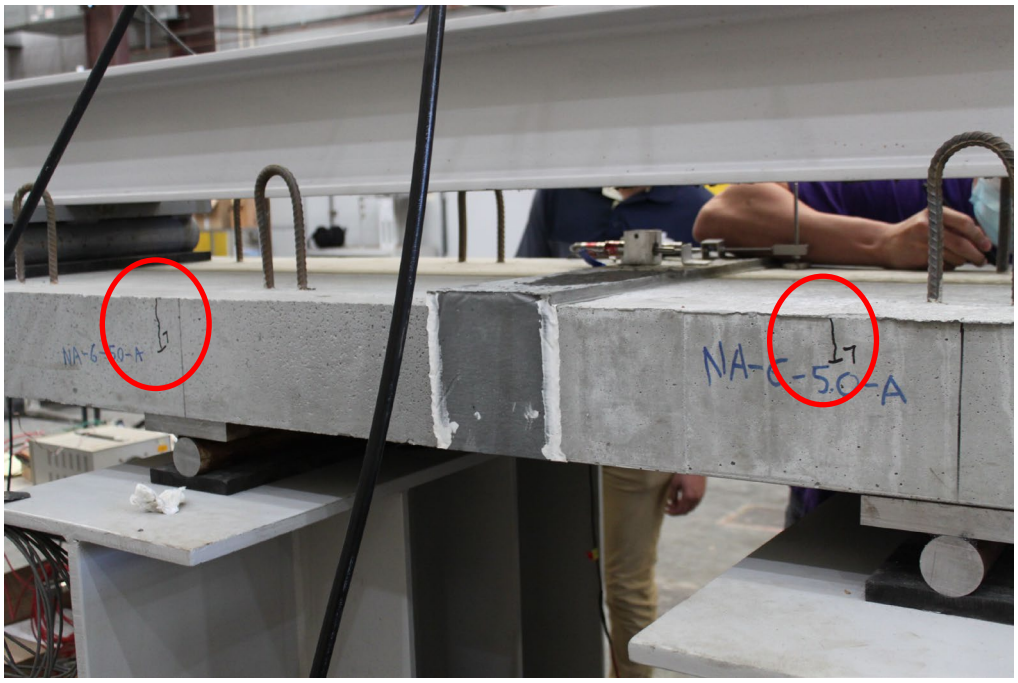

Figure 74: Cracks observed at M_{cr} circled in red.

5.4.2 Visual Assessment between M_{cr} and M_y

The load was held constant at $0.7M_y$ to inspect for any cracks in the deck panel specimen. More cracks propagated in the maximum moment region as shown in Figure 75. Cracks also occurred at the interface between the UHPC connection and concrete deck as

shown in Figure 76 and Figure 77. No cracks were visible on the surfaces of UHPC joint. The larger cracks in the concrete deck within the maximum moment region indicate engagement of steel reinforcement as the specimen is being loaded.

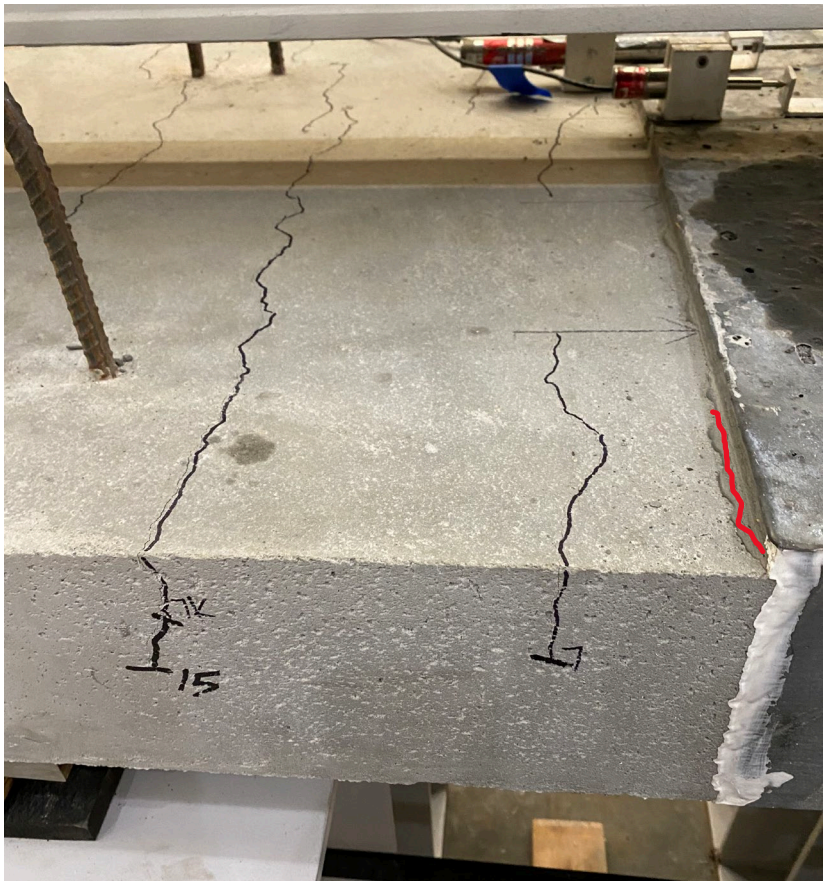

Figure 75: Cracks in the maximum moment region at $0.7M_y$.

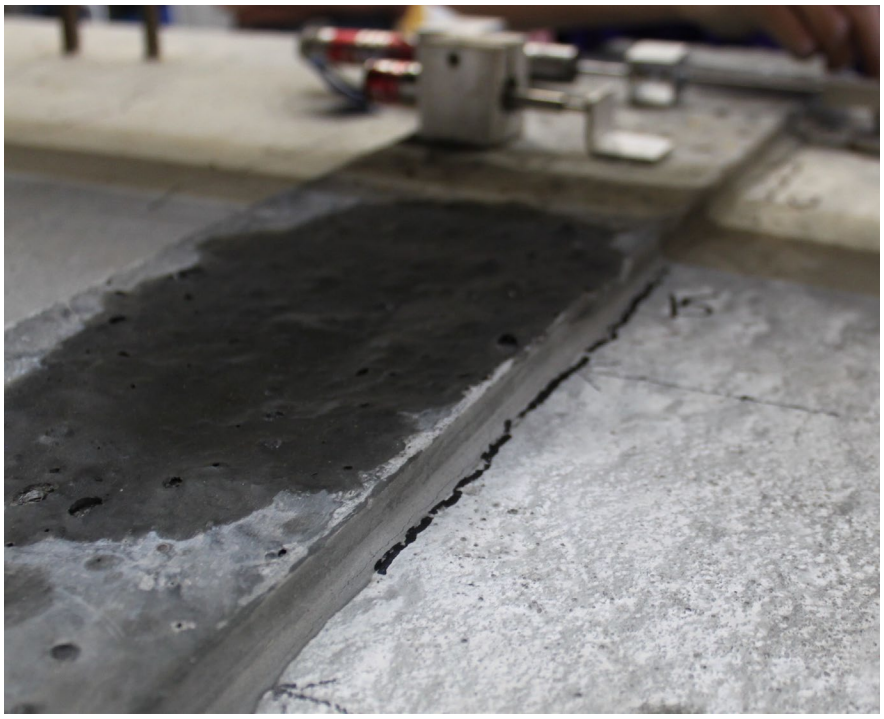

Figure 76: Cracks at the interface between the UHPC joint and concrete deck panel.

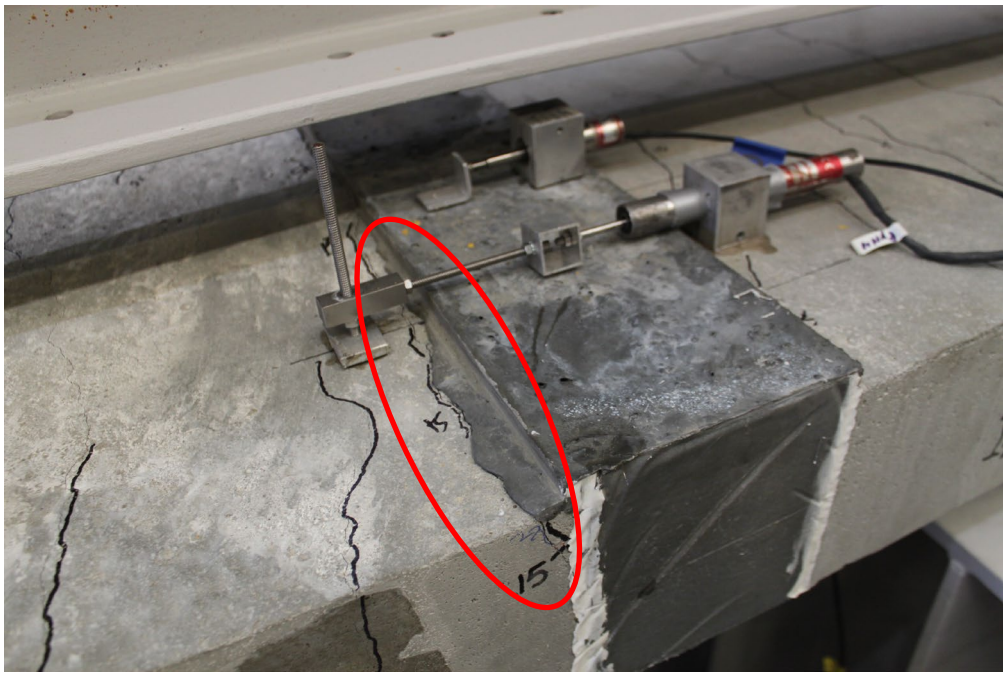

Figure 77: Cracks at the interface shown inside the red ellipse.

5.4.3 Visual Assessment at M_y

The applied load was held constant at M_y to inspect crack propagation in the specimen, especially in the UHPC connection. The previously observed interface crack had propagated as shown in Figure 78. This crack had a width of 0.007 in. The cracks in the concrete deck within the maximum moment region had a typical width of 0.020 in. These cracks have also propagated throughout the tension surface of the specimen as shown in Figure 79. No cracks were observed inside the connection region.

Figure 78: Propagation of interface crack at M_y.

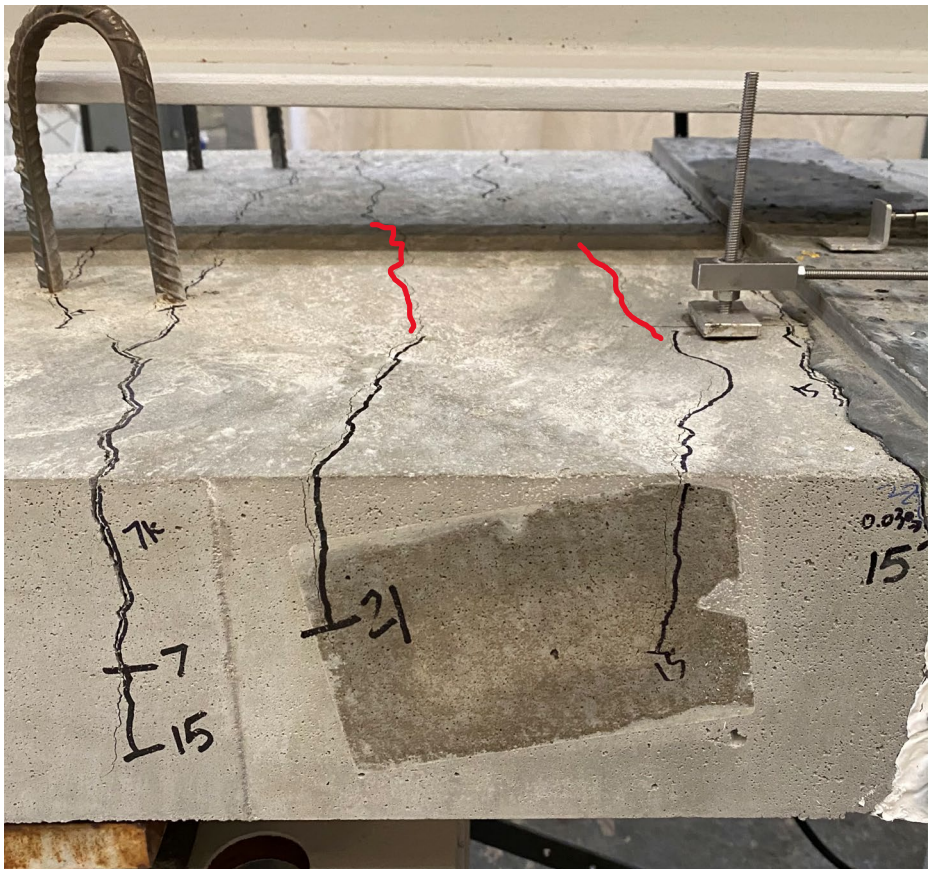

Figure 79: Crack propagation in the maximum moment region at M_y.

5.4.4 Visual Assessment at M_n

At the nominal flexural strength of the deck panel specimen, interface cracks had an increase in width from 0.007 in. to 0.03 in. The increase in crack width is shown in Figure 80. Thin cracks were also seen on the top face of the UHPC joint as shown in Figure 81.

Figure 80: Wider crack observed at the interface at M_u.

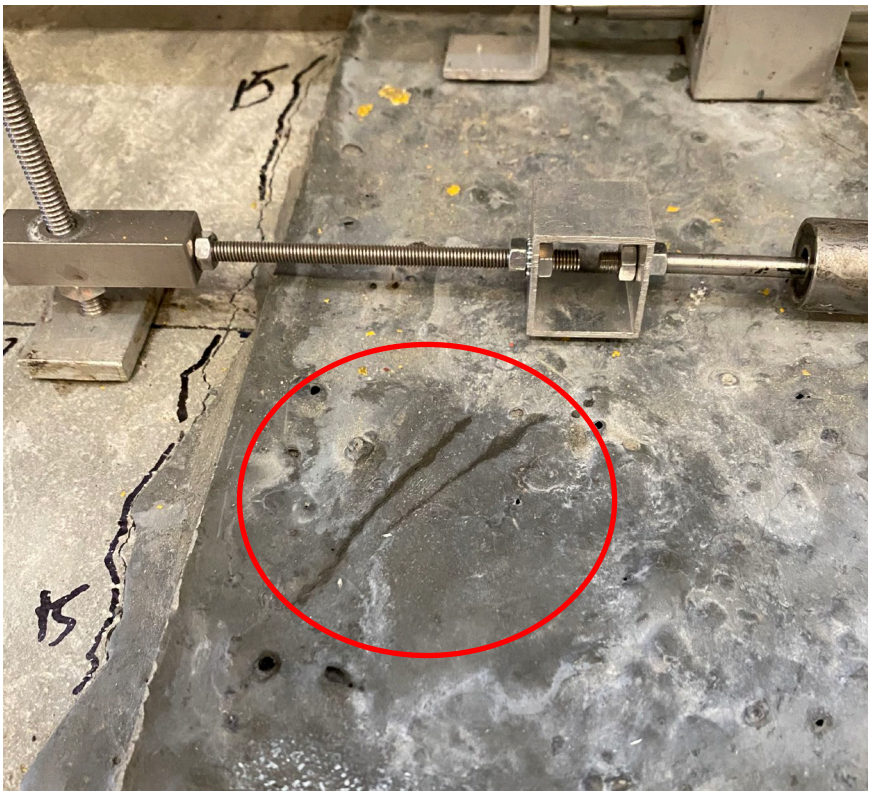

Figure 81: Cracks on the top face of UHPC joint at circled in red.

5.4.5 Visual Assessment beyond M_n

At $1.3M_n$, the load was held constant to observe any cracks within the UHPC joint. A number of cracks appeared on the surfaces of the UHPC. Figure 82 and Figure 83 show the surface cracks in UHPC at $1.3M_n$. UHPC surface cracks had typical widths of 0.01 in. The interface cracks widened from 0.03 in. to 0.07 in.

The string potentiometer malfunctioned during the test. Therefore, only data up until the malfunction (at approximately $0.66M_y$) is reported in Figure 85. In order to measure the approximate midspan deflection after the malfunction, an orange string was pulled taut along the length of the specimen. The vertical distance between the string and

the midspan was measured to be 2-7/16 in at the end of the test. Figure 84 shows how the deflection was measured.

Figure 82: Top surface crack in UHPC at $1.3M_n$.

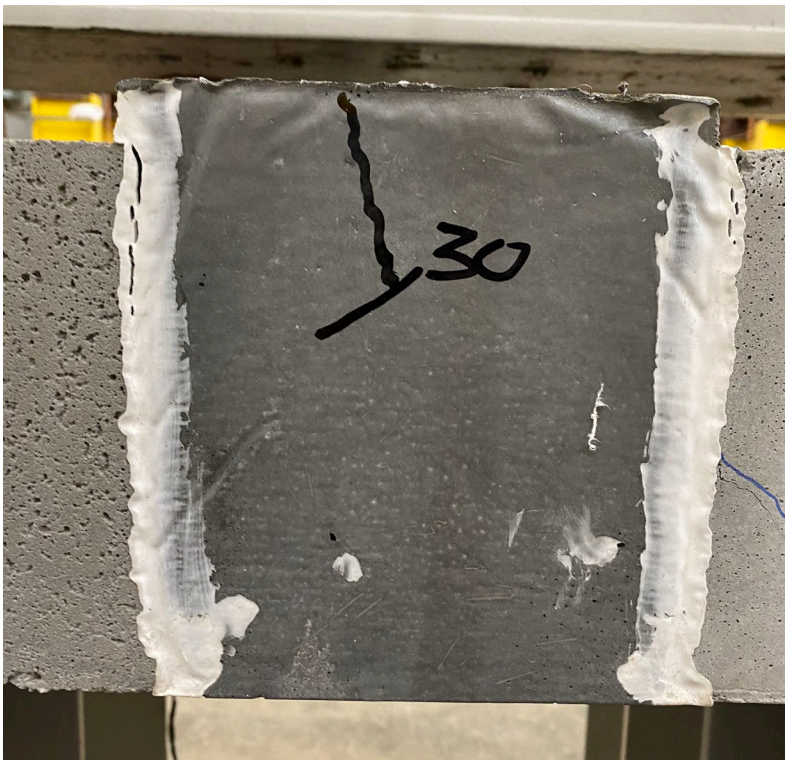

Figure 83: Side surface crack in UHPC at $1.3M_n$.

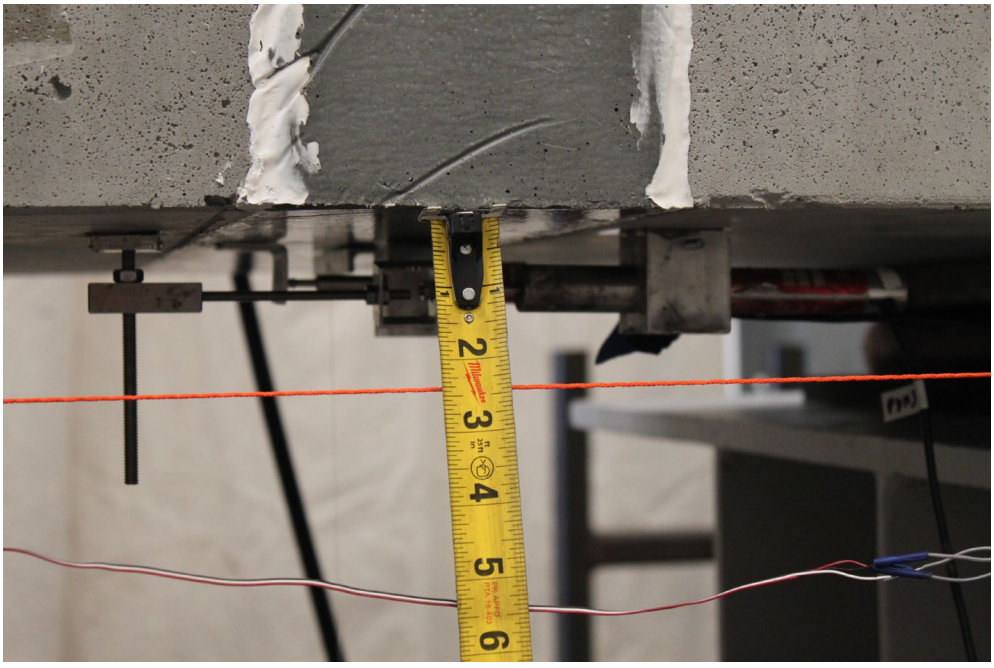

Figure 84: Approximate measurement of the midspan deflection at $1.3M_n$.

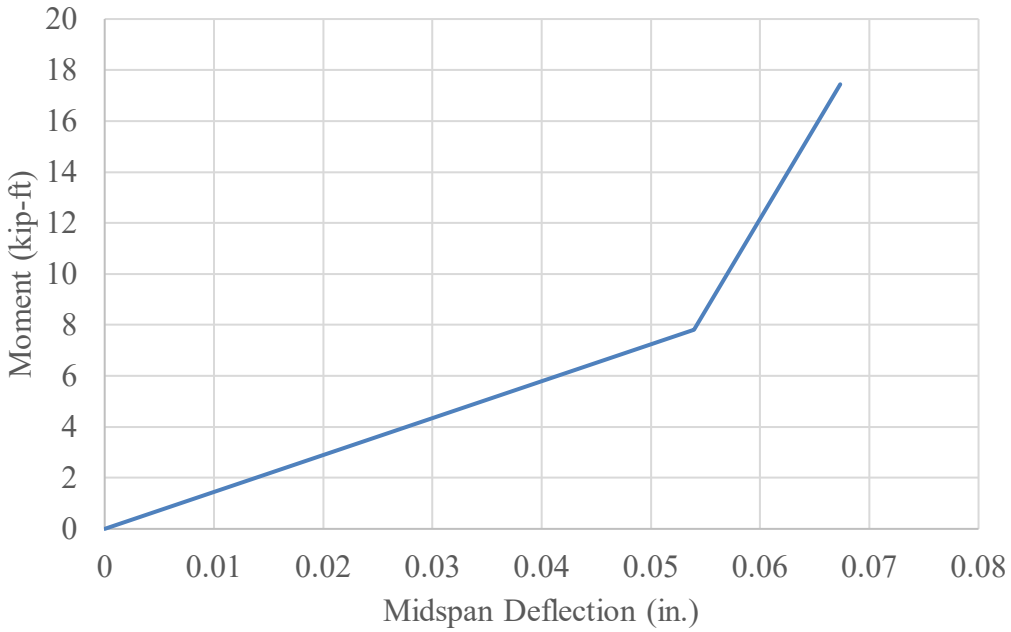

Figure 85: Applied moment versus midspan deflection before string potentiometer malfunctioned.

5.5 Moment-curvature and Strain Results

Data from LVDT readings were used to analyze moment-curvature relationships in the UHPC region and in the concrete deck. LVDTs on the tension side of the UHPC joint region showed erratic results. This made it difficult to formulate an accurate moment-curvature relationship within the UHPC joint. Theoretical measurements of the neutral axes at M_{cr}, M_y, and M_n are used to approximate the curvature within the UHPC connection. Figure 86 and Figure 87 show the approximate moment-curvature relationships in the UHPC connection and concrete deck panel, respectively. The data suggest higher curvature in the concrete deck than in the UHPC beyond M_{cr}.

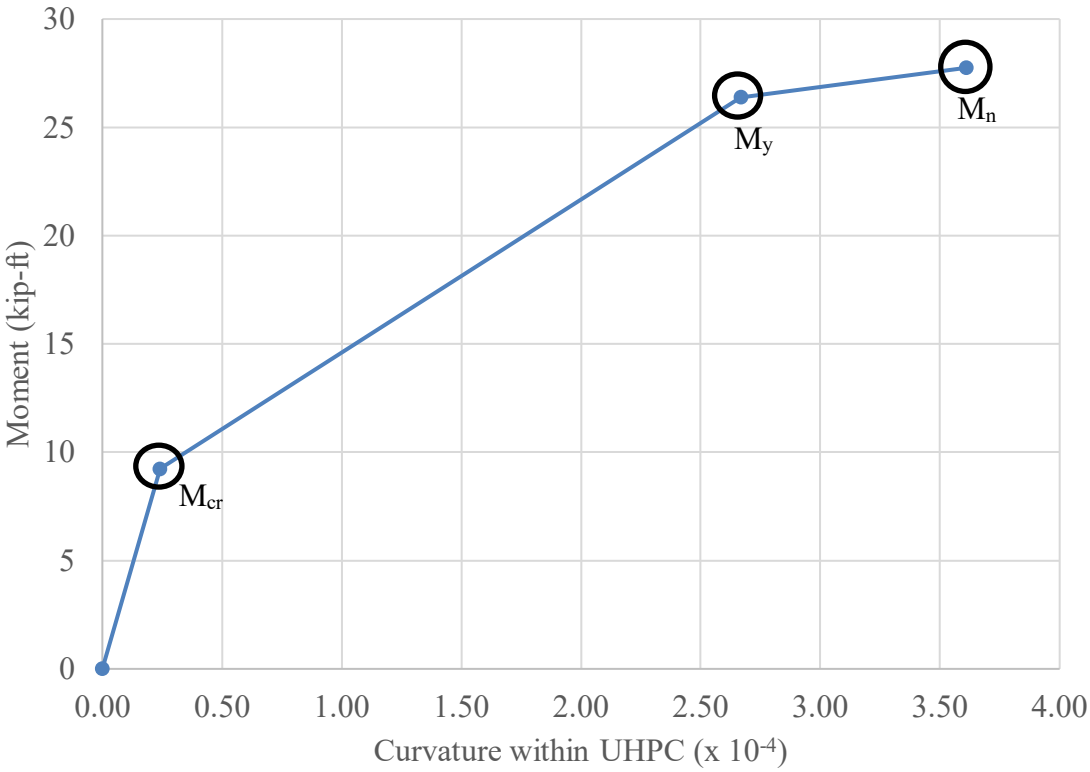

Figure 86: Approximate moment-curvature relationship within the UHPC connection.

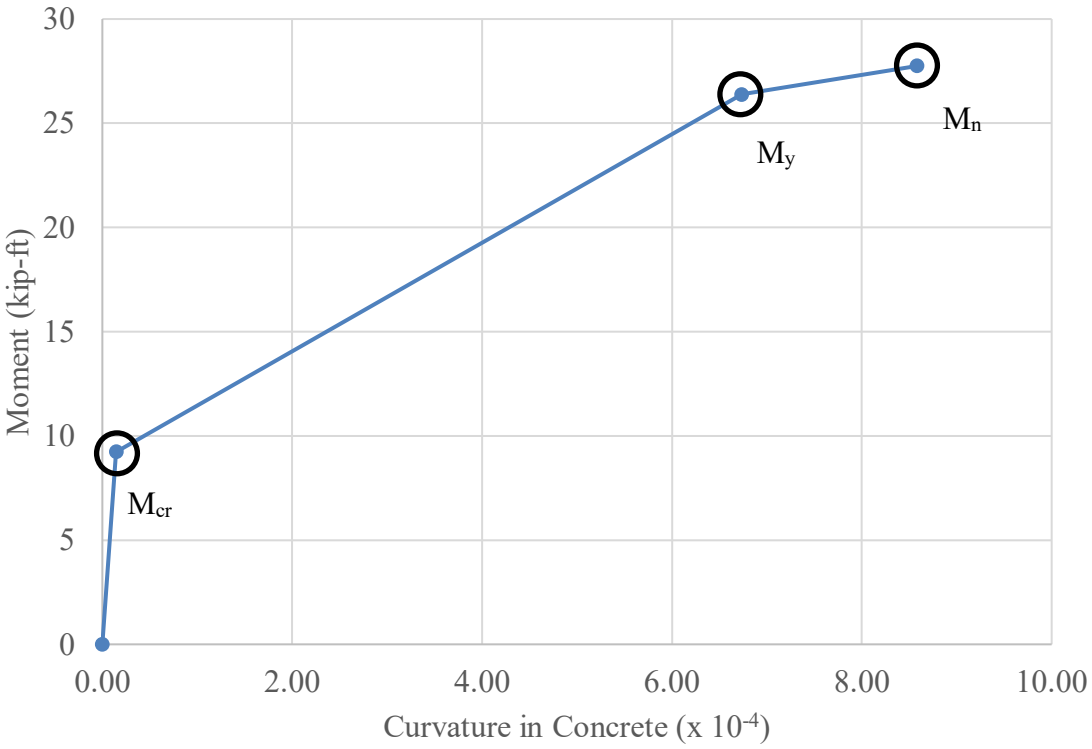

Figure 87: Approximate moment-curvature relationship in concrete deck panel.

The relationship between applied moment and strain of Grade 60 steel reinforcing bars in tension is shown in Figure 88. A theoretical yield strain of 0.002 is observed at $0.8M_y$. However, the moment versus strain graph of the steel reinforcement shows that the bars remain linear elastic until approximately M_y. This suggests that the bars may have a yield strength in the range of 70 to 75 ksi.

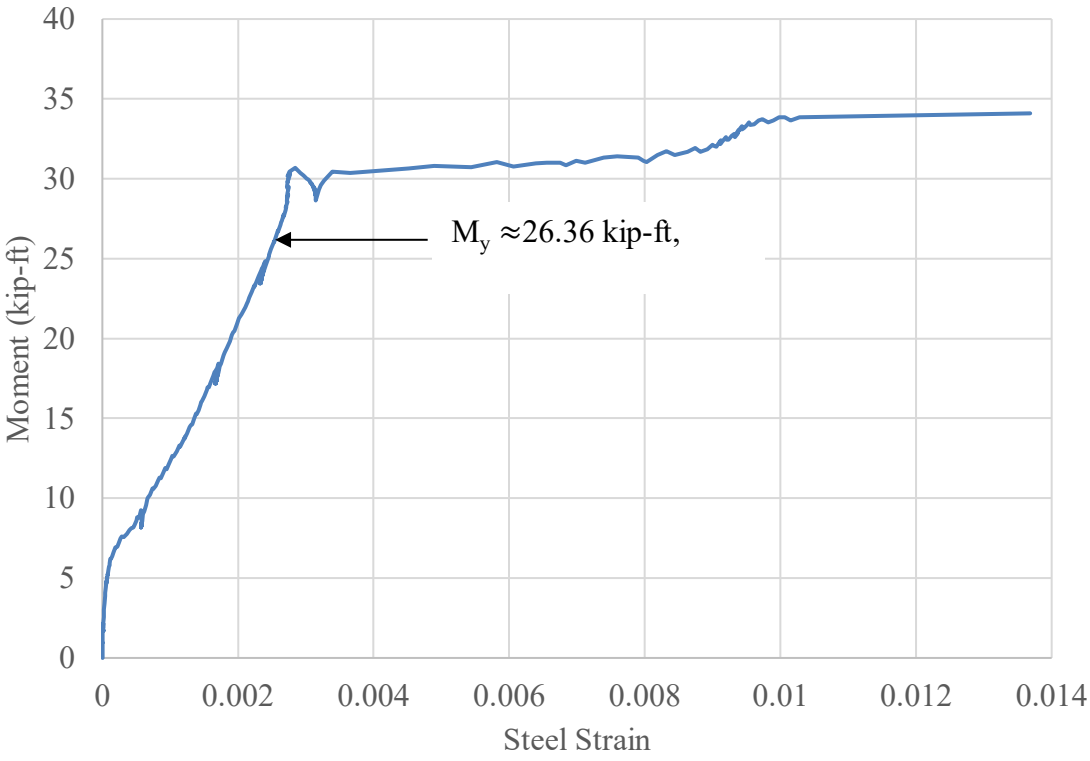

Figure 88: Moment-strain relationship of steel reinforcing bars in tension.

5.6 Remarks

The UHPC connection showed no cracks until M_y of the specimen was reached. As the specimen was loaded beyond M_y, thin cracks were observed on the surface of the connection region. Cracks at the interface between UHPC and concrete occurred at lower loads than M_y, but debonding of the two materials was not observed. The steel reinforcing bars have also undergone yielding prior to any observable failure in the connection. These observations indicate a satisfactory behavior of the deck panel specimen that employ the non-proprietary UHPC connection detail. Another important detail to note is the lack of a shear key geometry in the connection. The deck panels only incorporated EA surface with

1/8 in. amplitude. Additional tests will need to be performed to determine whether a shear key geometry can be eliminated entirely to ease fabrication of structural elements.

CHAPTER 6. CONCLUSION AND RECOMMENDATIONS FOR FUTURE RESEARCH

6.1 Conclusions

6.1.1 Development and Material Testing of Non-proprietary UHPC Mix Design

One of the primary objectives of this research was to develop a UHPC mix design that uses locally available materials in the state of Georgia while meeting the required strength parameters. The non-proprietary UHPC mix design, 1F31K8, was developed for this purpose. The mix design consists of Type I cement, Class F fly ash, metakaolin, masonry sand, HRWR, and steel fibers that are easily accessible within the state of Georgia. This mix has not only displayed good workability, but also met the required compressive strength of at least 18,000 psi at 28 days and tensile strength of 750 psi.

Mixing procedures and material testing protocols outlined in this work have demonstrated consistently satisfactory results. Dry blending of materials and a delayed addition of water helps improve the workability of UHPC without compromising its strength. Employing relevant standards from ASTM and BS to test for material properties helps increase the variety of available tests. Specifically, this research included the use of cubic compression specimen and small beam four-point bending experiments to determine the tensile strength. It was found that modifications to the load rate can be made in order to speed up the process of testing UHPC specimens, without affecting the results.

6.1.2 Structural Testing of 1F31K8 as a Closure Pour Material

In order to evaluate the performance of 1F31K8 as closure pour between concrete deck panels. a four-point negative bending test configuration was developed. Design and construction of these deck panel specimens have been outlined in this work. The test setup involves placing a deck panel specimen onto support pedestals using fabricated rollers. Two load plates were placed at the ends of the specimen supported a spreader beam. This spreader beam transferred the load from the hydraulic ram mounted to a load frame down to the specimen.

One proof-of-concept experiment was performed in this research. The setup of the four-point bending configuration overall performed as expected. Having the tension side face up makes identifying and inspecting cracks very easy. A few instrumentations such as the string potentiometer and LVDT on the tension side of UHPC did not provide adequate results.

Based on the overall behavior of the deck panel specimen, the non-proprietary UHPC developed works well as a closure pour. No damage was evident in the UHPC connection until at least the specimen was loaded to M_y. Additionally, the yielding of steel reinforcing bars prior to failure in the UHPC connection suggests that 5 in. of embedment length may be sufficient for a No. 5 bar to fully develop its strength.

6.2 Recommendations for Future Research

Future research can be conducted to potentially better evaluate the behavior of 1F31K8. A direct tension test of UHPC specimens could give more insight regarding

tensile properties. Chloride ion penetration, which causes corrosion in reinforcing bars in concrete, will need to be evaluated to ensure durability of structures that will potentially be built with 1F31K8 in the future. The relationship between steam treatment and other methods of curing and the mechanical properties of 1F31K8 can also be investigated.

Materials from suppliers other than the ones listed in this work should also be used to mix and test the performance of 1F31K8. Longer fibers or steel fibers with hooked ends can also be used to examine how properties of UHPC change. Adjustments may need to be made in the mix design depending on the properties of materials being used. This can potentially allow GDOT to have a variety of non-proprietary UHPC mix to choose from to best suit their project needs.

Work should also be done to ensure constructability of 1F31K8 in conditions similar to the field. A high shear mixer was used to make all UHPC in this research. However, a high shear mixer may not always be available at a construction site. A different type of mixer, such as a pan mixer, should be used to ensure that UHPC can be made with equipment that are more readily available in the field

Improvements to the structural test can be made by modifying the test configuration. The support and load plates were seated on rubber bearing pads in this research. To ensure even distribution of load in the specimen, the support and load plates should be seated on steel plates, which are then placed on rubber bearing pads. In order to reduce any tension stiffening effects in the specimen, the support and load plates should be designed so that they are not only free to rotate, but also move horizontally. Careful planning and arranging instrumentation is necessary to avoid any possible malfunctions

while testing. The wires of all instrumentation have to be rearranged to ensure that there is enough slack.

To better evaluate the structural service life performance of UHPC, cyclic loading tests should be performed to evaluate the fatigue strength. Pull-out tests of reinforcing bars should also be conducted in order to accurately determine the development length of various bars.

APPENDIX A. MATERIALS AND EXPERIMENTAL DATA

A.1 Sieve Analysis Data of Masonry Sand

Table 21: Masonry sand sieve analysis data.

Sieve #	Aggregate Retained (g)	Aggregate Retained (%)	% Retained (cumulative)	Aggregate Passing (g)	Aggregate Passing (%)
4	0	0.00	0.00	326.29	100
8	0.07	0.02	0.02	326.22	99.98
16	3.43	1.05	1.07	322.79	98.93
30	33.49	10.26	11.34	289.3	88.66
50	141.65	43.41	54.75	147.65	45.25
100	122.51	37.55	92.30	25.14	7.70
200	24.02	7.36	99.66	1.12	0.34
Tray	1.12	0.34	100.00	0	0

A.2 Compressive Strength Test Data of 1F31K8

Table 22: Compressive strength test data for Batches 2 to 4.

Mix Name	**Batch 2**	**Batch 3**	**Batch 4**
Mix Date	7/20/20	8/10/20	8/17/20
3 Day Test Date	**7/23/20**	**8/13/20**	**8/20/20**
Results (ksi)	15.65 14.50 15.16	13.57 14.32 13.98	14.19 13.82 15.63
Mean (ksi)	15.10	13.95	14.55
Standard Deviation (ksi)	0.57	0.38	0.96
COV (%)	3.80	2.70	6.58

7 Day Test Date	**7/27/20**	**8/17/20**	**8/24/20**
Results (ksi)	15.71 17.16 16.63	14.76 16.80 16.08	15.91 16.94 17.22
Mean (ksi)	16.50	15.88	16.69
Standard Deviation (ksi)	0.73	1.03	0.69
COV (%)	4.44	6.50	4.12

28 Day Test Date	**8/17/20**	**9/7/20**	**9/14/20**
Results (ksi)	16.08 18.18 17.99	18.23 17.11 19.07	18.61 17.27 16.57
Mean (ksi)	17.42	18.14	17.48
Standard Deviation (ksi)	1.16	0.98	1.03
COV (%)	6.66	5.43	5.92

Table 23: Compressive strength test data for Batches 5, 6, and 8.

Mix Name	**Batch 5**	**Batch 6**	**Batch 8**
Mix Date	11/16/20	11/23/20	12/15/20
3 Day Test Date	**11/19/20**	**11/26/20**	**12/18/20**
Results (ksi)	14.58 12.36 14.87	13.67 14.11 14.61	13.83 13.69 13.32
Mean (ksi)	13.94	14.13	13.61
Standard Deviation (ksi)	1.38	0.47	0.26
COV (%)	9.88	3.31	1.91

7 Day Test Date	**11/23/20**	**11/30/20**	**12/22/20**
Results (ksi)	16.02 16.90 16.10	16.11 15.95 15.84	14.57 15.57 15.96
Mean (ksi)	16.34	15.97	15.37
Standard Deviation (ksi)	0.49	0.14	0.72
COV (%)	2.99	0.88	4.68

28 Day Test Date	**12/14/20**	**12/21/20**	**1/12/21**
Results (ksi)	18.64 19.27 18.56	19.71 19.29 18.87	16.93 17.66 17.35
Mean (ksi)	18.82	19.29	17.31
Standard Deviation (ksi)	0.39	0.42	0.37
COV (%)	2.08	2.19	2.13

Table 24: Compressive strength test data for Batches 9 to 11.

Mix Name	**Batch 9**	**Batch 10**	**Batch 11**
Mix Date	2/8/21	2/15/21	2/22/21
3 Day Test Date	**2/11/21**	**2/18/21**	**2/25/21**
Results (ksi)	14.19 14.10 13.75	14.51 15.01 13.81	15.33 15.43 15.37
Mean (ksi)	14.01	14.44	15.38
Standard Deviation (ksi)	0.23	0.60	0.05
COV (%)	1.65	4.17	0.35

7 Day Test Date	**2/15/21**	**2/22/21**	**3/1/21**
Results (ksi)	16.50 15.22 16.26	15.70 16.27 15.50	16.73 16.30 17.14
Mean (ksi)	16.00	15.82	16.73
Standard Deviation (ksi)	0.68	0.40	0.42
COV (%)	4.25	2.53	2.51

28 Day Test Date	**3/8/21**	**3/15/21**	**3/22/21**
Results (ksi)	19.71 19.09 19.39	18.94 19.40 19.00	19.85 20.45 19.59
Mean (ksi)	19.40	19.12	19.97
Standard Deviation (ksi)	0.31	0.25	0.44
COV (%)	1.58	1.29	2.19

A.3 Compressive Strength Test Data of 1F24Sf25

Table 25: Compressive strength test data for Batches 1 and 7.

Mix Name	**Batch 1**	**Batch 7**
Mix Date	7/13/20	12/11/20
3 Day Test Date	**7/16/20**	**12/14/20**
Results (ksi)	13.02 12.84 13.05	12.85 12.88 12.51
Mean (ksi)	12.97	12.75
Standard Deviation (ksi)	0.12	0.21
COV (%)	0.90	1.62

7 Day Test Date	**7/20/20**	**12/18/20**
Results (ksi)	12.62 14.59 13.89	14.92 14.23 14.35
Mean (ksi)	13.70	14.50
Standard Deviation (ksi)	1.00	0.37
COV (%)	7.32	2.55

28 Day Test Date	**8/10/20**	**1/8/21**
Results (ksi)	16.84 16.24 18.47	15.95 16.05 16.87
Mean (ksi)	17.18	16.29
Standard Deviation (ksi)	1.16	0.50
COV (%)	6.73	3.09

A.4 Flexural Performance Results of 1F31K8

Graphs of load versus midspan deflection of 2 in. by 2 in. and 3 in. by 3 in. beams are shown in Figure 89 through Figure 97. Modulus of rupture at first crack and post crack are summarized in Table 26 through Table 34.

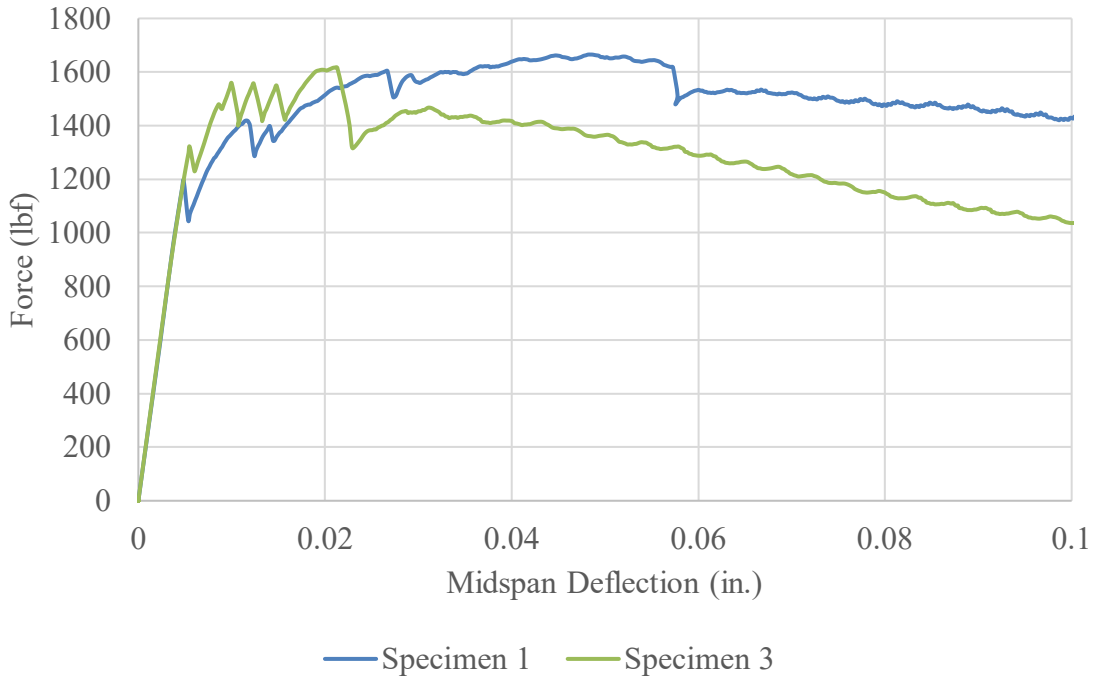

Figure 89: Applied load versus midspan deflection of 2 in. by 2 in. beams (Batch 7)

Table 26: Summary of f_r at first and post peak load (Batch 7) of 2 in. by 2 in. beams.

Specimen No.	f_r @ first peak load (psi)	f_r @ post peak load (psi)
1	1965	2725
2	--*	--*
3	2210	2685
COV (%)	8.31	1.05

*: major crack occurred outside of middle third, data discarded.

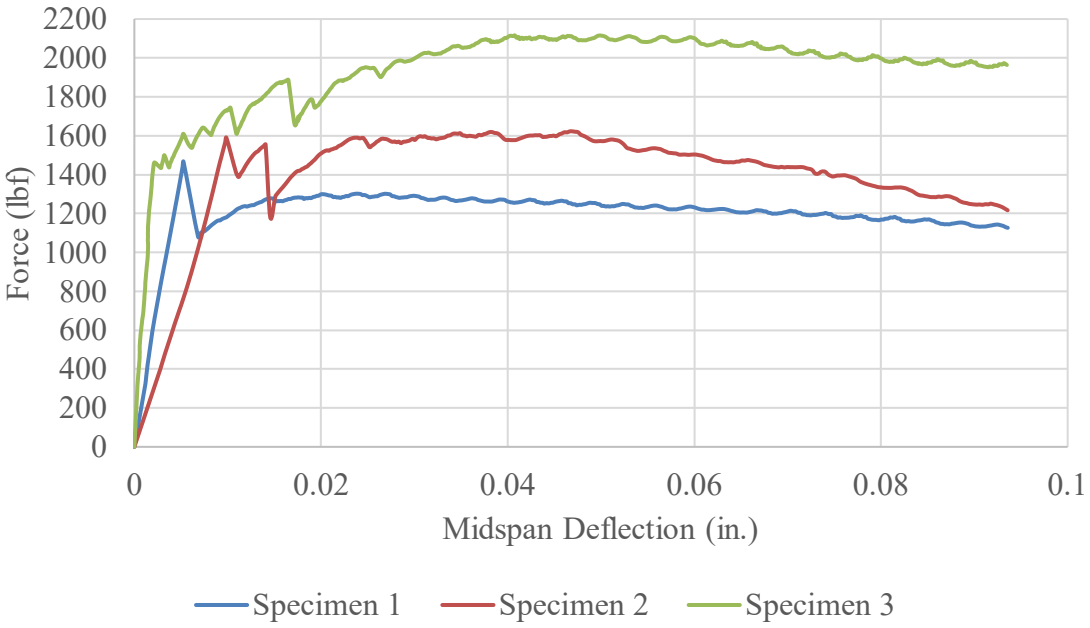

Figure 90: Applied load versus midspan deflection of 2 in. by 2 in. beams (Batch 8)

Table 27: Summary of f_r at first and post peak load (Batch 8) of 2 in. by 2 in. beams.

Specimen No.	f_r @ first peak load (psi)	f_r @ post peak load (psi)
1	2460	2460
2	2680	2735
3	2385	3450
COV (%)	6.12	17.74

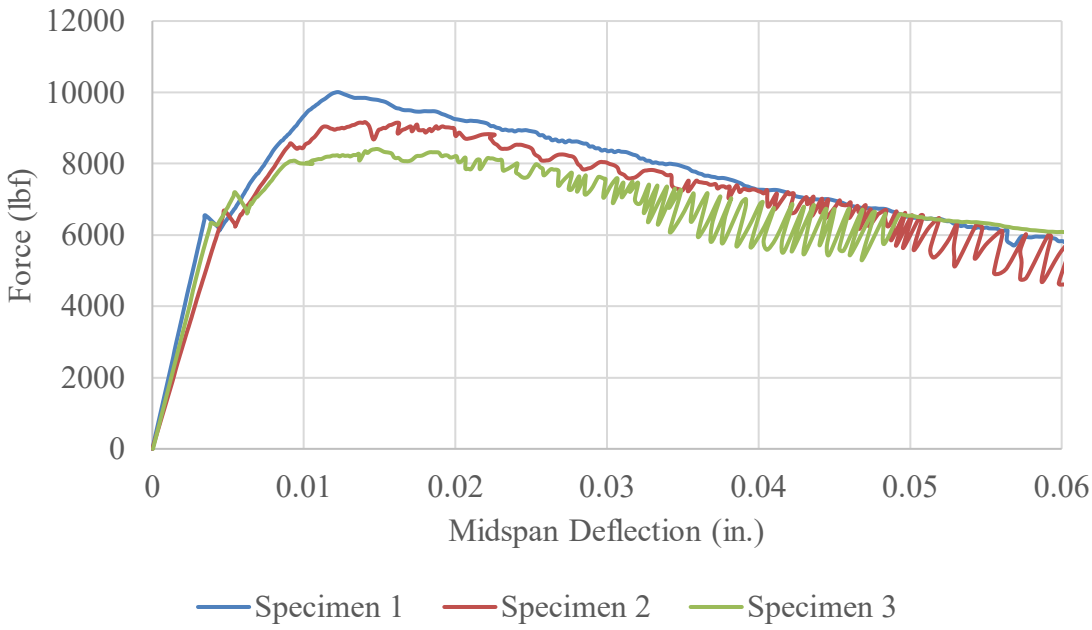

Figure 91: Applied load versus midspan deflection of 3 in. by 3 in. beams (Batch 8)

Table 28: Summary of f_r at first and post peak load (Batch 8) of 3 in. by 3 in. beams.

Specimen No.	f_r @ first peak load (psi)	f_r @ post peak load (psi)
1	2210	3380
2	2175	2985
3	2135	2835
COV (%)	1.73	9.19

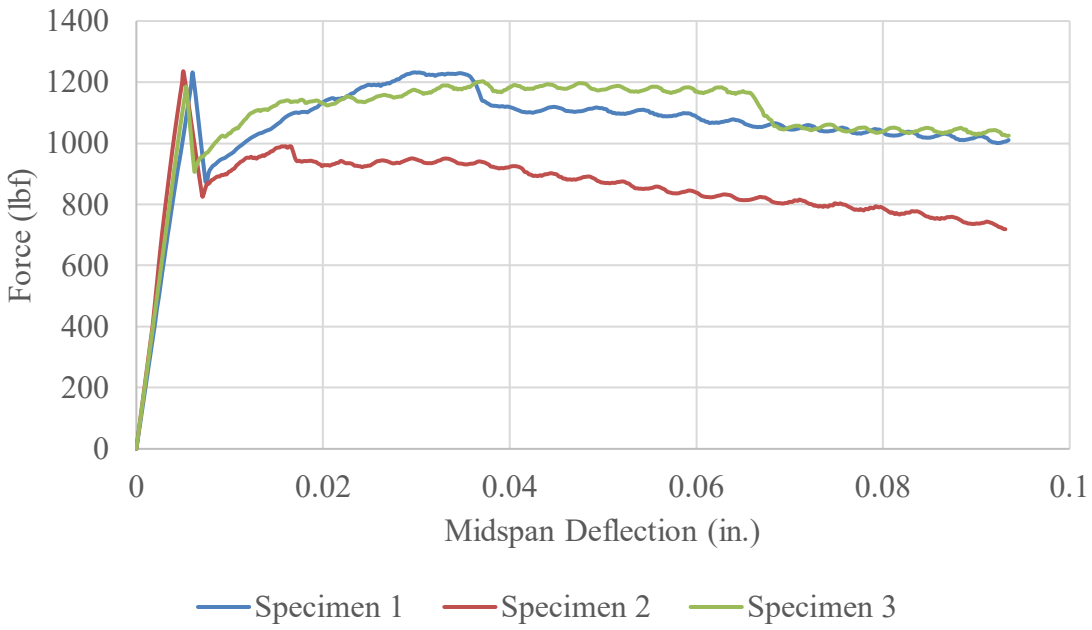

Figure 92: Applied load versus midspan deflection of 2 in. by 2 in. beams (Batch 9)

Table 29: Summary of f_r at first and post peak load (Batch 9) of 2 in. by 2 in. beams.

Specimen No.	f_r @ first peak load (psi)	f_r @ post peak load (psi)
1	2085	2090
2	2085	2085
3	1995	2025
COV (%)	2.53	1.75

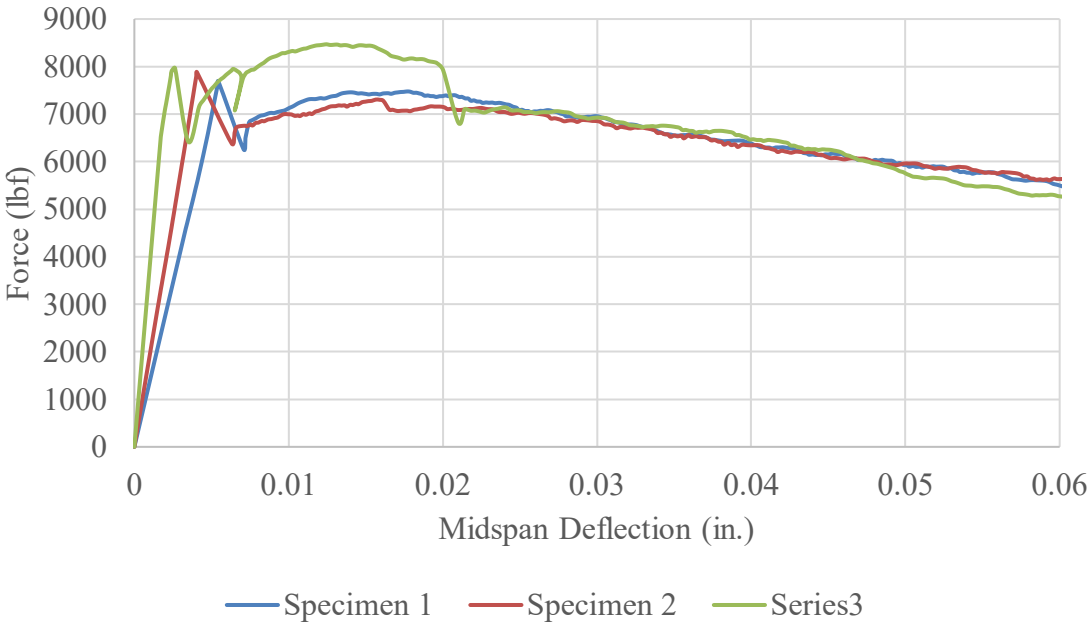

Figure 93: Applied load versus midspan deflection of 3 in. by 3 in. beams (Batch 9)

Table 30: Summary of f_r at first and post peak load (Batch 9) of 3 in. by 3 in. beams.

Specimen No.	f_r @ first peak load (psi)	f_r @ post peak load (psi)
1	2605	2605
2	2620	2620
3	2595	2760
COV (%)	0.48	3.21

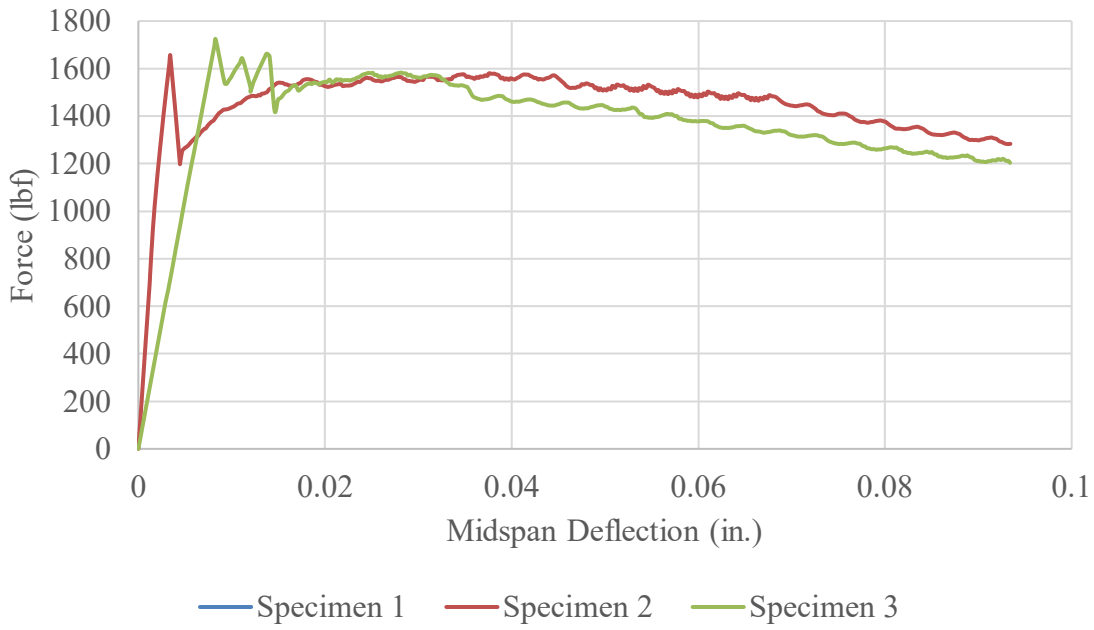

Figure 94: Applied load versus midspan deflection of 2 in. by 2 in. beams (closure pour 1)

Table 31: Summary of f_r at first and post peak load (closure pour 1) of 2 in. by 2 in. beams.

Specimen No.	f_r @ first peak load (psi)	f_r @ post peak load (psi)
1	--	--
2	2695	2695
3	2855	2855
COV (%)	4.08	4.08

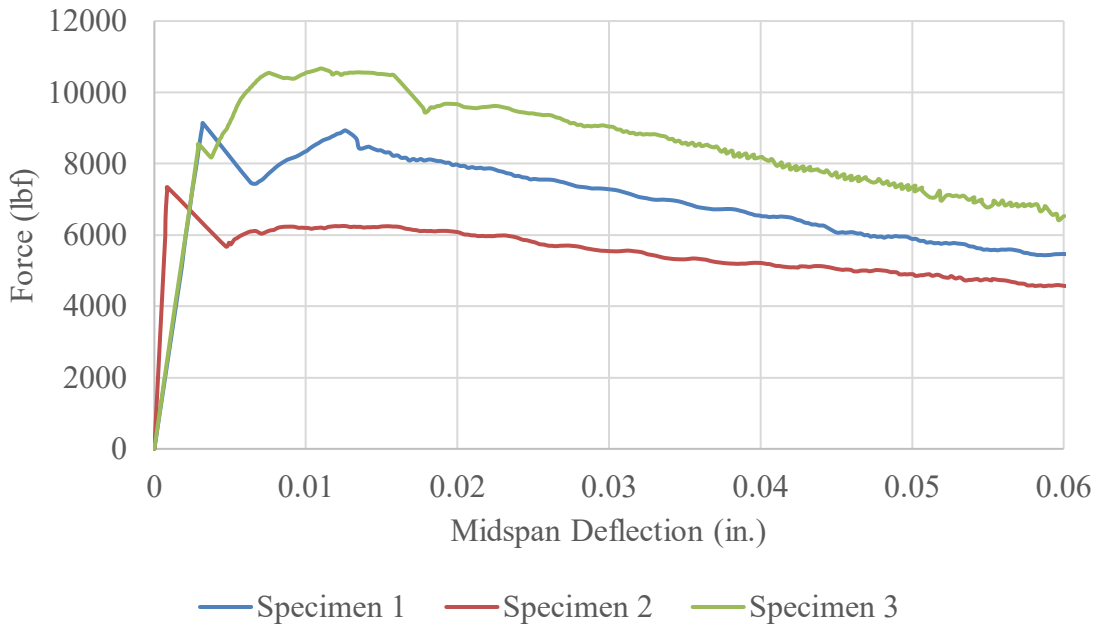

Figure 95: Applied load versus midspan deflection of 3 in. by 3 in. beams (closure pour 1)

Table 32: Summary of f_r at first and post peak load (closure pour 1) of 3 in. by 3 in. beams.

Specimen No.	f_r @ first peak load (psi)	f_r @ post peak load (psi)
1	2955	2955
2	2625	2625
3	2810	3510
COV (%)	5.92	14.76

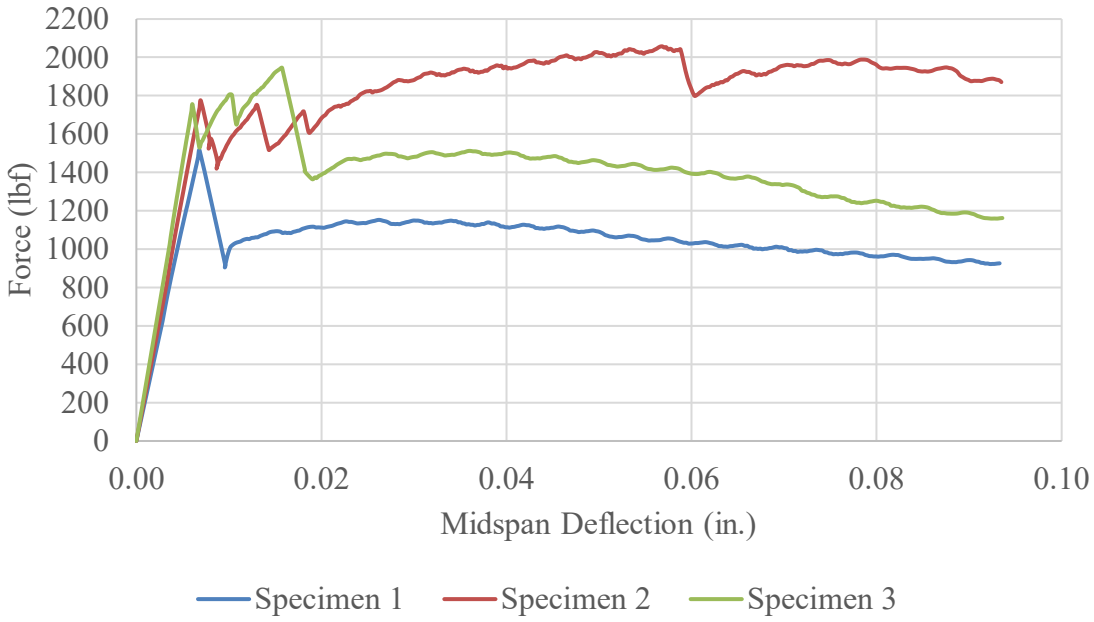

Figure 96: Applied load versus midspan deflection of 2 in. by 2 in. beams (closure pour 2)

Table 33: Summary of f_r at first and post peak load (closure pour 2) of 2 in. by 2 in. beams.

Specimen No.	f_r @ first peak load (psi)	f_r @ post peak load (psi)
1	2535	2535
2	2995	3475
3	2850	3165
COV (%)	3.51	6.60

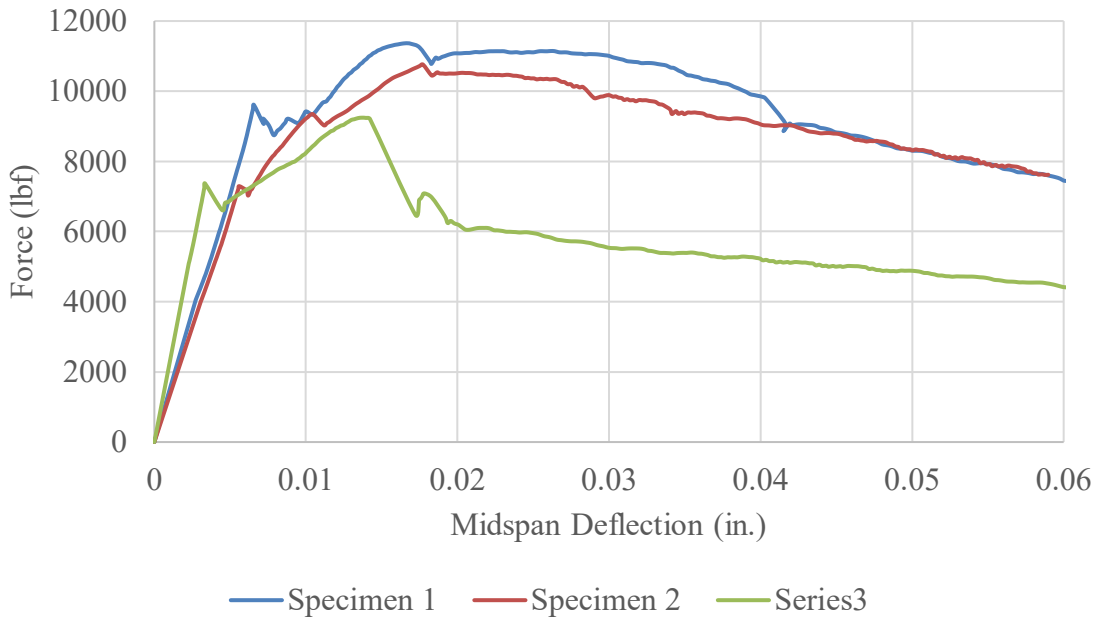

Figure 97: Applied load versus midspan deflection of 3 in. by 3 in. beams (closure pour 2)

Table 34: Summary of f_r at first and post peak load (closure pour 2) of 3 in. by 3 in. beams.

Specimen No.	f_r @ first peak load (psi)	f_r @ post peak load (psi)
1	3085	3650
2	2480	3660
3	2470	3100
COV (%)	13.17	9.24

APPENDIX B. PRECAST CONCRETE DECK PANEL STRENGTH CALCULATIONS

Calculations for 6" thick specimens (28"x102"x6")

Material Properties

$f_y := 60ksi$ $E_s := 29000ksi$

$K_1 := 1.0$ $w_c := 0.15\frac{kip}{ft^3}$

$f'_c := 6ksi$ $E_c := 120000 \cdot K_1 \cdot \left(\frac{w_c}{\frac{kip}{ft^3}}\right)^2 \cdot \left(\frac{f'_c}{ksi}\right)^{0.33} \cdot ksi = 4.877 \times 10^6 psi$

$\lambda := 1$

Initial length, width, and thickness values

$b := 28in$ $l := 48in$ $h := 6in$ Dimension of one precast deck

$h \geq \frac{b}{20} = 1$ Minimum thickness satisfied ACI 7.3.1.1

$A_g := b \cdot h = 168\,in^2$ Gross area of precast concrete section

Volume of UHPC required (no lips, flat joint)

$A_{UHPC} := (h + 0.25in) \cdot 6in = 37.5\,in^2$

$V_{UHPC} := A_{UHPC} \cdot b = 1.05 \times 10^3\,in^3$ $\frac{V_{UHPC}}{1728in^3} = 0.608\,ft^3$

Use #5 bars top and bottom

$A_{bar} := 0.31in^2$ $d_{bar} := \frac{5}{8}in$ Area and diameter of #5 bar

$n_{top} := 4$ $n_{bot} := 4$ Number of top and bottom rebars

$A'_s := n_{top} \cdot A_{bar} = 1.24\,in^2$ Total area of top rebar

$A_s := n_{bot} \cdot A_{bar} = 1.24\,in^2$ Total area of bottom rebar

$A_{s.min} := \max(0.0018 \cdot A_g, 0.0014 \cdot A_g) = 0.302\,in^2$ Minimum area of flexural reinf. ACI Table 7.6.1.1

$A_{s.min} \leq A_s = 1$ Minimum area satisfied

$d_{cover} := 1in$ Cover of 1-inch from Haber & Graybeal

$d' := d_{cover} + \frac{d_{bar}}{2} = 1.313\,in$ Depth to top steel from compression fiber

$d := h - d_{cover} - \frac{d_{bar}}{2} = 4.687\,in$ Depth to bottom steel from compression fiber

$\varepsilon_{t.min} := 0.004$ Minimum tensile strain

$\varepsilon_{cu} := 0.003$ Ultimate concrete strain

$\rho := \frac{A_s}{b \cdot h} = 7.381 \times 10^{-3}$ Reinforcement ratio

Cracking strength

$f_r := 0.24 \cdot \lambda \cdot \sqrt{\frac{f'_c}{ksi}} \cdot ksi = 587.878\,psi$ Modulus of rupture (AASHTO 5.4.2.6)

$\varepsilon_{cr} := \frac{f_r}{E_c} = 1.205 \times 10^{-4}$ Concrete strain at rupture

$n := \frac{E_s}{E_c} = 5.946$

$c := \frac{(n-1) \cdot A'_s \cdot d' + (n-1) \cdot A_s \cdot d + A_g \cdot \frac{h}{2}}{A_g + (n-1) \cdot A'_s + (n-1) \cdot A_s} = 3\,in$ Centroid of section from the top

$I_g := \frac{1}{12} \cdot b \cdot h^3 + A_g \cdot \left(\frac{h}{2} - c\right)^2 \ldots = 538.931\,in^4$ Moment of inertia using transformed section

$+ (n-1) \cdot A'_s \cdot (d' - c)^2 \ldots$

$+ (n-1) \cdot A_s \cdot (d - c)^2$

$M_{cr} := \frac{f_r \cdot I_g}{h - c} = 8.801\,ft \cdot kip$ Cracking strength using transformed section

Yield Strength

$\varepsilon_y := 0.002$ Assume tensile steel yields and "compression" steel is in compression

$f(c) := f_y \cdot A_s - \frac{\varepsilon_y}{d - c} \cdot (c - d') \cdot E_s \cdot A'_s - \frac{1}{2} \cdot \frac{\varepsilon_y \cdot c}{d - c} \cdot E_c \cdot c \cdot b$ Force equilibrium

$c := 2in$

$c := root(f(c), c) = 1.344\,in$ Centroid of section at yielding

$$\varepsilon'_s := \begin{cases} \frac{\varepsilon_y}{d - c} \cdot (d' - c) & \text{if } c < d' \\ \left[\frac{\varepsilon_y}{d - c} \cdot (c - d')\right] & \text{if } c \geq d' \end{cases} = 1.864 \times 10^{-5}$$

Compression steel strain

$M_y := f_y \cdot A_s \cdot \left(d - \frac{c}{3}\right) + \varepsilon'_s \cdot E_s \cdot A'_s \cdot \left(d' - \frac{c}{3}\right) = 26.334\,ft \cdot kip$ Yield strength using triangular stress block

Ultimate Strength

Force equilibrium

$c_g := 1.0in$ Initial guess of c

$f_s := -f_y$ Bottom steel stress

$\beta_1 := 0.85 - \frac{0.05 \cdot \left(\frac{f'_c}{psi} - 4000\right)}{1000} = 0.75$ Beta from ACI Table 22.2.2.4.3

$F(c_g) := E_s \cdot \left[\frac{\varepsilon_{cu}}{c_g} \cdot (c_g - d')\right] \cdot A'_s + f_s \cdot A_s \ldots + 0.85 \cdot f'_c \cdot (\beta_1 \cdot c_g \cdot b)$ Sum of forces

$c := root(F(c_g), c_g) = 1.004\,in$ Centroid of section at ultimate moment, measured from the top surface

$\varepsilon_t := \frac{\varepsilon_{cu}}{c} \cdot (d - c) = 0.011$ $\varepsilon_t \geq \varepsilon_{t.min} = 1$

$$\varepsilon'_s := \frac{\varepsilon_{cu}}{c}\cdot(c - d') = -9.215 \times 10^{-4}$$

Top steel strain
("Top steel" is used to describe steel on the compression side)

$$\text{TopTensComp} := \begin{cases} \text{"Top steel in compression"} & \text{if } \varepsilon'_s > 0 \\ \text{"Top steel in tension"} & \text{if } \varepsilon'_s < 0 \end{cases} = \text{"Top steel in tension"}$$

$$f'_s := \begin{cases} E_s\cdot\varepsilon'_s & \text{if TopTensComp} = \text{"Top steel in compression"} \\ 0 & \text{otherwise} \end{cases}$$

$$f'_s = 0\,\text{psi}$$

Top steel stress - ignore if in tension

$$F(c_g) := f'_s\cdot A'_s + f_s\cdot A_s + 0.85\cdot f'_c\cdot(\beta_1\cdot c_g\cdot b)$$

Reiterate force equilibrium

$$c_g := \text{root}(F(c_g), c_g) = 0.695\,\text{in}$$

Centroid of section

$$\varepsilon_s := \frac{\varepsilon_{cu}}{c}\cdot(d - c) = 0.017$$

Bottom steel strain

$$\varepsilon_s \geq \varepsilon_y = 1$$

Bottom steel yielded

$$\text{CompTransTens} := \begin{cases} \text{"Compression-controlled"} & \text{if } \varepsilon_t \leq \varepsilon_y \\ \text{"Transition"} & \text{if } \varepsilon_y < \varepsilon_t < 0.005 \\ \text{"Tension-controlled"} & \text{if } \varepsilon_t \geq 0.005 \end{cases} = \text{"Tension-controlled"}$$

$$M_n := \left| f'_s\cdot A'_s\cdot\left(d' - \frac{\beta_1\cdot c}{2}\right) + f_s\cdot A_s\cdot\left(d - \frac{\beta_1\cdot c}{2}\right)\right| = 27.447\,\text{ft}\cdot\text{kip}$$

Nominal strength using Whitney stress block

Test Configuration - 4 point bending (negative)

$w_{sw} := w_c \cdot b \cdot h = 0.175\,klf$ — Distributed load due to self weight of specimen

$x := 27in$ — Distance between support and load

$L_{concrete} := 2 \cdot l + 6in = 102\,in$ — Total length of concrete panel being tested, including 6-in UHPC joint

$L_{support} := 36in$ — Distance between two supports

$M_{sw} := w_{sw} \cdot \frac{(x + 6in)^2}{2} = 0.662\,ft \cdot kip$ — Maximum moment due to self weight of specimen

$M_{test} := \left[48plf \cdot \left(\frac{9.625ft}{2}\right) + 150lbf + 35lbf\right] \cdot x$

$M_{test} = 0.936\,ft \cdot kip$ — Maximum moment due to test configuration: weight of load plates and spreader beam*

$M_{DC} := M_{sw} + M_{test} = 1.598\,ft \cdot kip$ — Maximum moment due to dead load

*Actuator load to reach cracking, yield, and ultimate flexural capacity***

$P_{cr} := \frac{M_{cr} - M_{DC}}{x} \cdot 2 = 6.403 \times 10^3\,lbf$ — Load to reach cracking strength

$P_{yield} := \frac{M_y - M_{DC}}{x} \cdot 2 = 2.199 \times 10^4\,lbf$ — Load to reach yield of tensile steel

$P_{u.F} := \frac{M_n - M_{DC}}{x} \cdot 2 = 2.298 \times 10^4\,lbf$ — Load to reach ultimate flexural capacity

*: 9.625-ft long W8x48 as spreader beam; steel plates and roller that transfer load from the spreader beam and actuator weigh 35 lbf and 150 lbf, respectively.

**: Actuator loads will be different when more accurate loads from plates and beam are considered

Shear strength calculations (negative bending)

$V_c := 2\lambda \cdot \sqrt{\frac{f'_c}{psi}} \cdot psi \cdot b \cdot d = 2.033 \times 10^4 \, lbf$ Concrete shear strength

$V_{sw} := w_{sw} \cdot (x + 6in) = 481.25 \, lbf$ Maximum shear from self-weight

$V_{test} := 28plf \cdot \left(\frac{8ft}{2}\right) + 50lbf + 25lbf = 187 \, lbf$ Maximum shear from test configuration

$V_{DC} := V_{sw} + V_{test} = 668.25 \, lbf$ Maximum shear due to dead load

Actuator load to reach shear capacity

$P_{u.V} := (V_c - V_{DC}) \cdot 2 = 3.933 \times 10^4 \, lbf$ Load from actuator to cause shear failure

$$FailureMode := \begin{cases} \text{"Flexure"} & \text{if } \frac{P_{u.V}}{P_{u.F}} > 1 \\ \text{"Shear"} & \text{otherwise} \end{cases}$$

$FailureMode = \text{"Flexure"} \qquad \frac{P_{u.V}}{P_{u.F}} = 1.712$

REFERENCES

[1] Graybeal, B. A. (2013). Development of Non-Proprietary Ultra-High Performance Concrete for Use in the Highway Bridge Sector: TechBrief, United States. Federal Highway Administration.

[2] Russell, H.G., and Graybeal, B.A., "Ultra-high performance concrete: A state-of-the-art report for the bridge community," United States. Federal Highway Administration. Office of Infrastructure , 2013.

[3] Carey, A. S., I. L. Howard, D. A. Scott, R. D. Moser, J. Shannon and A. Knizley (2020). "Impact of Materials, Proportioning, and Curing on Ultra- High-Performance Concrete Properties." ACI Materials Journal **117**(1): 213-222.

[4] Graybeal, B. A., "Characterization of the ultra-high performance concrete," Doctor of Philosophy Dissertation, University of Maryland, College Park, 2005.

[5] Panesar, D.K., "3 - Supplementary cementing materials," in *Developments in the Formulation and Reinforcement of Concrete (Second Edition)*, S. Mindess Ed.: Woodhead Publishing, 2019, pp. 55-85.

[6] Graybeal, B. A., "Material property characterization of ultra-high performance concrete," United States. Federal Highway Administration. Office of Infrastructure …, 2006.

[7] Kusumawardaningsih, Y., Fehling, E., and Ismail, M., "UHPC compressive strength test specimens: Cylinder or cube?," *Procedia Engineering,* vol. 125, pp. 1076-1080, 2015.

[8] Graybeal, B. A., "Compressive behavior of ultra-high-performance fiber-reinforced concrete," *ACI materials journal,* vol. 104, no. 2, pp. 146-152, 2007.

[9] Scott, D.A., Long, W. R., Moser, R. D., Green, B. H., O'Daniel, J. L., and Williams, B. A., "Impact of steel fiber size and shape on the mechanical properties of ultra-high performance concrete," ENGINEER RESEARCH AND DEVELOPMENT CENTER, 2015.

[10] Kim, H., Hadl, P., and Nguyen, V. T., "A New Mix Design Method for UHPC based on Stepwise Optimization of Particle Packing Density," in *International Interactive Symposium on Ultra-High Performance Concrete*, 2016, vol. 1, no. 1: Iowa State University Digital Press.

[11] Ahlborn, T. M., Peuse, E. J., and Misson, D. L., "Ultra-high performance concrete for Michigan bridges, material performance: phase I," Michigan. Dept. of

Transportation, 2008.

[12] Berry, M., Snidarich, R., and Wood, C., "Development of non-proprietary ultra-high performance concrete," Montana. Dept. of Transportation. Research Programs, 2017.

[13] Ahmad, S, Hakeem, I., and Maslehuddin, M., "Development of an optimum mixture of ultra-high performance concrete," *European Journal of Environmental and Civil Engineering,* vol. 20, no. 9, pp. 1106-1126, 2016.

[14] Khaloo A., Karimi H., Asadollahi S., and Dehestani M., "A new mixture design method for ultra-high-strength concrete," *ACI Materials Journal,* vol. 114, no. 2, pp. 215-224, 2017.

[15] B. Reichard, B., Stewart, L., Weaver, M., and Morrill, K., "Coupled Hydraulic System for Tensile Testing in Compression-only Machines," *Experimental Mechanics,* vol. 56, no. 7, pp. 1179-1190, 2016.

[16] Graybeal, B. A. and Baby F., "Tension testing of ultra-high performance concrete," Federal Highway Administration, 2019.

[17] *Standard Test Method for Flexural Performance of Fiber-Reinforced Concrete (Using Beam With Third-Point Loading)*, A. International, West Conshohocken, PA, 2019.

[18] Roth, M. J., Rushing, T. S., Flores, O. G., Sham, D. K., and Stevens, J. W., "Laboratory investigation of the characterization of Cor-Tuf flexural and splitting tensile properties," 2010.

[19] Mindess, S., Young, J.F., and Darwin, D. (2003). "Concrete 2nd Edition." Pearson Education, Inc., Upper Saddle River, New Jersey.

[20] *Standard Test Method for Electrical Indication of Concrete's Ability to Resist Chloride Ion Penetration*, West Conshoshocken, PA, 2019.

[21] Kizhakommudom, H., Li, Z., and Schiff, S. D., "Research Project No. 682 Development of High-Strength/High Performance Concrete/Grout Mixtures for," 2014.

[22] Graybeal, B.A., "Field-cast UHPC connections for modular bridge deck elements," Federal Highway Administration, 2010.

[23] Graybeal, B.A., "Design and construction of field-cast UHPC connections," United States. Federal Highway Administration, 2014.

[24] Haber, Z. B., "Ultra-High Performance Concrete (UHPC)," Federal Highway Administration, Presentation for 2016 FDOT Design Training Expo, 2016.

[25] Graybeal, B.A., "Behavior of Ultra-High Performance Concrete Connections between Precast Bridge Deck Elements," 2010.

[26] Haber, Z. B. and Graybeal, B. A., "Performance of grouted connections for prefabricated bridge deck elements," United States. Federal Highway Administration. Office of Infrastructure …, 2018.

[27] ASTM International. *C1856/C1856M-17 Standard Practice for Fabricating and Testing Specimens of Ultra-High Performance Concrete*. West Conshohocken, PA; ASTM International, 2017. doi: https://doi.org/10.1520/C1856_C1856M-17

[28] *EIRICH Intensive Mixer*, 2018, pp. 1-16.

[29] Schachinger, I., Schubert, J., and Mazanec, O., "Effect of mixing and placement methods on fresh and hardened ultra high performance concrete (UHPC)," in *International Symposium on Ultra High Performance Concrete*, 2004, pp. 575-586.

[30] *Testing Hardened Concrete - Part 3: Compressive Strength of Test Specimens*, EN-12390-3, E. Standard, 2019.

[31] *MasterGlenium 7920 High-Range Water Reducing Admixture*, Master Builders Solutions, 2020.

[32] *Dramix Data Sheet*, Bekaert, 2014.

[33] Rougeau, P., and Borys, B., "Ultra high performance concrete with ultrafine particles other than silica fume," in *Proceedings of the International Symposium on Ultra High Performance Concrete*, 2004, vol. 32, pp. 213-225.

[34] Miller, A. A., Loreto, G., Gao, N., Kurtis, K. E., and Stewart, L. K., "Applications of UHPC to Bridge Construction in Georgia," in *International Interactive Symposium on Ultra-High Performance Concrete*, 2019, vol. 2, no. 1: Iowa State University Digital Press.